Measurements of jet cross-section ratios in 13 TeV proton-proton collisions with ATLAS

G. Aad *et al.*[*]

(ATLAS Collaboration)

Measurements of jet cross-section ratios between inclusive bins of jet multiplicity are performed in 140 fb^{-1} of proton-proton collisions with $\sqrt{s} = 13$ TeV center-of-mass energy, recorded with the ATLAS detector at CERN's Large Hadron Collider. These ratios are constructed from double-differential cross-section measurements that are made in bins of jet multiplicity and other observables that are sensitive the energy scale and angular distribution of radiation due to the strong interaction in the final state. Additionally, the scalar sum of the two leading jets' transverse momenta is measured triple differentially, in bins of the third jet's transverse momentum and of jet multiplicity. These measurements are unfolded to account for acceptance and detector-related effects. The measured distributions are used to construct ratios of the inclusive jet-multiplicity bins, which have been shown to be sensitive to the strong coupling α_S while being less sensitive than other observables to systematic uncertainties and parton distribution functions. The measured distributions are compared with state-of-the-art QCD calculations, including next-to-next-to-leading-order predictions for two- and three-jet events. These predictions are generally found to model the data well and perform best in bins with a modest requirement on the third jet's transverse momentum. Significant differences between data and Monte Carlo predictions are observed in events with large rapidity gaps and invariant masses of the leading jet pair. Studies leading to reduced jet energy scale uncertainties significantly improve the precision of this work and are documented herein.

I. INTRODUCTION

Quantum chromodynamics (QCD) is the theory of the strong interaction, which describes the interactions of quarks and gluons. It is therefore fundamental to understanding both initial-state and final-state physics at hadron colliders such as CERN's Large Hadron Collider (LHC). Recent theoretical advances have led to fixed-order predictions of three-jet cross sections in proton-proton (pp) collisions at next-to-next-to-leading order (NNLO) [1]. Comparisons between experimental results and these state-of-the-art predictions provide powerful tests of perturbative QCD. Discrepant models of QCD processes impact the accuracy of physics simulations and Monte Carlo event generators, which in turn often limits experimental precision. Better understanding of the modeling of QCD processes is therefore needed to achieve the highest possible levels of precision in physics analysis, both at the LHC and at future experimental facilities [2,3].

In this analysis, multiple facets of QCD are studied by measuring differential cross sections of multijet events, and their ratios, in $\sqrt{s} = 13$ TeV pp collisions at the LHC. One set of measured observables is sensitive to the energy scale of the hard-scattering process in the event and can be used to test the accuracy of fixed-order matrix-element predictions. A complementary set of observables is sensitive to the angular distributions of hadronic energy flow in the final state and hence can probe other aspects of QCD modeling. The differential cross sections for each observable are used to construct cross-section ratios between different inclusive jet-multiplicity bins, reducing the sensitivity of the measurements to systematic uncertainties and parton distribution functions.

This procedure was used previously by the ATLAS [4] and CMS [5,6] Collaborations at the LHC to measure the three-jet to two-jet cross-section ratio, R_{32}, in pp collisions at $\sqrt{s} = 7$ TeV. Prior to those results, this quantity was measured at other hadron colliders by the UA1 [7], UA2 [8], CDF [9], and D0 [10,11] Collaborations. Here, R_{32} is presented for the first time in $\sqrt{s} = 13$ TeV pp collisions and is compared with fixed-order QCD predictions at NNLO accuracy. Although such high-precision predictions do not yet exist for events with larger jet multiplicities, the higher multiplicity ratios R_{43}, R_{42}, and R_{54} are experimentally accessible with the complete run 2

---

dataset. These ratios were also measured in this analysis, to serve as a reference for future theoretical developments.

The structure of this paper is as follows. A description of the ATLAS detector, the run 2 dataset, and the multijet simulations used in this analysis are given in Sec. II. In Sec. III, an overview of the event selection and observables used in this analysis is provided, along with a description of the unfolding procedure used to correct the measured distributions for effects related to detector resolution. The estimated systematic uncertainties from various sources are described in Sec. IV, and modeling improvements leading to smaller jet energy scale uncertainties are highlighted. Fixed-order QCD calculations that are compared with the measured data are then described in Sec. V. The main results of the analysis are presented in Sec. VI and compared with fixed-order QCD predictions and Monte Carlo simulated event samples. Concluding remarks follow, in Sec. VII.

II. THE ATLAS DETECTOR, RUN 2 DATASET, AND SIMULATION

A. The ATLAS detector

The ATLAS detector [12] at the LHC covers nearly the entire solid angle around the collision point.[1] It consists of an inner tracking detector surrounded by a thin superconducting solenoid, electromagnetic and hadron calorimeters, and a muon spectrometer incorporating three large superconducting air-core toroidal magnets.

The inner-detector system is immersed in a 2 T axial magnetic field and provides charged-particle tracking in the range $|\eta| < 2.5$. The high-granularity silicon pixel detector covers the vertex region and typically provides four measurements per track, the first hit normally being in the insertable B-layer installed before run 2 [13,14]. It is followed by the silicon microstrip tracker, which usually provides eight measurements per track. These silicon detectors are complemented by the transition radiation tracker (TRT), which enables radially extended track reconstruction up to $|\eta| = 2.0$. The TRT also provides electron identification information based on the fraction of hits (out of a typical total of 30) above a higher energy-deposit threshold corresponding to transition radiation.

The calorimeter system covers the pseudorapidity range $|\eta| < 4.9$. Within the region $|\eta| < 3.2$, electromagnetic

calorimetry is provided by barrel and end cap high-granularity lead/liquid-argon (LAr) calorimeters, with an additional thin LAr presampler covering $|\eta| < 1.8$ to correct for energy loss in material upstream of the calorimeters. Hadron calorimetry is provided by a steel/scintillator-tile calorimeter ("tile calorimeter"), segmented into three barrel structures within $|\eta| < 1.7$ and two copper/LAr hadron end cap calorimeters. The solid angle coverage is extended by forward copper/LAr and tungsten/LAr calorimeter modules optimized for electromagnetic and hadronic energy measurements, respectively.

The muon spectrometer comprises separate trigger and high-precision tracking chambers measuring the deflection of muons in a magnetic field generated by the superconducting air-core toroidal magnets. The field integral of the toroids ranges between 2.0 and 6.0 Tm across most of the detector. Three layers of precision chambers, each consisting of layers of monitored drift tubes, cover the region $|\eta| < 2.7$, complemented by cathode-strip chambers in the forward region, where the background is highest. The muon trigger system covers the range $|\eta| < 2.4$ with resistive-plate chambers in the barrel and thin-gap chambers in the end cap regions.

Interesting events are selected by the first-level trigger system implemented in custom hardware, followed by selections made by algorithms implemented in software in the high-level trigger [15]. The first-level trigger accepts events from the 40 MHz bunch crossings at a rate below 100 kHz, which the high-level trigger reduces in order to record events to disk at about 1 kHz.

An extensive software suite [16] is used in data simulation, in the reconstruction and analysis of real and simulated data, in detector operations, and in the trigger and data acquisition systems of the experiment.

B. Data

This analysis is performed using data from LHC pp collisions with a center-of-mass energy of $\sqrt{s} = 13$ TeV, collected during 2015–2018 with the ATLAS detector. The total integrated luminosity of this dataset is 140 fb^{-1}. The uncertainty in the combined 2015–2018 integrated luminosity is 0.83% [17], obtained using the LUCID-2 detector [18] for the primary luminosity measurements, complemented by measurements using the inner detector and calorimeters. Due to the high instantaneous luminosity and the large total inelastic pp cross section, there are, on average, 33.7 simultaneous ("pileup") collisions in each bunch crossing. Data events must satisfy quality requirements to be included in the analysis [19].

C. Simulation

Samples of Monte Carlo (MC) simulated multijet events are used in this analysis for comparison with the data, to unfold the detector-level measurement to particle-level and

---

[1]ATLAS uses a right-handed coordinate system with its origin at the nominal interaction point (IP) in the center of the detector and the z-axis along the beam pipe. The x-axis points from the IP to the center of the LHC ring, and the y-axis points upward. Cylindrical coordinates (r, ϕ) are used in the transverse plane, ϕ being the azimuthal angle around the z-axis. The pseudorapidity is defined in terms of the polar angle θ as $\eta = -\ln\tan(\theta/2)$. Angular distance is measured in units of $\Delta R \equiv \sqrt{(\Delta y)^2 + (\Delta \phi)^2}$, where $y = (1/2)\ln[(E + p_z)/(E - p_z)]$ is the object's rapidity defined by its energy and longitudinal momentum.

to achieve the reductions in jet energy scale uncertainties described in Sec. IV. Since the jet production cross section is much larger than the cross sections for other processes, these multijet samples are sufficient to describe data in the fiducial region of the measurement.

PYTHIA8.230 [20] is used as the nominal MC generator in this analysis and is also referred to here as the "nominal" simulation. Samples of $2 \rightarrow 2$ dijet events were generated using the A14 set of tuned parameters ("tune") [21], the Lund string hadronization model [22], and the NNPDF2.3LO leading-order (LO) parton distribution function (PDF) set [23]. The PYTHIA parton shower (PS) algorithm uses a transverse-momentum-ordered evolution [24], and its renormalization and factorization scales were set to the geometric mean of the squared transverse masses of the outgoing particles. EVTGEN [25] was used to model decays of heavy-flavor hadrons.

Three sets of SHERPA2.2.5 [26] multijet events were used with the default AHADIC cluster hadronization model [27] or with the SHERPA interface to the Lund string hadronization model as implemented in PYTHIA6.4, and its decay tables. These samples include LO matrix-element calculations for $2 \rightarrow 2$ processes and use the SHERPA parton shower algorithm based on Catani-Seymour dipole subtraction [28]. The CT14NNLO NNLO PDF set [29] was used for matrix-element calculations and the CT10 PDF set [30] was used for multiparton interactions (MPIs). One additional SHERPA sample was generated with SHERPA2.2.11, using the same settings as the sample with cluster-based hadronization described above, except that the parameters of the hadronization model were retuned to achieve better agreement with large electron positron (LEP) data [31]. This retuning changes the description of the baryon production rate inside jets and was found to make the description of the ATLAS detector's jet energy response more consistent between SHERPA and PYTHIA jets. Further details can be found in Ref. [32].

Another set of multijet events was generated using HERWIG7.1.6 [33–35] with the default cluster hadronization model and either the default angle-ordered PS or the alternative dipole PS [27]. In these samples the $2 \rightarrow 2$ matrix elements are modeled with LO accuracy and interfaced with the NNPDF2.3LO PDF set. The angle-ordered sample is compared with measurements from this analysis, and both samples are used in the studies of jet energy scale systematic uncertainties presented in Sec. IV.

Two additional samples of multijet events with next-to-leading-order (NLO) matrix-element accuracy were produced with POWHEGv2 [36–38] using the multijet process implemented in POWHEG BOXv2 [39], matched to either the PYTHIA8 or angle-ordered HERWIG7 parton shower configured as for the corresponding samples described above. The renormalization and factorization scales in these samples were set to the transverse momentum (p_T) of the underlying Born-level configuration. For the PYTHIA

PS, the default Lund string hadronization model was used with the NNPDF3.0NLO PDF set [40] and A14 tune. The NNPDF3.0NLO PDF set was also used for the HERWIG sample, but with the default HERWIG cluster-based hadronization model. These samples are referred to as the "POWHEG+PYTHIA" and "POWHEG+HERWIG" samples.

All generated events were passed through a full detector simulation [41] based on GEANT4 [42] and overlaid with simulated minimum-bias interactions generated using PYTHIA8 with the A3 tune [43] and NNPDF2.3LO PDF set to represent pileup interactions. The distribution of the average number of pileup interactions in simulation is reweighted during data analysis to match that observed in run 2 data.

Additional details of the MC samples used in this measurement may be found in Ref. [44].

III. METHODOLOGY

A. Object and event selection

All jets in this analysis are reconstructed using the anti-k_t algorithm [45] as implemented in FASTJET [46], with a jet radius parameter $R = 0.4$.

"Particle-level" jets are reconstructed in simulated events without detector simulation. All detector-stable particles, with a lifetime τ in the laboratory frame such that $c\tau > 10$ mm, are used, except those that are expected to deposit little or no energy in the calorimeters (i.e., muons and neutrinos). Particle-level jets are required to have $p_T > 60$ GeV and absolute rapidity $|y| < 4.5$ to enter this analysis.

Detector-level jets are reconstructed from particle flow (PFlow) objects [47], which combine measurements from the ATLAS inner detector and calorimeters [48] to improve the jet energy resolution and increase the jet reconstruction efficiency, especially at low jet p_T. Jets are calibrated such that the average detector-level jet energy scale (JES) matches that of the corresponding particle-level jets, using a combination of simulation-based and *in situ* techniques [49]. Signals originating from detector noise, cosmic rays, and beam-induced backgrounds can be reconstructed as spurious jets, but these are efficiently rejected by following the methodology described in Ref. [50], updated for particle flow jets but utilizing the same observables. For this study, detector-level jets are required to have $p_T > 60$ GeV and absolute rapidity $|y| < 4.5$. After applying these kinematic selections, the likelihood that a particle flow jet originates from a pileup interaction is sufficiently low that no additional pileup-jet rejection is applied [51,52].

To be included in the analysis, both the particle- and detector-level events are required to have at least two selected jets ($N_{jets} \geq 2$), and the scalar p_T sum of the leading jet pair (ordered in p_T), $H_{T2} = p_{T,1} + p_{T,2}$, must satisfy $H_{T2} \geq 250$ GeV.

All detector-level events are required to have at least one vertex reconstructed from two or more inner-detector tracks with $p_T > 500$ MeV and to pass the data quality requirements described in Ref. [19]. The data were collected using a set of single-jet triggers [53], whose thresholds depended on the data-taking year during run 2. By design, the minimum H_{T2} requirement ensures that the measurement is performed in a region where the single-jet triggers are fully efficient for the analysis selection. It also ensures that the measurement's fiducial region does not include phase-space regions that are divergent at fixed order [54,55].

Combinations of central and forward single-jet triggers are used to select events in ranges of H_{T2} where the combination is fully efficient. For triggers that were prescaled during data taking, events in data are reweighted by the appropriate prescale factor to recover a smoothly falling jet p_T spectrum. The prescale factors applied to central- and forward-jet triggers differ, so they are logically combined using the "inclusion method" described in Ref. [56].

B. Measured observables

The two observables chosen for their sensitivity to fixed-order effects are H_{T2} and $p_T^{N\text{incl}}$. As introduced in Sec. III A, H_{T2} is the scalar sum of the transverse momenta of the leading two jets in the event: $H_{T2} = p_{T,1} + p_{T,2}$. It is a proxy for the energy scale of the hard-scattering interaction. For events with more than two jets, the p_T of the third leading jet, $p_{T,3}$, determines the sensitivity to resummation effects, and varying the $p_{T,3}$ threshold leads to better understanding of these effects. The cross section is measured triple differentially, as a function of H_{T2} and in bins of jet multiplicity N_{jets} and bins of $p_{T,3}$.

The $p_T^{N\text{incl}}$ distribution is the inclusive jet p_T spectrum, measured in bins of inclusive jet multiplicity. For example, the $p_T^{2\text{incl}}$ distribution is the p_T spectrum of the two leading jets in any selected event, and $p_T^{3\text{incl}}$ would include the leading and subleading jet contributions in addition to the third jet, if one passes the selection.

Configurations with large logarithmic corrections can be preferentially selected by measuring jet cross-section ratios as a function of either the absolute value of the leading jet pair's rapidity difference, or the absolute value of the maximum rapidity difference between selected jets in the event (Δy_{jj} and $\Delta y_{jj,\text{max}}$, respectively). Similarly, the invariant mass of the two leading jets and the maximum dijet invariant mass found among all selected jets in the event (forming the m_{jj} and $m_{jj,\text{max}}$ distributions, respectively) also contain a region at large invariant mass where the cross section receives large logarithmic contributions. These four observables are measured to probe the resummation in different ways: for example, logarithmic corrections will be larger for $m_{jj,\text{max}}$ than for m_{jj}. Large invariant masses for m_{jj} tend to be dominated by the contributions from large p_T, which are well described by fixed-order predictions.

Conversely, $m_{jj,\text{max}}$ includes greater contributions from the large angular separations that directly probe these effects. This set of measurements provides a novel way to indirectly test analytic descriptions of vector-boson scattering/fusion (VBS/VBF) interactions and MC calculations. Observables such as m_{jj} and Δy_{jj} are also sensitive to PDFs and were used in prior PDF fitting studies by the CMS Collaboration [57]. The analysis selection imposes a single-jet p_T requirement on all jets, which allows the logarithmic structure of VBS/VBF events to be probed without introducing additional complications from hierarchies in the jet selection.

C. Unfolding

All data presented in Sec. VI are unfolded using an iterative D'Agostini unfolding procedure [58] to account for effects arising from the limited efficiency, acceptance, and resolution of the ATLAS detector. For each observable, the binning used in this measurement is varied in accord with the detector's resolution. The unfolding algorithm was implemented using the ROOUNFOLD toolkit [59]. Four iterations of the unfolding procedure are used, because this ensures the unfolding converges well and either minimizes or minimally affects the total uncertainty from all sources for all observables. For most observables the unfolding is performed double differentially, in bins of the observable and in exclusive bins of jet multiplicity N_{jets}, to allow the unfolding procedure to account for migrations between relevant bins. The H_{T2} measurement is unfolded triple differentially in bins of H_{T2}, N_{jets}, and $p_{T,3}$. For the double-differential measurements and triple-differential measurement, the purity of the response matrices (i.e., the size of the diagonal elements) is typically above 50% or 30%, respectively.

These exclusive bins of N_{jets} are used to construct inclusive bins of N_{jets}. The unfolded absolute differential cross sections are presented in Sec. VI A. These unfolded cross sections are used to construct the cross-section ratios R_{32}, R_{42}, R_{43}, and R_{54}, which are presented in Sec. VI B.

IV. SYSTEMATIC UNCERTAINTIES

A. Jet energy scale

Systematic uncertainties in the $R = 0.4$ JES and jet energy resolution (JER) are evaluated using a series of simulation-based techniques and *in situ* measurements, documented in Ref. [49]. These uncertainties are propagated by building a response matrix from each variation representing a systematic uncertainty component, then unfolding the nominal prior distribution using the varied response matrix. The difference between the unfolded nominal and systematically varied cross sections is taken as the systematic uncertainty. They are the dominant sources of experimental uncertainty in the analysis.

The impact of certain components of the JES uncertainty has been reduced by updating the prescriptions given in
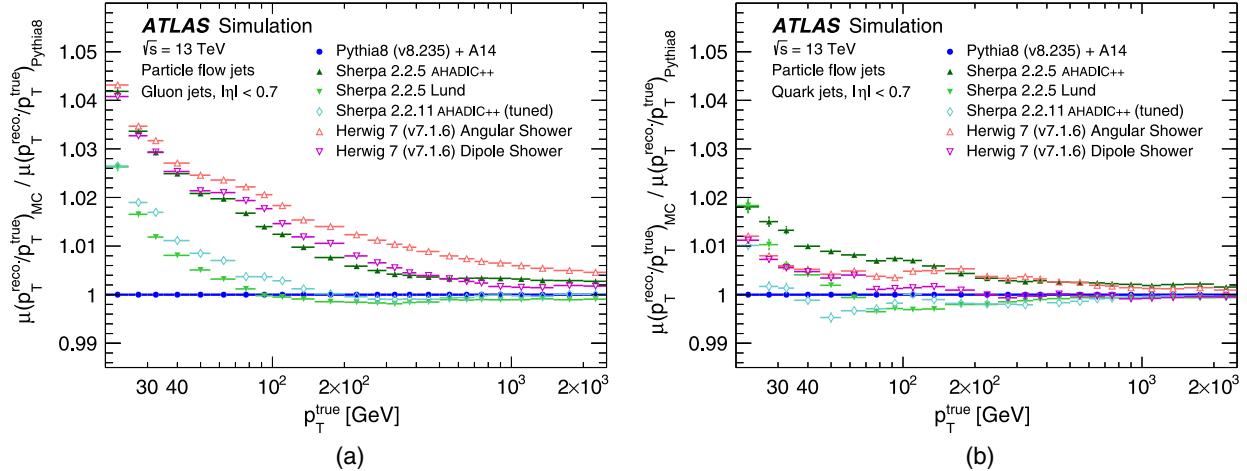
FIG. 1. The ratio of the average jet energy response for (a) gluon-initiated and (b) quark-initiated jets in various MC simulation samples to the jet energy response of the nominal PYTHIA sample, as a function of the true jet p_T for jets within the pseudorapidity range $|\eta| < 0.7$.

Ref. [49]. Uncertainties can also arise because the relative jet energy response for simulated quark- and gluon-initiated jets varies between different MC generators; they are called "jet flavor response/composition" uncertainties in Ref. [49]. These uncertainties were significantly reduced relative to their prior treatment, and the improvements are explained below in Sec. IV A 1. Following this updated treatment, the component of the JES uncertainty due to the jet flavor is reduced from a leading source of uncertainty in the measurement to a completely subdominant effect.

Improvements were also made to the component of the jet energy scale uncertainty related to the extrapolation of single-hadron response measurements [60–62] to jets, discussed below in Sec. IV A 2. This component of the JES uncertainty is reduced by roughly a factor of 3 compared to that reported in Ref. [49].

The JES/JER uncertainties can result in asymmetric variations, and they are left unsymmetrized in the presentation of the measured cross sections and their ratios.

1. Updated jet flavor response uncertainty

The internal dynamics of a jet are determined in part by the flavor of the parton that initiated it.[2] The response of the ATLAS detector to jets depends on the underlying particle

spectra, which can vary significantly between different MC generator setups. An uncertainty related to our limited knowledge of the actual spectra in data and its relationship with the JES is therefore necessary: this component of the ATLAS JES uncertainties is referred to as the "flavor response uncertainty." Historically, it has been defined by the difference between the responses to gluon-initiated jets from different MC generator setups multiplied by the fraction of gluon-initiated jets in the measured phase space (e.g., in Ref. [49], as the difference between PYTHIA8 and HERWIG++).

The jet energy response is defined as the ratio of the jet transverse momentum at detector-level (p_T^{reco}) to that at particle-level (p_T^{true}). The ratio of the average jet response, $\mu(p_T^{reco}/p_T^{true})$, between several MC generator setups and the nominal PYTHIA sample is shown in Figs. 1(a) and 1(b) for $R = 0.4$ particle flow jets that are initiated by either gluons or quarks and antiquarks, respectively. For gluon-initiated jets, differences between PYTHIA and alternative models are as large as 2.5% at $p_T = 60$ GeV. For quark-initiated jets, the differences are smaller, with a spread below $\sim 1\%$ above $p_T = 60$ GeV.

Several fragmentation- and hadronization-related effects can change the jet response. The calorimeter energy response to hadrons rises with energy [61,62], so the momentum spectrum of the particles associated with the jet is expected to play an important role in jet response modeling. The particle composition also plays a role because the calorimeter response to neutral pions, which decay via $\pi^0 \rightarrow \gamma\gamma$, is significantly higher than for hadronic showers, and for charged hadrons the particle flow algorithm is able to use track measurements. Additionally, the ATLAS detector's response to hadrons has also been found to vary slightly depending on the species of particle [61], which is consistent with analysis of test-beam data for pions, protons, and charged kaons [68,69]. While the

---

[2]The notion of a "quark-initiated" or "gluon-initiated" jet is not well defined beyond leading order in QCD [63,64]: quark-initiated jets are narrower and have fewer constituents and a harder particle spectrum, on average, than gluon-initiated jets with the same p_T. For simplicity, these studies use labels based on the identity of the highest-energy ghost-associated [65] parton that the MC generator's "truth" record matches to the reconstructed jet. While this definition can be MC-generator-dependent, this label nevertheless reflects the expected differences between quark- and gluon-initiated jet fragmentation in experimental settings [66,67] and is therefore well suited to characterize differences in how these jets interact with the detector material.

particle composition is partly determined by isospin symmetries, the production of baryons and kaons occurs via different mechanisms in hadronization models that are parameterized and tuned to experimental data [70–72].

Since both the particle spectra from jet fragmentation and the particle content of a jet can affect the detector response, their modeling must be tuned to experimental measurements. Many measurements of jet fragmentation functions and other pertinent substructure observables have been performed at the SPS [73–75], LEP [76–87], the LHC [67,88–95], and other colliders [96–110], typically without explicit particle identification. However, the ALICE experiment has performed some measurements [111–113] that do probe the particle content.

Figure 2 shows the mean baryon energy fractions for central ($|\eta| < 0.7$), particle-level, gluon-initiated jets in MC samples generated by PYTHIA and either HERWIG7.1.6 with the angle-ordered or dipole PS algorithms [Fig. 2(a)] or SHERPA2.2.5 with cluster- or string-based hadronization models and SHERPA2.2.11 with a cluster hadronization model that was retuned to LEP data [31] [Fig. 2(b)]. The mean baryon energy fraction for quark-initiated jets in the PYTHIA MC sample is also shown, to indicate the size of possible differences arising due to the jet flavor. Significant differences between the different MC generator setups are observed. The mean baryon energy fraction varies between 12% and 20% for the different generators and slowly decreases as the jet p_T increases. Variation of the PS model in HERWIG samples does not change the distribution much. In both HERWIG samples and the SHERPA2.2.5 sample with cluster-based hadronization the fraction of energy carried by baryons is lower than for the nominal PYTHIA sample, while for the SHERPA2.2.5 sample

with string-based hadronization it is higher. The SHERPA2.2.11 sample with the retuned cluster-based hadronization is in better agreement with the PYTHIA sample.

To further investigate the dependence of the jet response on the particle content of the jet, Fig. 3 shows the PFlow jet response of gluon- and quark-initiated jets as a function of the fraction of the true jet energy carried by baryons. It is seen that larger baryon fractions lead to lower jet energy responses for both gluon- and quark-initiated jets. This is expected, as the majority of these baryons will be protons or neutrons, or their antiparticles. The average response of these particles is typically lower than that of a mixture of charged and neutral pions, as neutral pions decay mainly into two photons and the calorimeter is calibrated for electromagnetic showers. Additionally, while protons, antiprotons, and charged pions will have reconstructed tracks during particle flow reconstruction, neutrons and antineutrons will rely solely on calorimeter measurements and thus have a lower response (due to signal leakage, dead material, etc.). Together, these lead to the observed trend that, when a larger fraction of the jet's energy is carried by baryons, the jet energy response is lower.

A similar, but smaller, dependence of the jet response on the kaon energy fraction is also observed and can be explained similarly.

Based on these observations, the treatment of the ATLAS JES flavor response uncertainty was revisited in order to consider differences between the underlying simulated particle spectra more carefully and to use updated MC generator setups. Instead of the previous two-point comparison of the gluon-initiated jet response between PYTHIA8 and HERWIG++, three separate uncertainty components are

(a)

(b)
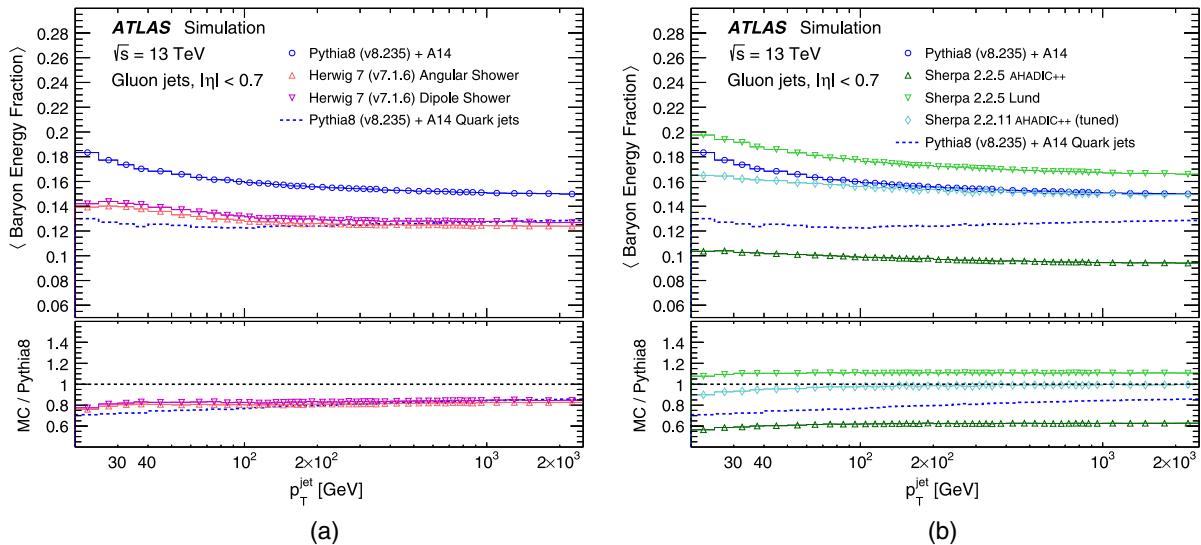
FIG. 2.   The average fraction of the gluon-initiated jet's energy carried by baryons as a function of the jet p_T for jets within $|\eta| < 0.7$. The nominal PYTHIA sample is compared with (a) several HERWIG samples with different parton shower models, and (b) several SHERPA samples with different hadronization models and sets of tuned parameters. The dashed line provides a comparison with quark-initiated jets in the nominal PYTHIA sample.
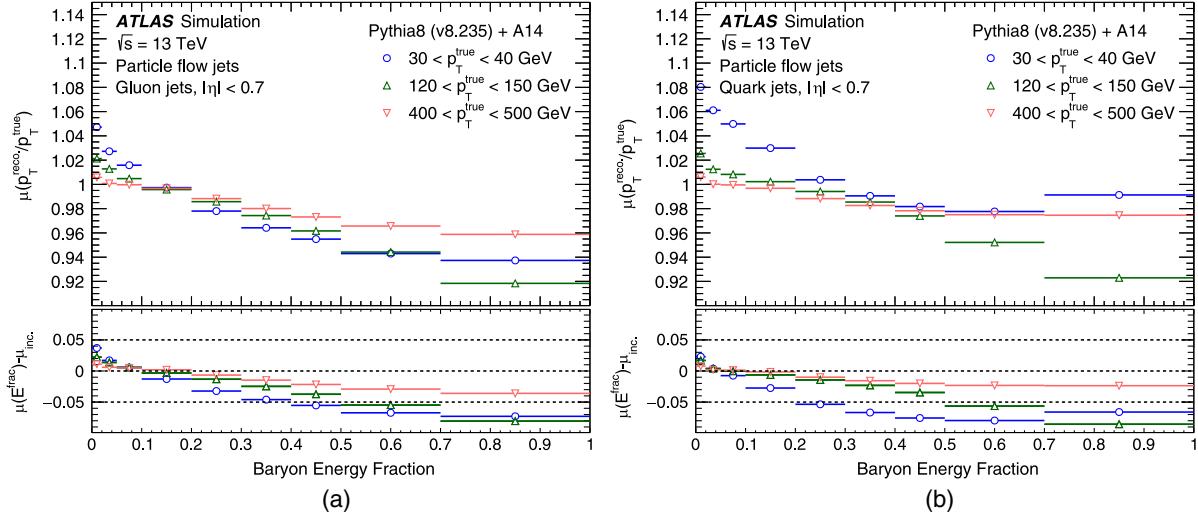
FIG. 3. The jet energy response for (a) gluon- and (b) quark-initiated jets as a function of the baryon energy fraction, for various true jet p_{T} bins in the nominal PYTHIA sample.

defined by directly comparing MC generator setups that factorize different physical effects:

(1) Flavor generator/shower: PYTHIA8 vs SHERPA2.2.5 with Lund string hadronization. This comparison varies the UE/MPI model and aspects of the PS model (p_{T} ordered vs dipole).

(2) Flavor hadronization: SHERPA2.2.11 with AHADIC cluster-based hadronization vs SHERPA2.2.5 with Lund string hadronization. This comparison varies the nonperturbative hadronization model, between the updated SHERPA AHADIC cluster-based model and the Lund string model as implemented in PYTHIA6.

(3) Flavor shower: HERWIG7.1 with angle-ordered PS vs HERWIG7.1 with dipole PS. This comparison between the angle-ordered and dipole PS models implemented in HERWIG ensures that all three major PS schemes used in ATLAS MC generators are considered.

These comparisons ensure that three plausible PS models (p_{T} ordered, angle ordered and dipole) are compared and that the comparison of nonperturbative models of hadronization physics (AHADIC cluster-based hadronization and Lund string hadronization) does not include model parameterizations that are disfavored by data. Different PDF sets and color reconnection models are also used for various setups: for complete details of the MC setups used, see Sec. II C or Ref. [44].

These uncertainties are derived separately for five different jet flavors (u or d, and s, c, b, and g) and applied according to a per-jet label in simulated event samples. This per-jet treatment eliminates the need for the earlier "jet flavor composition" uncertainty based on the aggregate flavor composition of an analysis' selection relative to the compositions used for *in situ* JES calibrations.

Since the $Z + \text{jet}$ topology is used directly for the *in situ* JES calibration, the flavor response uncertainty should not

vary the response in such events. In order to maintain a fixed energy scale in the $Z + \text{jet}$ topology while providing an uncertainty for extrapolation to other flavor compositions, the flavor response uncertainty scales the JES of gluon-initiated jets as $+f_q \Delta(q-g)$ and that of quark-initiated jets as $-(1-f_q)\Delta(q-g)$, where f_q is the p_{T}-dependent fraction of quark-initiated jets in the $Z + \text{jet}$ sample, and $\Delta(q-g)$ is the difference in the jet response between generators,

$$\Delta(q-g) = (R_q^{\mathrm{MC1}} - R_g^{\mathrm{MC1}}) - (R_q^{\mathrm{MC2}} - R_g^{\mathrm{MC2}})$$
$$= (R_q^{\mathrm{MC1}} - R_q^{\mathrm{MC2}}) - (R_g^{\mathrm{MC1}} - R_g^{\mathrm{MC2}}).$$

This procedure is applied to each of the three MC sample comparisons listed above, resulting in three independent uncertainty components for the JES. These three components have no effect on samples with the same flavor composition as the $Z + \text{jet}$ events used in the *in situ* calibration. The uncertainties in the fractions of quark- and gluon-initiated jets in the simulated samples are evaluated by unfolding data with different MC models as described in Sec. IV B.

2. Updated single-particle deconvolution uncertainty

At high jet p_{T}, the component of the jet energy scale uncertainty determined by the extrapolation of single-particle response measurements to jets via the "deconvolution" procedure, described in Refs. [61,114], has been reduced by updating several inputs. In particular, the response to electromagnetic showers has been updated [115], and the response to high-p_{T} pions has been measured *in situ* up to $p_{\mathrm{T}} = 250$ GeV using $W \to \tau(\to \pi\nu)\nu$ events [62], replacing previous test-beam measurements. The extrapolation of these measurements to other types of hadrons and higher energies is assessed by using updated alternative GEANT4 physics

lists [42] and variations of the detector geometry. Together, these changes result in a reduction of this uncertainty by roughly a factor of 3 compared to the uncertainty reported in Ref. [49].

3. Summary of run 2 jet energy scale uncertainty

The final run 2 JES uncertainty as a function of the jet p_T for central jets is shown separately for gluon- and quark-initiated jets in Figs. 4(a) and 4(b). The components due to the flavor generator/shower, shower and hadronization uncertainties are shown, and the overall size of the uncertainty is compared between this updated flavor

prescription and the previous one. Anticorrelations between these uncertainties for gluon- and quark-initiated jets can reduce the aggregate uncertainty for topologies with mixed flavor compositions, such as the dijet flavor composition shown in Fig. 4(c). For both gluon- and quark-initiated jets, the flavor hadronization component is largest for low-p_T jets, up to ~0.8% below $p_T = 100$ GeV. The flavor shower component increases for high-p_T jets, up to ~0.5% for jets above $p_T = 400$ GeV. The flavor shower/generator component is small (below 0.5%) everywhere, but largest for low-p_T jets (below $p_T \sim 100$ GeV). The updated flavor uncertainty reduces the overall size of the JES uncertainty by up to a factor of 2 around $p_T \sim 100$ GeV and renders the

(a)

(b)

(c)
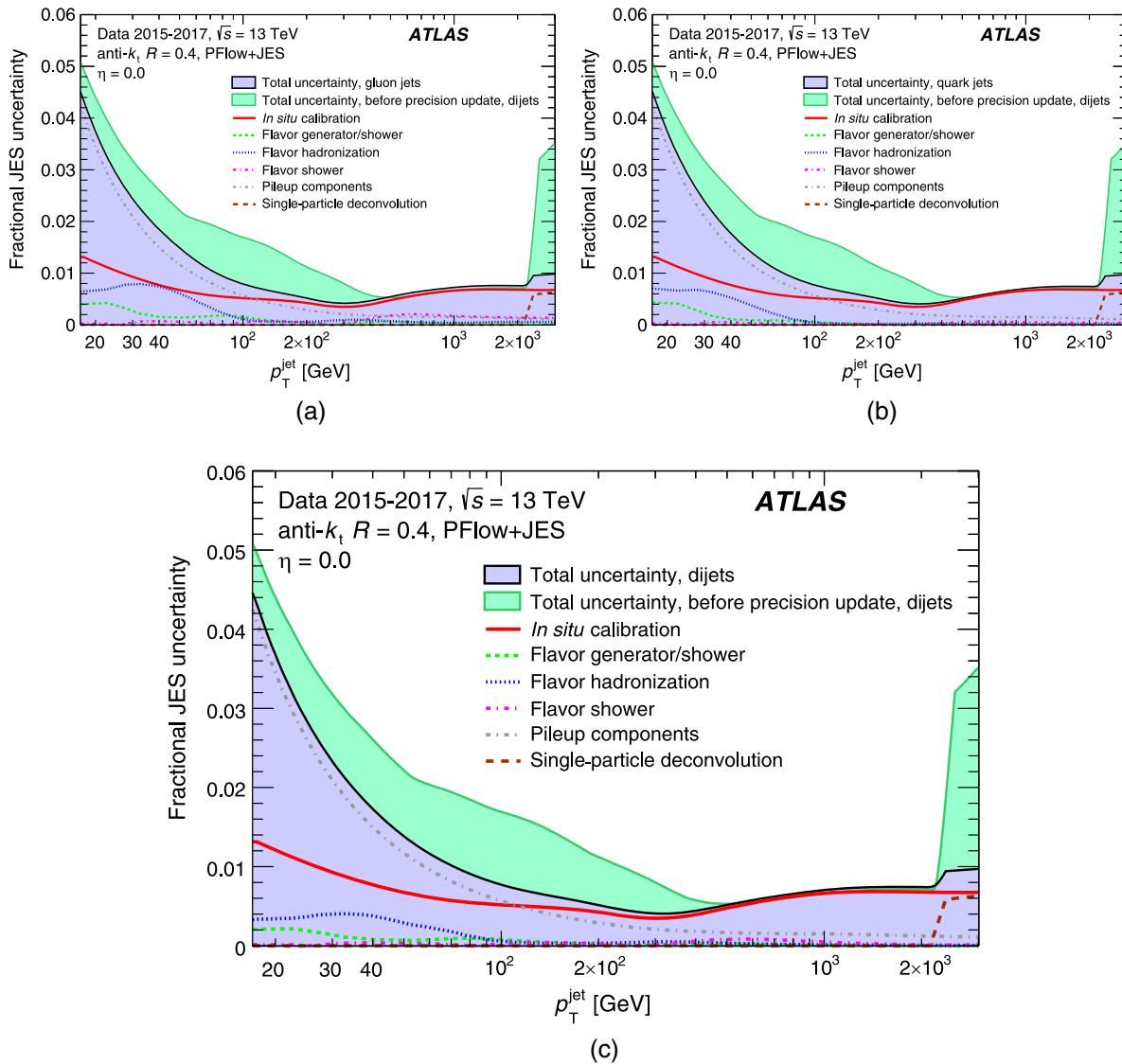
FIG. 4.   The jet energy scale uncertainty for (a) gluon- and (b) quark-initiated jets produced at central pseudorapidities ($|\eta| = 0$). In (c), the overall uncertainty for a dijet flavor composition is shown. The difference between the total uncertainty obtained from the previous prescriptions documented in Ref. [49] and that obtained from the updated uncertainties is indicated by a filled green region, while the new total uncertainty is indicated by the filled blue region. Subcomponents of the uncertainty originating from the flavor generator/shower, shower and hadronization comparisons are indicated by different lines.

component of the JES uncertainty that was previously dominant for $p_T = 30$–400 GeV subdominant everywhere. The updated single-particle deconvolution uncertainty results in a reduction of this component of the JES at high p_T by roughly a factor of 3 compared to the uncertainty reported in Ref. [49].

B. Choice of MC models

When unfolding a measurement using iterative Bayesian unfolding, one must select a nominal MC simulation to construct the response matrix that is applied to data. Different results can be obtained if a different MC model is used to define the unfolding procedure, as the alternative underlying particle spectrum can change the prior, response matrix, and fake and efficiency factors. To account for the uncertainty related to the choice of nominal MC model, the unfolding procedure is repeated with the nominal PYTHIA prior but a response matrix, fake factors, and efficiency factors constructed using an alternative MC simulation.

The alternative sample used to define this uncertainty is the SHERPA2.2.5 sample with cluster-based hadronization, which varies many aspects of the simulation with respect to the nominal PYTHIA sample (Sec. II C), including the PS algorithm and PDF set. Despite the differences between these setups, both provide good descriptions of the measured data. In order to factorize modeling effects due to the JES and reduce double counting, the average JES of the alternative SHERPA samples was recalibrated to match that of the PYTHIA sample when evaluating this uncertainty. This MC-to-MC correction procedure significantly reduces the size of the MC modeling systematic uncertainty, from a few percent to less than 1% for most of the measurement.

When changing the MC model, the effects on the analysis efficiencies, acceptance, and unfolding response matrix are considered individually. The three components of this uncertainty are summed in quadrature to obtain the total modeling uncertainty.
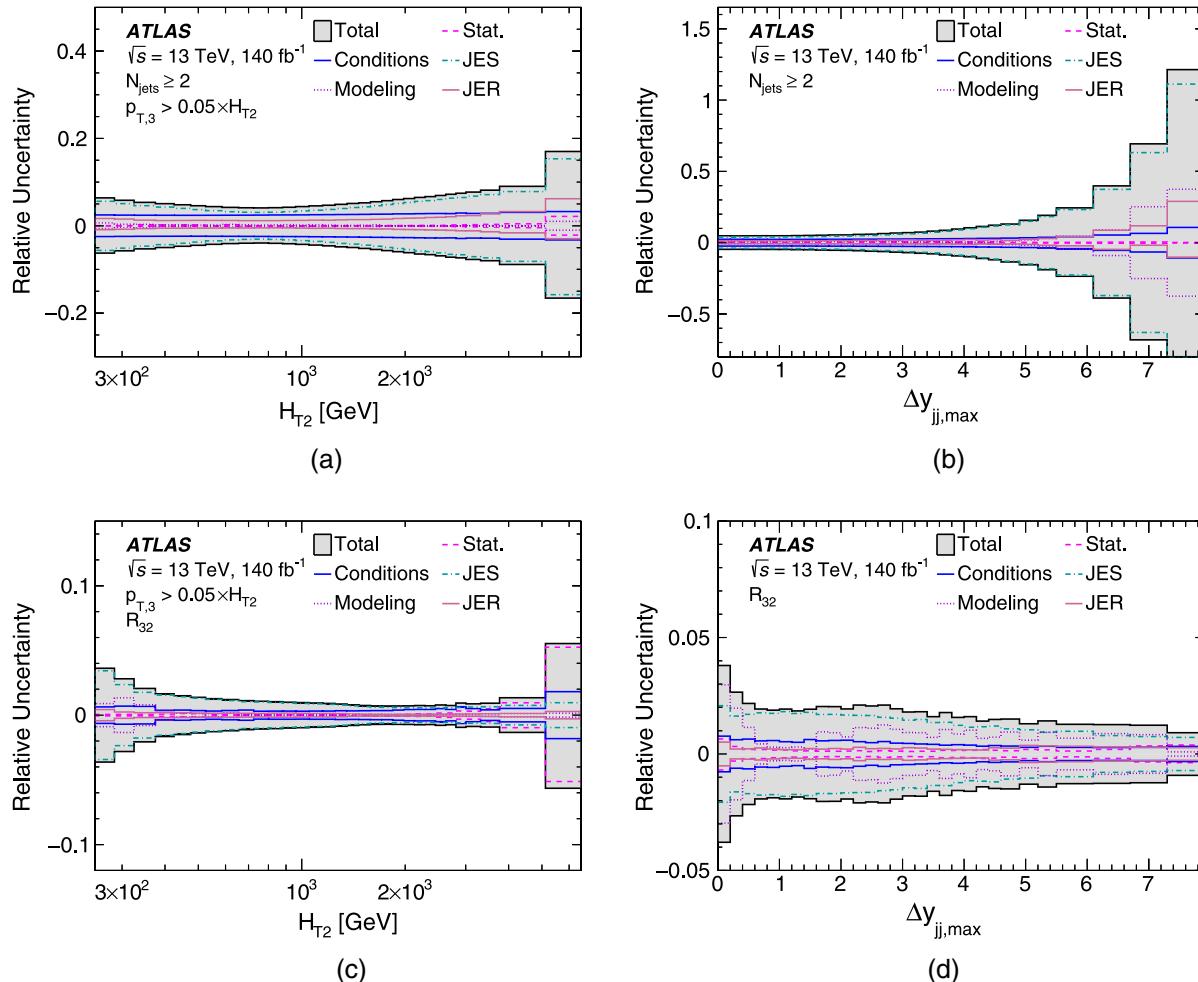
FIG. 5.   The breakdown of the experimental uncertainties for the (a),(b) inclusive two-jet cross-section measurement and (c),(d) R_{32} measurement, differential in (a),(c) H_{T2} with $p_{T,3} > 60$ GeV and (b),(d) $\Delta y_{jj,max}$.
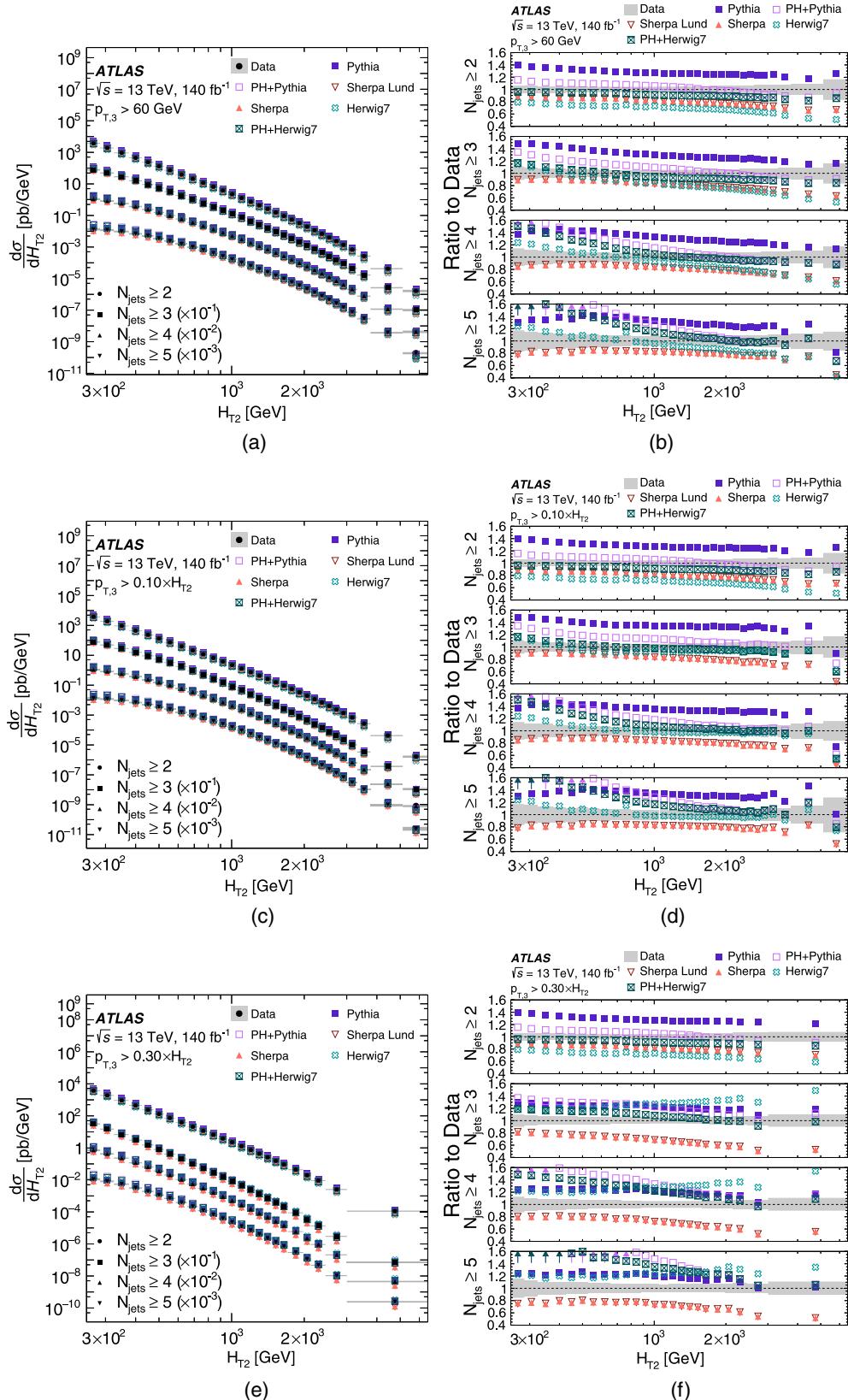
FIG. 6. (a),(c),(e) The differential cross section as a function of H_{T2}, in inclusive bins of N_{jets}, and (b),(d),(f) the ratios of MC predictions to the measured data distribution vs (a),(b) $p_{T,3} > 60$ GeV, (c),(d) $p_{T,3} > 0.10 \times H_{T2}$, and (e),(f) $p_{T,3} > 0.30 \times H_{T2}$. The data error bands show the statistical and systematic components summed in quadrature. Arrows are used to indicated cases where the ratio falls outside of the plotted ratio range.

C. Unfolding methodology: Statistical uncertainties and nonclosure

Statistical uncertainties arise from the finite MC and data sample sizes in the measurement and are estimated during the unfolding procedure with Poissonian pseudoexperiments, as described in Ref. [116]. For the MC simulation, pseudoexperiments are used to vary the response matrix used for the unfolding procedure. The input MC prior is unfolded with each varied response matrix. The efficiencies and acceptances are allowed to vary during this process. For the data statistical uncertainty, pseudoexperiments are generated to vary the input data spectrum ("prior") for the unfolding procedure and are then unfolded using the nominal PYTHIA response matrix. In both cases, 100 pseudoexperiments are generated; using larger numbers of pseudoexperiments did not alter the results significantly. The 68% interquantile range of the output distributions generated as a result of these variations is taken as the corresponding statistical uncertainty.

The nonclosure uncertainty in the unfolding procedure is evaluated using a data-driven reweighting procedure [117]. The detector-level PYTHIA spectrum is reweighted to match the observed data spectrum and then unfolded with the nominal PYTHIA response matrix. The difference between this unfolded result and the nominal PYTHIA particle-level spectrum is taken as a systematic uncertainty.

D. Other experimental uncertainties

Other uncertainties related to experimental effects are accounted for in this analysis. They are typically small, but can occasionally be significant in certain measurement bins.
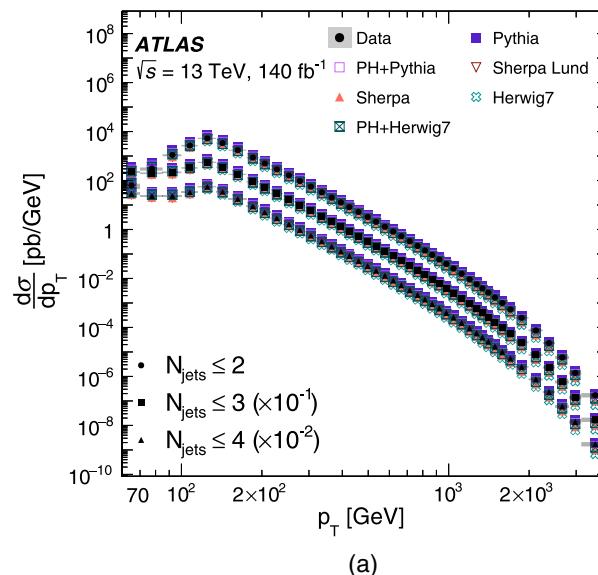
The uncertainty in the absolute luminosity measurement is applied as a 0.83% variation of the normalization of the data [17]. This uncertainty is negligible for the measurement of cross-section ratios.

Uncertainties due to the mismodeling of pileup events are included by reweighting the distribution of the average number of pileup interactions and are found to be negligible throughout the measurement.

During certain run 2 data-taking periods, specific modules of the tile calorimeter were disabled due to technical problems. Some of these modules are also disabled in the simulated events corresponding to a given data-taking period, while other modules that were temporarily disabled during data taking were not disabled in the simulation. No additional correction is applied to the p_T of jets which may have deposited energy in disabled tile modules. The impact of the disabled tile modules on the unfolded distributions is evaluated by repeating the measurement and vetoing events with jets directed at disabled modules in either data or the nominal PYTHIA sample. Differences between these results with vetoed events and the nominal set are taken as a source of systematic uncertainty.

E. Summary of experimental uncertainties

A breakdown of the experimental uncertainties for two representative distributions, H_{T2} with $p_{T,3} > 60\,\text{GeV}$ and $\Delta y_{jj,\text{max}}$, for the cross sections and their ratios is shown in Fig. 5. For H_{T2}, the JES uncertainties dominate
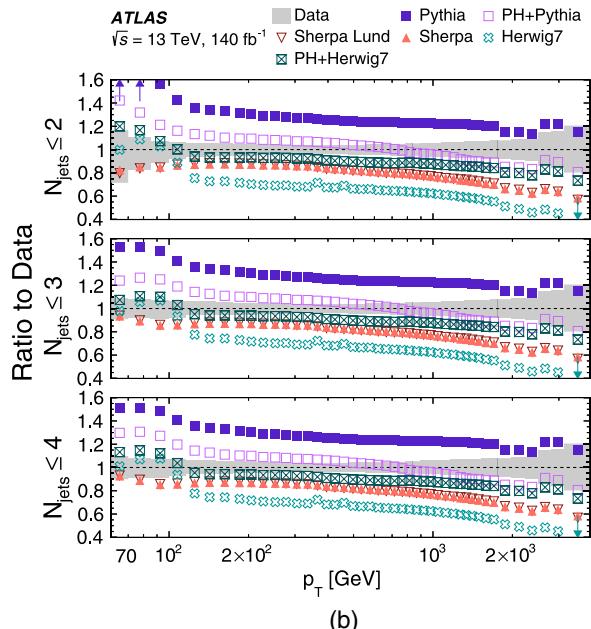
FIG. 7.   (a) The differential cross section is shown as a function of $p_T^{N\text{incl}}$, in inclusive bins of N_{jets}, and (b) the ratios of MC predictions to the measured data distribution. The data error bands show the statistical and systematic components summed in quadrature. Arrows are used to indicated cases where the ratio falls outside of the plotted ratio range.
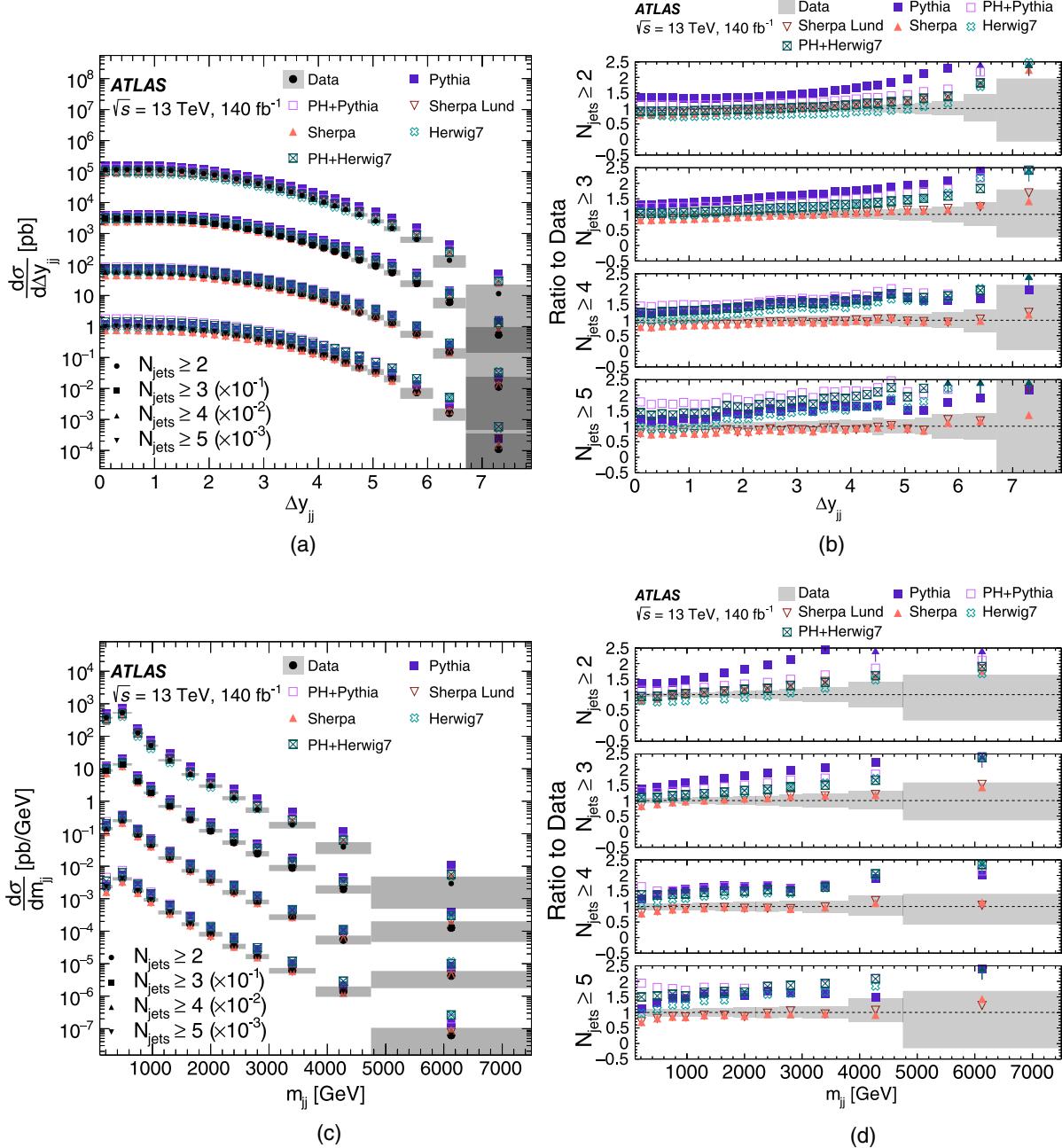
FIG. 8.   The differential cross section as a function of (a) Δy_{jj} and (c) m_{jj}, in inclusive bins of N_{jets}, and the ratios of MC predictions to the measured data distribution in bins of N_{jets} vs (b) Δy_{jj} and (d) m_{jj}. The data error bands show the statistical and systematic components summed in quadrature. Arrows are used to indicated cases where the ratio falls outside of the plotted ratio range.

everywhere, highlighting the importance of the JES uncertainty reductions. The MC-to-MC correction improves the consistency of the jet p_T modeling between MC generators, rendering this a subleading source of uncertainty for H_{T2}. For $\Delta y_{jj,max}$, the JES uncertainties dominate everywhere except the smallest rapidity differences, where the modeling uncertainty dominates.

V. FIXED-ORDER QCD PREDICTIONS

A. NLO prediction

The theoretical predictions for three- and two-jet cross sections are calculated at NLO in perturbative QCD using the NLOJET++ program [118,119]. The partonic cross section is convolved with NNLO PDFs obtained from
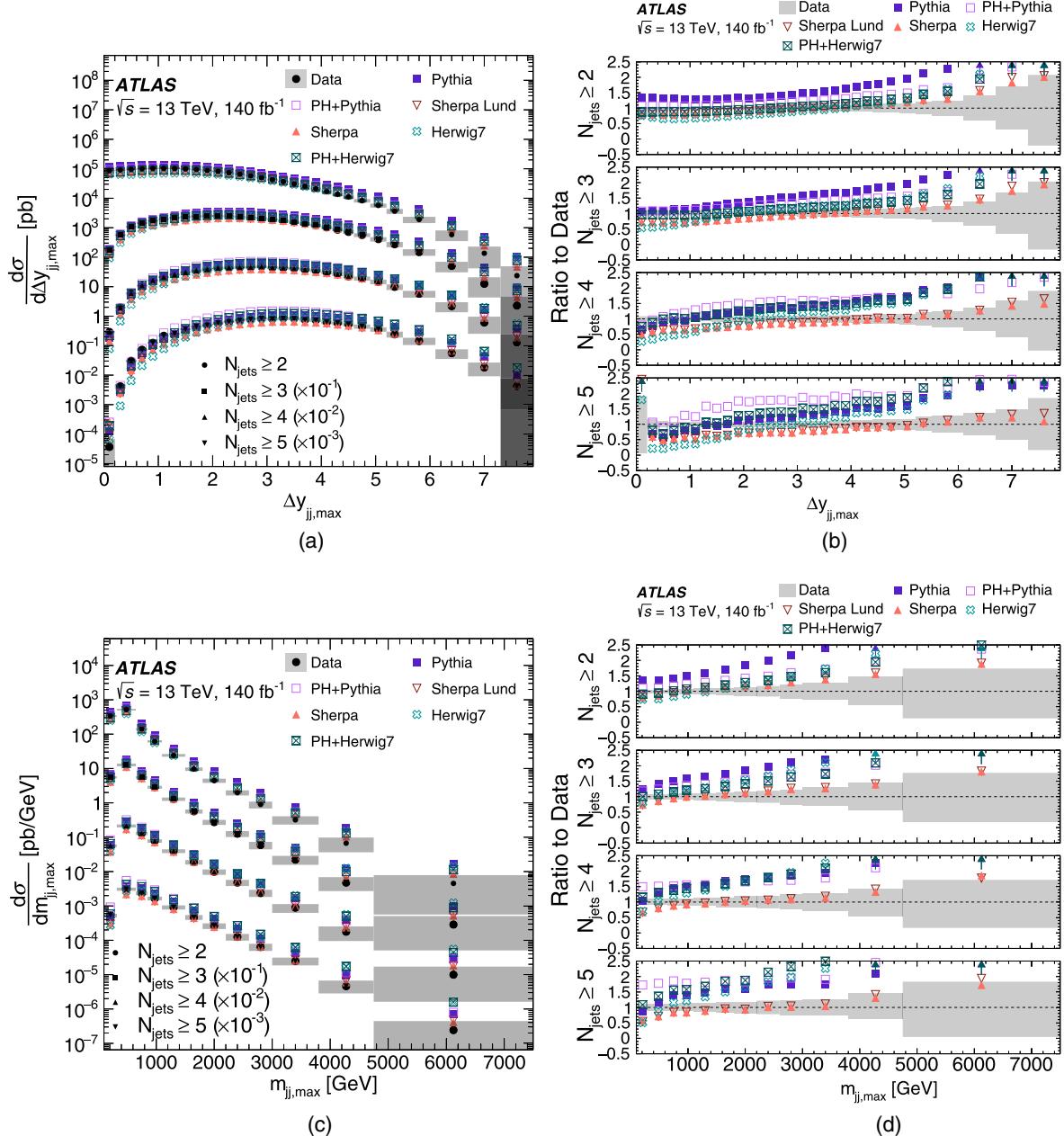
FIG. 9. The differential cross section as a function of (a) $\Delta y_{jj,\max}$ and (c) $m_{jj,\max}$, in inclusive bins of N_{jets}, and the ratios of MC predictions to the measured data distribution in bins of N_{jets} vs (b) $\Delta y_{jj,\max}$ and (d) $m_{jj,\max}$. The data error bands show the statistical and systematic components summed in quadrature. Arrows are used to indicated cases where the ratio falls outside of the plotted ratio range.

the LHAPDF interfaces [120] to CT18 [121], NNPDF4.0 [122], MSHT20 [123], and ATLASpdf21 [124]. The PDFs are based on the $N_F = 5$ scheme, where N_F is the number of parton flavors. The value of $\alpha_S(m_Z)$ is set consistently between the partonic matrix-element calculation and the PDF; the central value is taken to be $\alpha_S(m_Z) = 0.118$. The partonic events are clustered with the anti-k_t algorithm ($R = 0.4$) before the phase-space requirements of this measurement are applied. The renormalization and factorization scales (μ_r and μ_f, respectively) are set to the scalar

sum of the p_T of all partons in the final state, as recommended in Ref. [125],

$$\mu_r = \mu_f = \hat{H}_T = \sum_i p_{T,i}, \tag{1}$$

where i is the parton index.

The uncertainty of the CT18 PDF set is smaller than 2% throughout the fiducial volume of the measurement. It covers the differences between the studied PDF sets, with
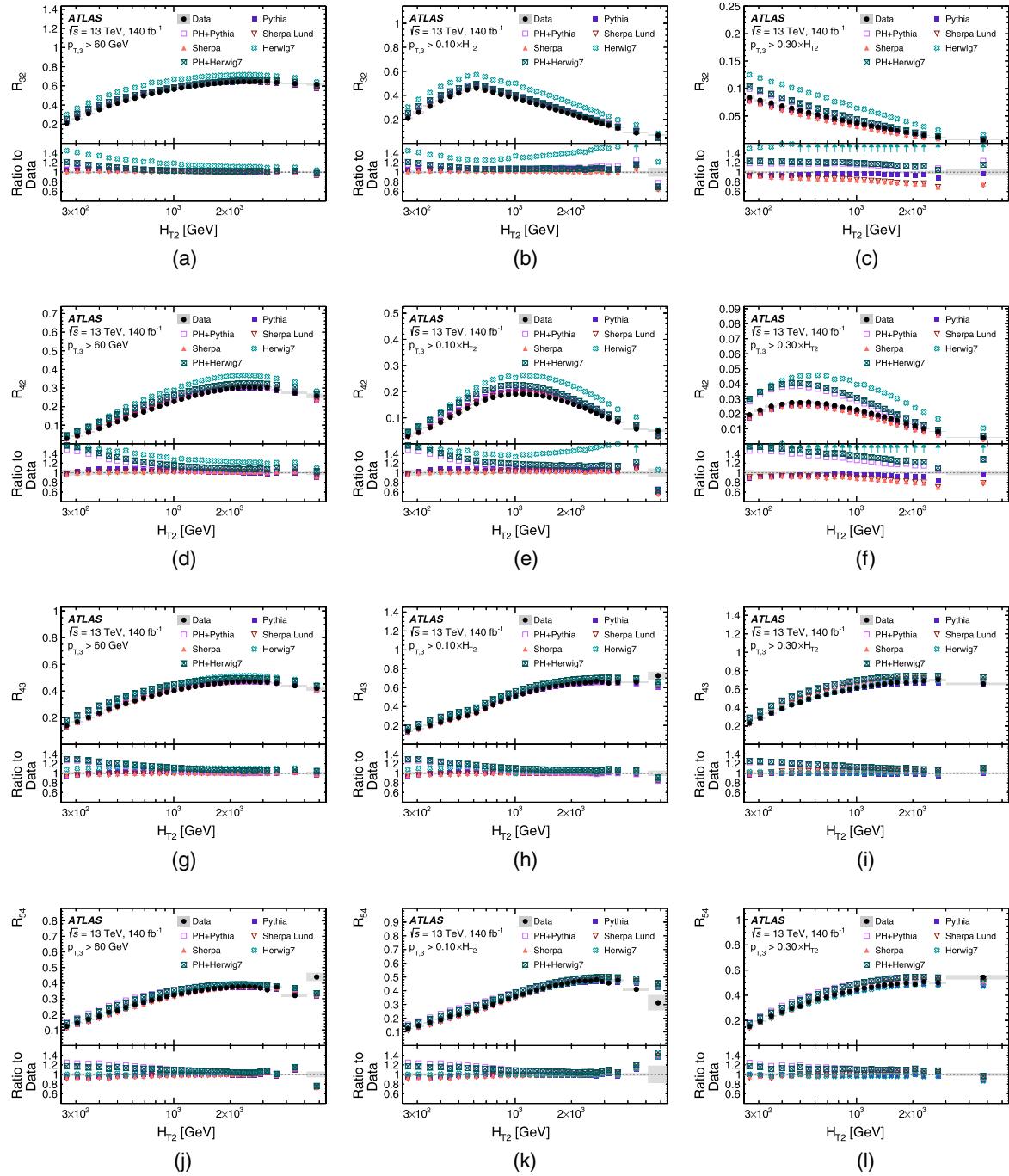
FIG. 10.   (a)–(c) R_{32} vs H_{T2}, (d)–(f) R_{42} vs H_{T2}, (g)–(i) R_{43} vs H_{T2}, and (j)–(l) R_{54} vs H_{T2}, with (a), (d), (g), (j) $p_{T,3} > 60$ GeV, (b), (e), (h), (k) $p_{T,3} > 0.10 \times H_{T2}$, and (c), (f), (i), (l) $p_{T,3} > 0.3 \times H_{T2}$. The data error bands show the statistical and systematic components summed in quadrature. The lower parts of each panel provide ratios of the MC predictions to the unfolded data. Arrows are used to indicated cases where the ratio falls outside of the plotted ratio range.

the exception of NNPDF4.0, which differs by around 2σ (1σ) at low (high) H_{T2}.

Renormalization and factorization scale uncertainties are estimated by varying μ_r and μ_f up and down by a factor of 2, avoiding configurations in which the scales are varied in different directions. The envelope of results from this seven-point scale variation is taken as the uncertainty, which tends to be 5% or smaller throughout the measurement. For comparisons with ratios of jet cross-section measurements, the NLO prediction is defined as the ratio of the NLO prediction for three-jet production to the NLO prediction for two-jet production.

B. NNLO prediction

Fixed-order predictions for the (differential) R_{32} ratios are obtained at NNLO in perturbative QCD using the computational framework in Refs. [1,126–128]. The evaluation of scattering amplitudes makes use of AVHLIB [129], OPENLOOPS2 [130], FIVEPOINTAMPLITUDES [131], and PENTAGONFUNCTIONS++ [132]. The partonic cross sections are convolved with PDFs provided by the LHAPDF package, using the NNLO MSHT20 PDF set as the nominal one. The perturbative QCD calculations are performed with $N_F = 5$ massless quark flavors, i.e., without top-quark contributions to scattering amplitudes. The contribution from top-quark pair production is estimated to be below 0.3% in the relevant phase space. The value of $\alpha_S(m_Z)$ used in the partonic matrix-element calculation and PDFs is chosen to be 0.118. The partonic events are clustered with the anti-k_t algorithm ($R = 0.4$) before the phase-space requirements of this measurement are applied. The renormalization and the factorization scale for each event are chosen to be the scalar sum of the p_T of all partons in the final state [Eq. (1)] and varied with the same seven-point scheme used for the NLO prediction. For comparisons with ratios of jet cross-section measurements, the NNLO prediction is defined as the ratio of the NNLO prediction for three-jet production to the NNLO prediction for two-jet production.

C. Nonperturbative corrections for fixed-order predictions

In order to compare the theoretical predictions with the measured data (Sec. VI), nonperturbative QCD effects from hadronization and the underlying event (UE) must be included. To determine the size of these corrections, MC predictions are obtained at hadron-level including the UE, and compared with parton-level distributions where the UE contribution is disabled in the MC generator. The ratio of these two predictions is applied as a bin-by-bin correction to the theoretical prediction. The nonperturbative corrections are typically found to deviate from unity by about 2% for the two- and three-jet selections separately and generally by about 0.5% for the R_{32} ratio itself.

The uncertainty in this correction is estimated by changing the set of tuned parameters used for the PYTHIA MC generator. While the nominal correction makes use of the A14-NNPDF3.1NLO ATLAS tune [21], an alternative
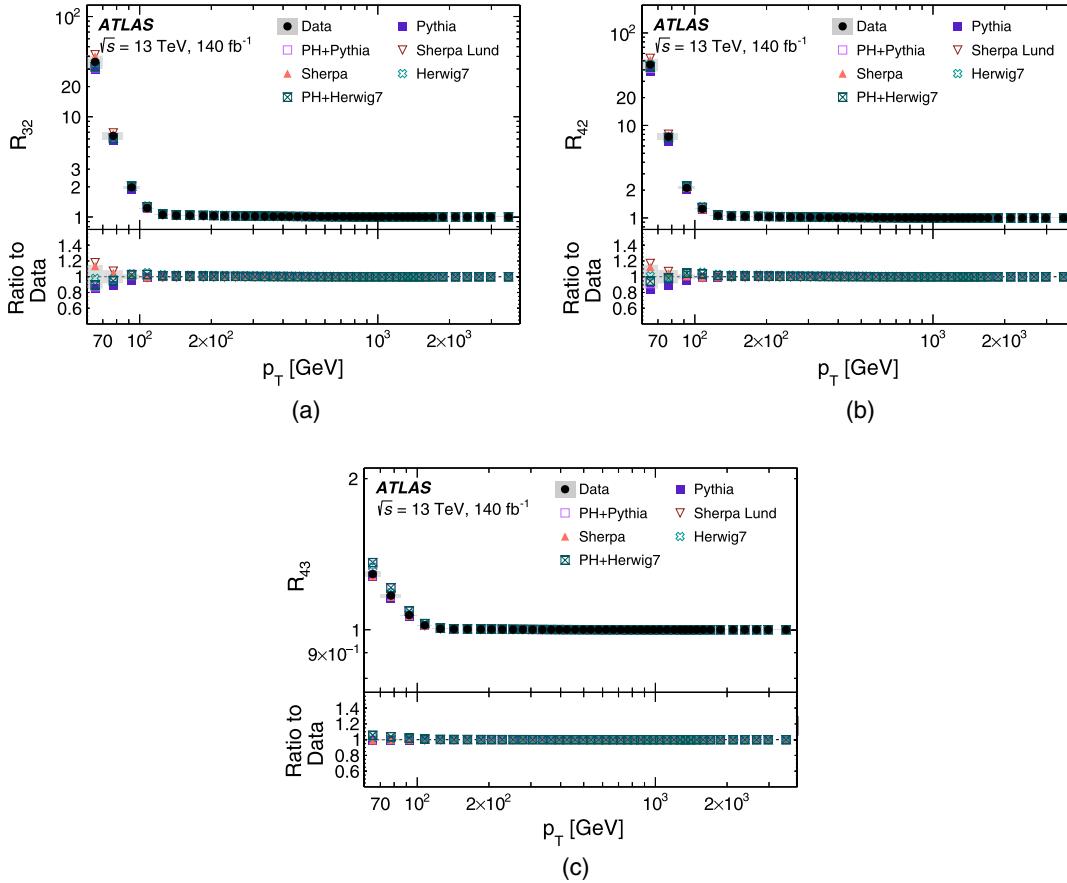
FIG. 11. (a) R_{32} vs $p_T^{N\mathrm{incl}}$, (b) R_{42} vs $p_T^{N\mathrm{incl}}$, and (c) R_{43} vs $p_T^{N\mathrm{incl}}$. The data error bands show the statistical and systematic components summed in quadrature. The lower parts of each panel provide ratios of the MC predictions to the unfolded data. Arrows are used to indicated cases where the ratio falls outside of the plotted ratio range.

correction factor is calculated using the MONASH tune [133], which uses a larger value of α_S for final-state radiation (0.1365 vs 0.1270). The difference between the two correction factors defines the systematic uncertainty of the nonperturbative corrections and is generally smaller than 0.5%.

D. High-energy jet prediction

The high-energy jet (HEJ) framework [134–136] calculates the tower of leading logarithmic QCD corrections in $\hat{s}/p_T^2$ (where $\hat{s}$ is the parton center-of-mass energy) to all orders in the strong coupling α_S for all relevant Standard Model processes. These corrections are relevant in regions of phase space where jets span a large range of rapidity or where pairs of jets have a large invariant mass. The predictions from HEJ contain both the resummation of logarithmic corrections and the matching of these to fixed-order accuracy. This includes matching of all processes of $pp \to 2j, 3j, 4j, 5j,$ and $6j$ to tree-level accuracy point-by-point in phase space. All the predictions are obtained using a renormalization and factorization scale of $\hat{H}_T/2$, with an

independent seven-point variation of the scales by factors of 2. The PDF set is NNPDF3.1NLO ($\alpha_S = 0.118$), and $R = 0.4$ and $p_{T,min} = 60$ GeV are used throughout the anti-k_t algorithm.

VI. RESULTS

A. Measured cross sections

The unfolded cross-section measurements for the different observables studied in this analysis are shown in Figs. 6–9.

The differential cross section as a function of H_{T2} is compared to several MC generator predictions in Fig. 6, for various requirements on the inclusive jet multiplicity and the transverse momentum of the third jet ($p_{T,3}$). No single MC prediction is able to describe the data across all H_{T2} and multiplicity bins. The PYTHIA prediction has an approximately constant offset relative to the data, with the offset decreasing at larger values of $p_{T,3}$. The two SHERPA models have nearly identical behavior, since the
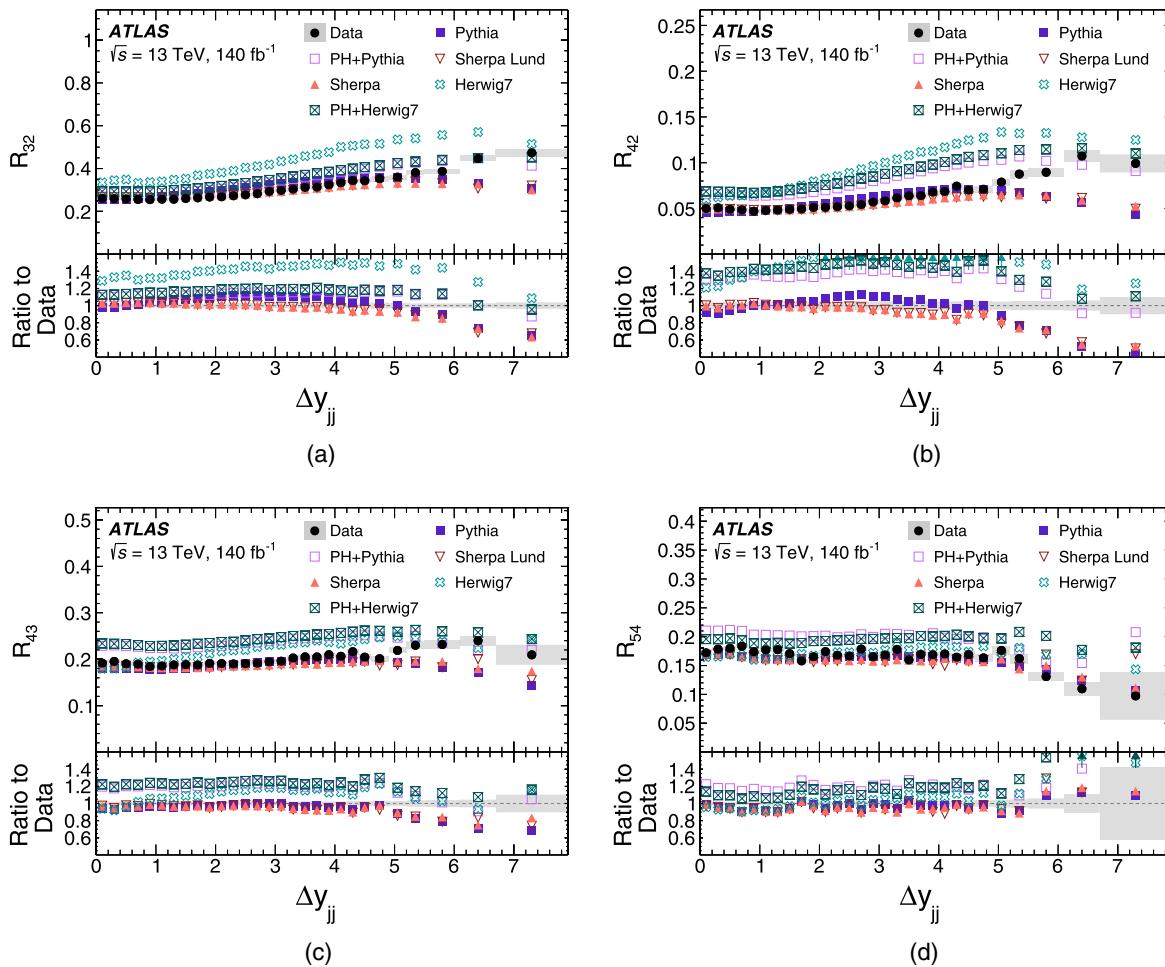

FIG. 12. (a) R_{32}, (b) R_{42}, (c) R_{43}, and (d) R_{54} vs Δy_{jj} with $p_{T,3} > 60$ GeV. The data error bands show the statistical and systematic components summed in quadrature. The lower parts of each panel provide ratios of the MC predictions to the unfolded data. Arrows are used to indicated cases where the ratio falls outside of the plotted ratio range.

H_{T2} cross section is not significantly impacted by the hadronization model. The HERWIG model underestimates the two-jet cross section, but provides a good description of higher multiplicities, except for the highest $p_{T,3}$ bin, where no models provide a good description.

The differential cross section as a function of p_T^{Nincl} is shown in Fig. 7, differentially in bins of the inclusive number of jets. Because of the event selection requirement that $H_{T2} > 250$ GeV combined with the minimum p_T cut of 60 GeV, each event has at least two jets with p_T around 125 GeV, resulting in a sharp downturn in p_T^{Nincl} around half of the value of the H_{T2} cut. The MC predictions have an offset in the cross section, which is generally constant as a function of p_T, except for $p_T < 100$ GeV where there is also a shape difference in the predictions. The exception to this is the SHERPA predictions, which do not show this shape difference at low p_T.

The differential cross section as a function of Δy_{jj} and m_{jj} is presented in Fig. 8, in bins of inclusive jet multiplicity. For both observables, SHERPA provides the best description

of the data. HERWIG models the data well for small rapidity differences and small dijet masses, but its performance quickly deteriorates at larger rapidity differences and masses. PYTHIA and POWHEG+PYTHIA overestimate the data everywhere, while POWHEG+HERWIG provides a reasonable description of the data for low jet multiplicities and small values of Δy_{jj} and m_{jj}, with a poor description of the data elsewhere.

Finally, the differential cross section as a function of $\Delta y_{jj,max}$ and $m_{jj,max}$ is presented in Fig. 9, in bins of inclusive jet multiplicity. Overall, SHERPA provides the best description of the data, but it underestimates the cross section at low $\Delta y_{jj,max}$ and $m_{jj,max}$. POWHEG+HERWIG describes the data well at low multiplicities, but significantly overestimates the cross section at high multiplicities, particularly for large $\Delta y_{jj,max}$ and $m_{jj,max}$. For $m_{jj,max}$, PYTHIA and POWHEG+PYTHIA overestimate the cross section everywhere, with agreement worsening at high $m_{jj,max}$. Similar behavior is observed for $\Delta y_{jj,max}$, except in the low $\Delta y_{jj,max}$ region, where there is fair agreement. The HERWIG
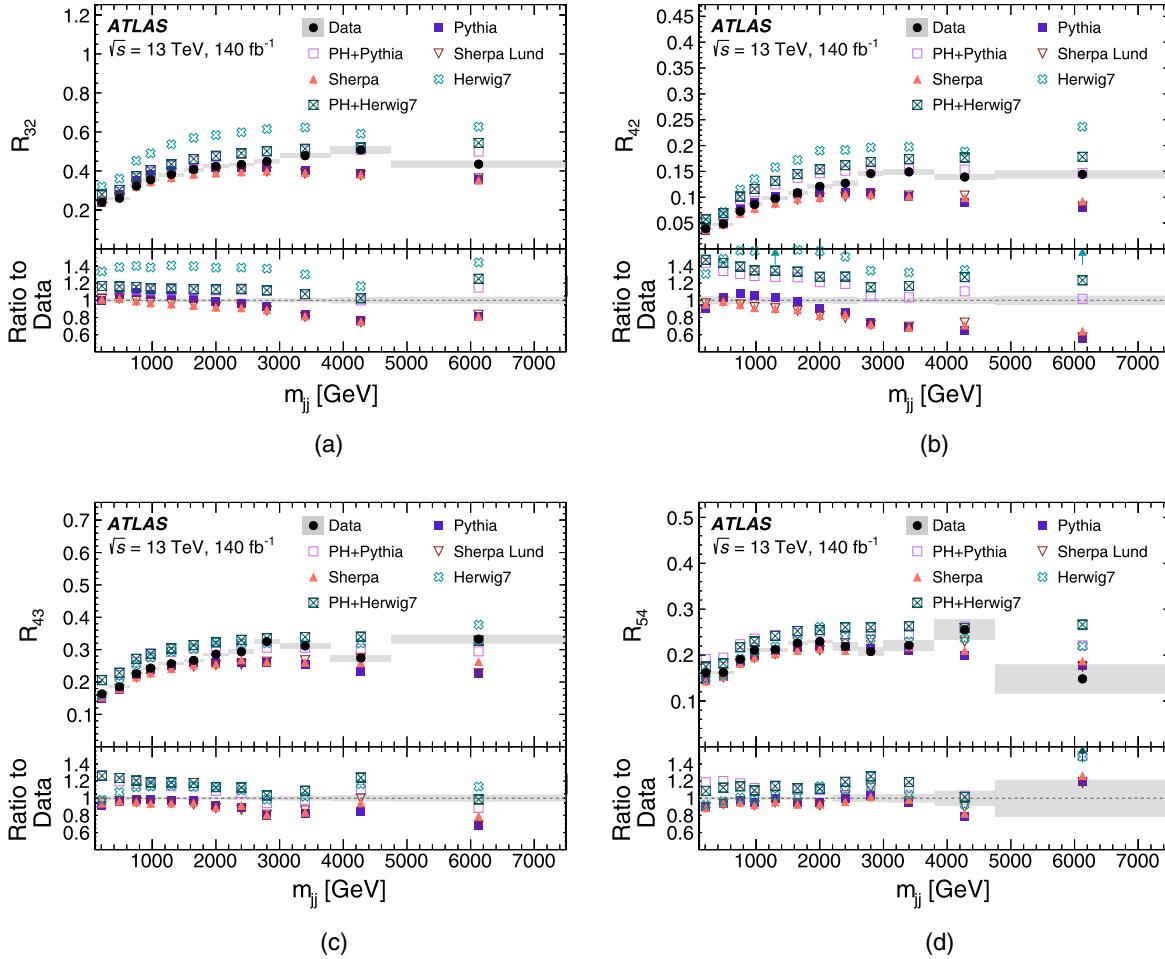
FIG. 13. (a) R_{32}, (b) R_{42}, (c) R_{43}, and (d) R_{54} vs m_{jj} with $p_{T,3} > 60$ GeV. The data error bands show the statistical and systematic components summed in quadrature. The lower parts of each panel provide ratios of the MC predictions to the unfolded data. Arrows are used to indicated cases where the ratio falls outside of the plotted ratio range.

prediction differs from the data in overall shape for both observables and does not provide a good description of the data for any multiplicity.

B. Cross-section ratios

Ratios of the measured observables between different bins of inclusive jet multiplicity are presented in this section. When compared with the cross-section measurements, the uncertainties are generally reduced because correlated systematic variations in the numerator and denominator partially cancel out.

The ratios of the measured H_{T2} distributions are shown in Fig. 10. The shape of the R_{32} distribution changes as the $p_{T,3}$ threshold is varied, because the $p_{T,3}$ requirement depends on the event's H_{T2} value. When the $p_{T,3}$ cut does not depend on H_{T2} [Fig. 10(a)], the R_{32} ratio increases smoothly until dropping slightly at the highest H_{T2} values, as the probability to emit a third hard parton increases with the energy scale of the event. At the highest values of H_{T2}, events with a soft third jet are often in a back-to-back

configuration: the third jet can be merged with one of the leading two, causing the ratio to decrease slightly [137,138]. When the $p_{T,3}$ cut is made to depend on H_{T2}, a feature related to this dependence appears at a value of H_{T2} corresponding to the ratio of the third jet's p_T threshold (60 GeV in this case) to the fraction of H_{T2} that $p_{T,3}$ must satisfy in that bin: for example, in Fig. 10(b) where $p_{T,3}/H_{T2} > 0.10$, the distribution turns over at a value of 60 GeV/0.10 = 600 GeV. This turnover point shifts to lower values as the fractional H_{T2} requirement is increased in higher $p_{T,3}$ bins. The R_{32} value decreases after this point because of the steeply falling p_T spectrum of the third jet.

In general, agreement between the data and predictions worsens as the third jet's p_T cut is increased, and the R_{43} and R_{54} ratios tend to be better modeled than the R_{32} and R_{42} ratios. PYTHIA tends to predict slightly higher values of R_{32} and R_{42} than seen in data, with better agreement at larger $p_{T,3}$, and agrees fairly well with the data for R_{43} and R_{54}. POWHEG+PYTHIA overestimates the value of all four ratios, particularly at low H_{T2}. Both SHERPA predictions
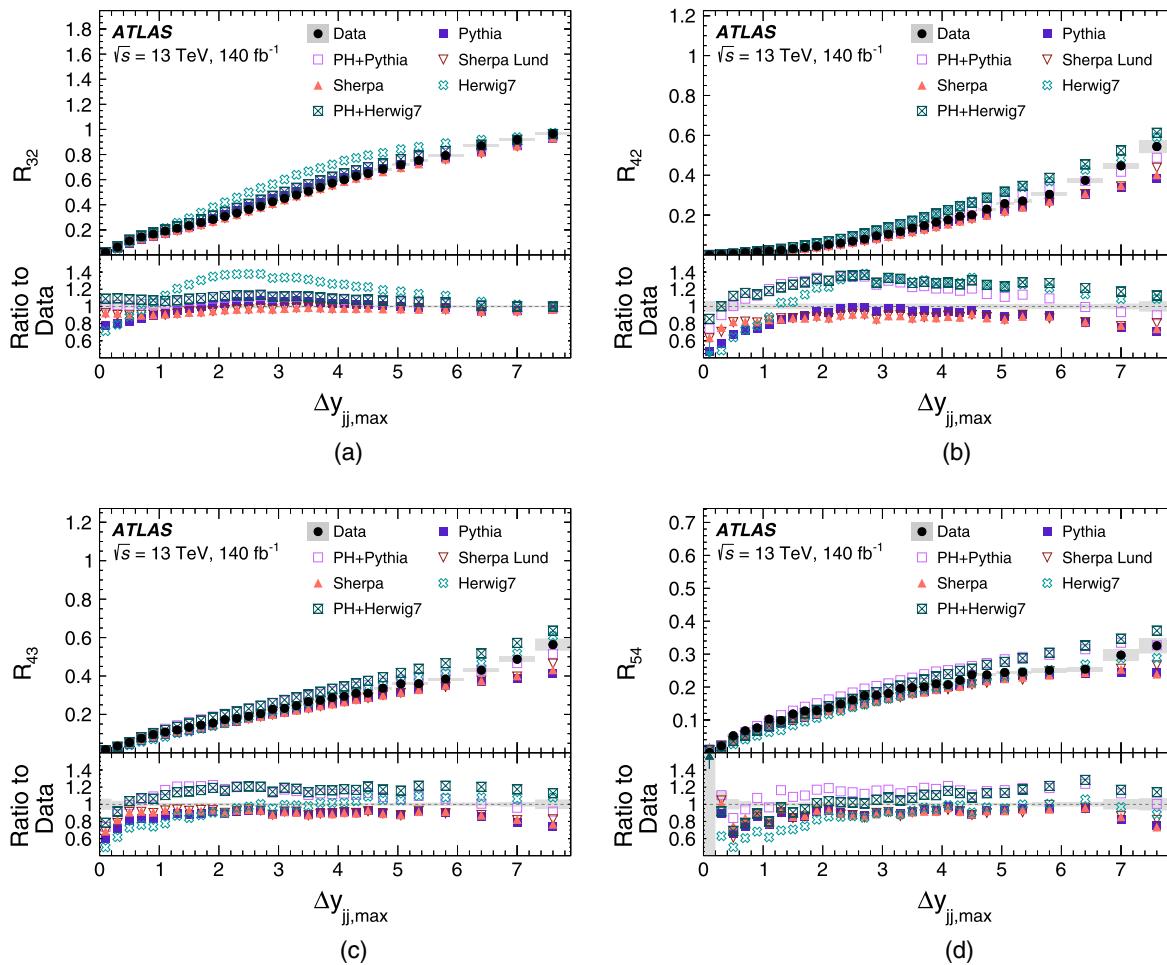
FIG. 14. (a) R_{32}, (b) R_{42}, (c) R_{43}, and (d) R_{54} vs $\Delta y_{jj,max}$ with $p_{T,3} > 60$ GeV. The data error bands show the statistical and systematic components summed in quadrature. The lower parts of each panel provide ratios of the MC predictions to the unfolded data. Arrows are used to indicated cases where the ratio falls outside of the plotted ratio range.

describe the data well for small values of $p_{T,3}$, but tend to underestimate the values of R_{32} and R_{42} for large values of $p_{T,3}$, particularly at high H_{T2}. For R_{32} and R_{42}, HERWIG predicts significantly fewer two-jet events than are seen in data, particularly for large values of $p_{T,3}$, while POWHEG+ HERWIG gives a better description of the data, particularly for large values of H_{T2}. Both HERWIG and POWHEG+HERWIG provide poorer descriptions of the data than PYTHIA and SHERPA for R_{32} and R_{42}. For R_{43} and R_{54}, HERWIG provides a relatively good description of the data, while POWHEG+ HERWIG tends to overestimate both of these ratios.

The ratios of the measured p_T^{Nincl} distributions are shown in Fig. 11. The ratios tend toward 1 at high p_T, since very few events have more than two jets with p_T above a few hundred GeV. While the uncertainties cancel out significantly for the entire p_T distribution, the differences between data and the MC predictions are generally covered by the uncertainties.

The ratios of the measured Δy_{jj} and m_{jj} distributions are shown in Figs. 12 and 13, respectively. For both

observables, the HERWIG, POWHEG+HERWIG, and POWHEG+ PYTHIA predictions significantly overestimate all four ratios for all rapidity differences. The PYTHIA and SHERPA predictions provide a good description of the data for all four ratios for rapidity differences $\Delta y_{jj} < 6$ and dijet masses above 2 TeV, while at larger rapidity differences and larger dijet masses, they underestimate the ratios, with the exception of R_{54}, which is modeled well across all bins.

The ratios of the measured $\Delta y_{jj,max}$ and $m_{jj,max}$ distributions are shown in Figs. 14 and 15, respectively. For the $\Delta y_{jj,max}$ ratios, the PYTHIA and SHERPA predictions model the data well, except in the low and high rapidity-difference regions. Similar features are seen for $m_{jj,max}$, although the mismodeling at low dijet masses is only seen in the lowest $m_{jj,max}$ bin. POWHEG+HERWIG and POWHEG+PYTHIA do not model any of the ratios well, with the smallest disagreement seen for R_{32}. HERWIG does not describe R_{32} or R_{42} well for either observable, but provides a reasonable description for R_{43} and R_{54}, except for the low rapidity-difference region, where it underestimates the ratio.
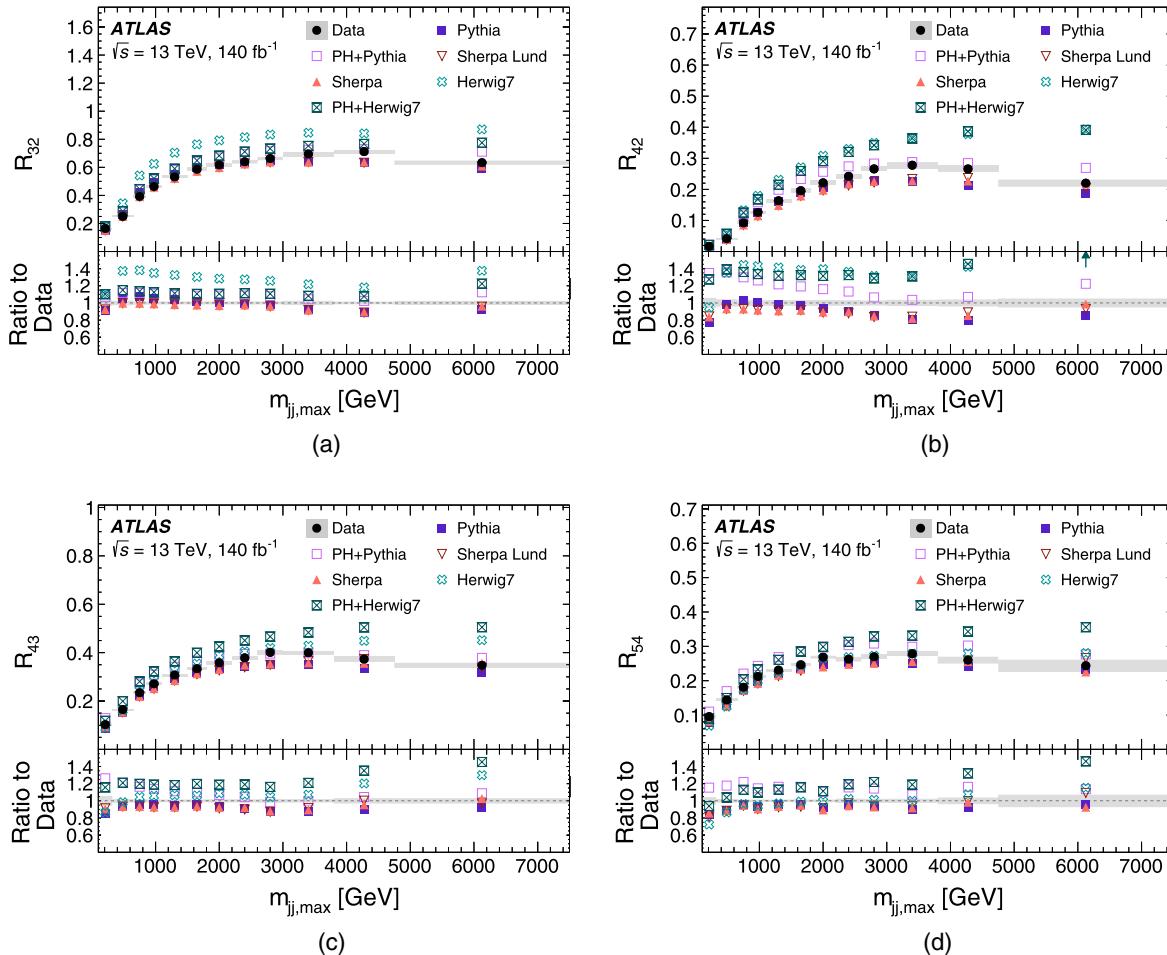
FIG. 15. (a) R_{32}, (b) R_{42}, (c) R_{43}, and (d) R_{54} vs $m_{jj,max}$ with $p_{T,3} > 60$ GeV. The data error bands show the statistical and systematic components summed in quadrature. The lower parts of each panel provide ratios of the MC predictions to the unfolded data. Arrows are used to indicated cases where the ratio falls outside of the plotted ratio range.

C. Comparisons with fixed-order and resummed calculations

The ratios R_{32} of the measured H_{T2} distributions are shown in Fig. 16, compared with the NLO and NNLO predictions. The NNLO prediction provides an accurate description of the value and shape of R_{32} for all the different $p_{T,3}$ bins of the measurement, while the NLO prediction tends to overestimate R_{32}. This highlights the importance of the higher-order predictions in describing multijet production. For low cuts on $p_{T,3}$ and at larger values of H_{T2}, the NNLO prediction slightly overestimates the data. This is the region where effects from resummation play a more important role, and higher cuts on $p_{T,3}$ reduce these differences. Some statistical fluctuations in the NNLO prediction are observed, due to the significant computational requirements of these predictions. The statistical

error of the theory predictions is treated independently between bins.

For each $p_{T,3}$ cut, the value of χ^2 per degree of freedom (d.o.f.) is shown in Table I. The individual experimental and theoretical uncertainties are considered to be uncorrelated with each other and fully correlated across the H_{T2} bins. For all $p_{T,3}$ cuts, the highest H_{T2} bin is excluded from the χ^2 calculation, due to the large statistical fluctuation in the NNLO prediction in this bin: this results in 19 degrees of freedom (bins). The χ^2/d.o.f. values for the NLO and NNLO predictions agree well with the data in all bins except the highest $p_{T,3}$ bin, which has poor agreement due to a fluctuation in the second-highest H_{T2} bin. The χ^2/d.o.f. values are often less than 1 for the smallest $p_{T,3}$ cuts (the two lowest cuts for the NLO comparison, the four lowest for the NNLO comparison). For the NLO
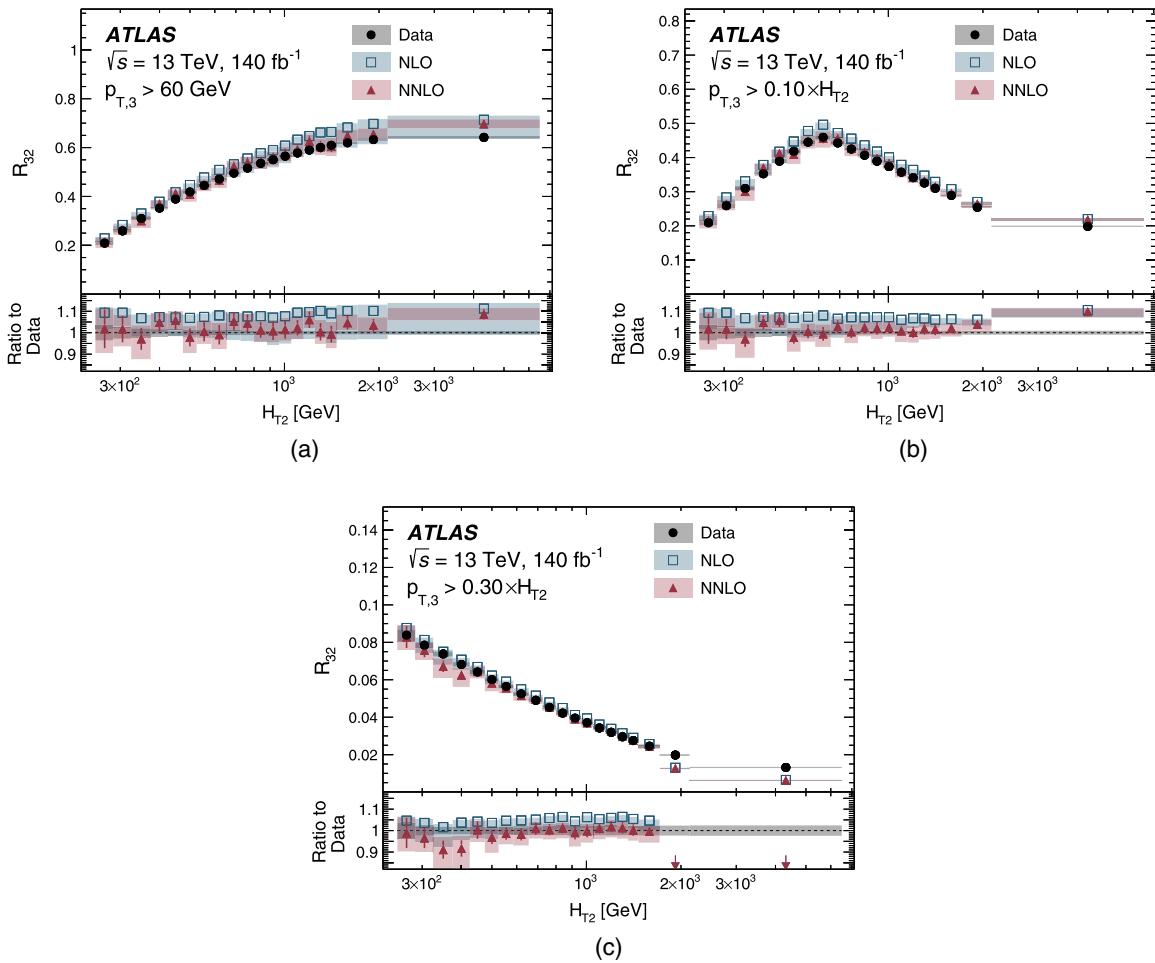
FIG. 16. R_{32} vs H_{T2} with (a) $p_{T,3} > 60$ GeV, (b) $p_{T,3} > 0.10 \times H_{T2}$, and (c) $p_{T,3} > 0.30 \times H_{T2}$. The data error bands show the statistical and systematic components summed in quadrature. The theory error bands include contributions from the statistical, PDF, and scale variations, where the scale variations are determined from a seven-point variation of the renormalization and factorization scales used in the prediction. The statistical uncertainty on the theory predictions is illustrated with a vertical line. The lower parts of each panel provide ratios of the predictions to the unfolded data. Arrows are used to indicated cases where the ratio falls outside of the plotted ratio range.

TABLE I. Summary of the χ^2/d.o.f. values from the comparison of the measurement of R_{32} and the NLO and NNLO predictions.

	χ^2/d.o.f.	
	NLO	NNLO
$p_{T,3} > 60$ GeV	0.48	0.36
$p_{T,3} > 0.05 \times H_{T2}$	0.55	0.32
$p_{T,3} > 0.10 \times H_{T2}$	1.05	0.24
$p_{T,3} > 0.20 \times H_{T2}$	1.11	0.30
$p_{T,3} > 0.30 \times H_{T2}$	9.24	5.49

prediction, this is primarily due to the large theory scale uncertainties. Despite their smaller uncertainty due to scale variations, the NNLO predictions have smaller χ^2/d.o.f. values than the NLO predictions and are more often less than 1: this is partially due to both an overall improved description of the shape of the measured data and the presence of a non-negligible statistical uncertainty on the prediction.

The ratios of three- to two-jet cross sections measured as a function of Δy_{jj}, $\Delta y_{jj,max}$, m_{jj}, and $m_{jj,max}$ are compared with HEJ predictions in Fig. 17. The HEJ predictions underestimate the multiplicity at low values of Δy_{jj} for R_{32}, while providing a better prediction of the region with large rapidity differences. For $\Delta y_{jj,max}$, the HEJ predictions significantly overestimate the multiplicity distribution for intermediate rapidity differences while providing a good description of the largest-rapidity-difference region. The HEJ predictions provide good modeling of the R_{32} distribution for m_{jj} and $m_{jj,max}$, where the results agree with the data within uncertainties.
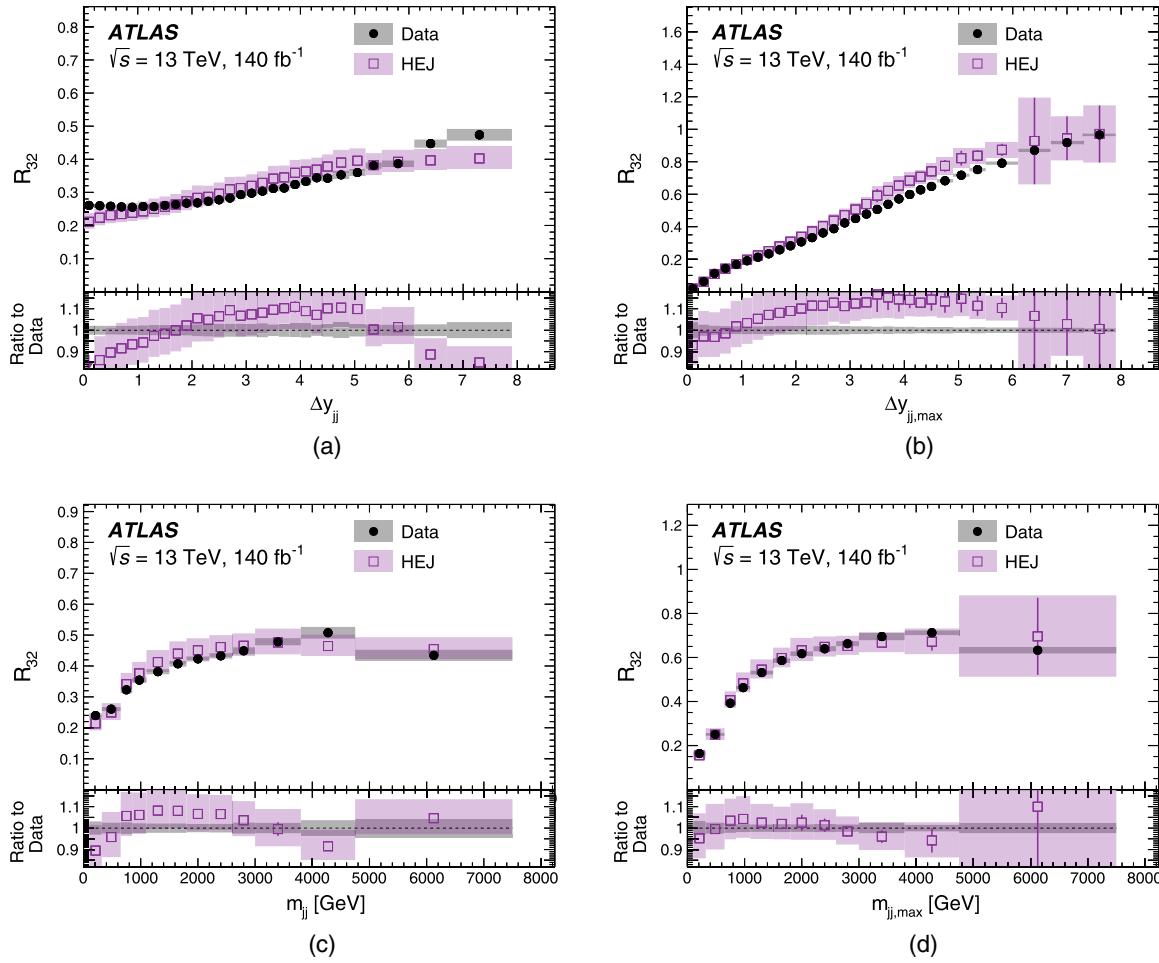
FIG. 17. R_{32} vs (a) Δy_{jj}, (b) $\Delta y_{jj,max}$, (c) m_{jj}, and (d) $m_{jj,max}$ with $p_{T,3} > 60$ GeV. The data error bands show the statistical and systematic components summed in quadrature. The theory error bands are determined from a seven-point variation of the renormalization and factorization scales used in the prediction. The statistical uncertainty on the theory predictions is illustrated with a vertical line. The lower parts of each panel provide ratios of the predictions to the unfolded data. Arrows are used to indicated cases where the ratio falls outside of the plotted ratio range.

VII. CONCLUDING REMARKS

This paper reports a measurement of jet cross-section ratios between inclusive bins of jet multiplicity, performed in 140 fb^-1 of proton-proton collisions with $\sqrt{s} = 13$ TeV center-of-mass energy that were recorded with the ATLAS detector at CERN's Large Hadron Collider. Observables that are sensitive to either the energy scale (H_{T2}, p_T^{Nincl}) or angular distribution (m_{jj}, $m_{jj,max}$, Δy_{jj}, $\Delta y_{jj,max}$) of hadronic energy flow in the final state are measured double differentially, in bins of inclusive jet multiplicity, and the scalar sum of the two leading jets' transverse momenta is measured triple differentially, in bins of the third jet's transverse momentum as well as bins of jet multiplicity. Several improvements to the modeling of jet energy scale uncertainties are described, and these result in a significant reduction of the overall ATLAS jet energy scale uncertainty. In particular, improvements in the Monte Carlo models used to define the jet flavor response uncertainty have reduced that source of uncertainty by up to a factor of 2 for jets with $p_T = 100$ GeV. An updated procedure for the jet energy scale uncertainties derived from a single-particle deconvolution method at high jet p_T has reduced that source of uncertainty by roughly a factor of 3 for jets with $p_T = 2$ TeV, leading to increased precision of the differential cross sections reported in this work.

The measured distributions are used to construct ratios of the inclusive three- to two-jet, four- to three-jet, four- to two-jet, and five- to four-jet multiplicity bins, reducing sensitivity to systematic uncertainties and parton distribution functions. Because uncertainties partially cancel out in the ratios, good precision is achieved for all observables, with the remaining uncertainties typically being less than a few percent for the measurements of the ratios of H_{T2} cross sections and less than 10% for the dijet mass and Δy observables. The H_{T2} distribution is compared with NNLO fixed-order QCD predictions, which are found to model the behavior well across most $p_{T,3}$ bins. For the dijet mass and Δy observables, significant differences between data and Monte Carlo predictions are observed at large values. A prediction with additional resummation for logarithmic contributions that arise in topologies characteristic of VBS/VBF events, where high-energy jets are present in the forward region, provides a good description of the measured ratios in regions where the logarithmic terms make significant contributions.

A RIVET routine is available for this measurement [139], and the measured data points have been made publicly available [140] for use in future Monte Carlo tuning campaigns and other studies of QCD at the electroweak scale.

ACKNOWLEDGMENTS

[1] M. Czakon, A. Mitov, and R. Poncelet, Next-to-next-to-leading order study of three-jet production at the LHC, Phys. Rev. Lett. **127,** 152001 (2021).

[2] M. Begel *et al.*, Precision QCD, hadronic structure & forward QCD, heavy ions: Report of energy frontier topical groups 5, 6, 7 submitted to Snowmass 2021, arXiv:2209.14872.

[3] J. Bonilla *et al.*, Jets and jet substructure at future colliders, Front. Phys. **10,** 897719 (2022).

[4] ATLAS Collaboration, Measurement of multi-jet cross sections in proton-proton collisions at a 7 TeV center-of-mass energy, Eur. Phys. J. C **71,** 1763 (2011).

[5] CMS Collaboration, Measurement of the ratio of the 3-jet to 2-jet cross sections in pp collisions at $\sqrt{s} = 7$ TeV, Phys. Lett. B **702,** 336 (2011).

[6] CMS Collaboration, Measurement of the ratio of the inclusive 3-jet cross section to the inclusive 2-jet cross section in pp collisions at $\sqrt{s} = 7$ TeV and first determination of the strong coupling constant in the TeV range, Eur. Phys. J. C **73,** 2604 (2013).

[7] UA1 Collaboration, Comparison of three-jet and two-jet cross-sections in $p\bar{p}$ collisions at the CERN SPS $p\bar{p}$ collider, Phys. Lett. B **158,** 494 (1985).

[8] UA2 Collaboration, A study of three-jet events at the CERN $\bar{p}p$ collider, Z. Phys. C **30,** 341 (1986).

[9] CDF Collaboration, Properties of high-mass multijet events at the Fermilab proton-antiproton collider, Phys. Rev. Lett. **75,** 608 (1995).

[10] D0 Collaboration, Studies of topological distributions of inclusive three- and four-jet events in $\bar{p}p$ collisions at $\sqrt{s} = 1800$ GeV with the D0 detector, Phys. Rev. D **53,** 6000 (1996).

[11] D0 Collaboration, Ratios of multijet cross sections in $p\bar{p}$ collisions at $\sqrt{s} = 1.8$ TeV, Phys. Rev. Lett. **86,** 1955 (2001).

[12] ATLAS Collaboration, The ATLAS experiment at the CERN Large Hadron Collider, J. Instrum. **3,** S08003 (2008).

[13] ATLAS Collaboration, ATLAS Insertable B-layer: Technical Design Report, ATLAS-TDR-19; CERN-LHCC-2010-013, 2010, https://cds.cern.ch/record/1291633, Addendum: ATLAS-TDR-19-ADD-1; CERN-LHCC-2012-009, 2012, https://cds.cern.ch/record/1451888.

[14] B. Abbott *et al.*, Production and integration of the ATLAS Insertable B-Layer, J. Instrum. **13,** T05008 (2018).

[15] ATLAS Collaboration, Performance of the ATLAS trigger system in 2015, Eur. Phys. J. C **77,** 317 (2017).

[16] ATLAS Collaboration, The ATLAS Collaboration Software and Firmware, Report No. ATL-SOFT-PUB-2021-001, 2021, https://cds.cern.ch/record/2767187.

[17] ATLAS Collaboration, Luminosity determination in pp collisions at $\sqrt{s} = 13$ TeV using the ATLAS detector at the LHC, Eur. Phys. J. C **83,** 982 (2023).

[18] G. Avoni *et al.*, The new LUCID-2 detector for luminosity measurement and monitoring in ATLAS, J. Instrum. **13,** P07017 (2018).

[19] ATLAS Collaboration, ATLAS data quality operations and performance for 2015–2018 data-taking, J. Instrum. **15,** P04003 (2020).

[20] T. Sjöstrand *et al.*, An introduction to PYTHIA8.2, Comput. Phys. Commun. **191,** 159 (2015).

[21] ATLAS Collaboration, ATLAS PYTHIA8 tunes to 7 TeV data, Report No. ATL-PHYS-PUB-2014-021, 2014, https://cds.cern.ch/record/1966419.

[22] B. Andersson, G. Gustafson, G. Ingelman, and T. Sjöstrand, Parton fragmentation and string dynamics, Phys. Rep. **97,** 31 (1983).

[23] R. D. Ball *et al.* (NNPDF Collaboration), Parton distributions with LHC data, Nucl. Phys. **B867,** 244 (2013).

[24] T. Sjöstrand and P. Z. Skands, Transverse-momentum-ordered showers and interleaved multiple interactions, Eur. Phys. J. C **39,** 129 (2005).

[25] D. J. Lange, The EVTGEN particle decay simulation package, Nucl. Instrum. Methods Phys. Res., Sect. A **462,** 152 (2001).

[26] E. Bothmann *et al.*, Event Generation with SHERPA2.2, SciPost Phys. **7,** 034 (2019).

[27] B. R. Webber, A QCD model for jet fragmentation including soft gluon interference, Nucl. Phys. **B238,** 492 (1984).

[28] S. Schumann and F. Krauss, A parton shower algorithm based on Catani-Seymour dipole factorisation, J. High Energy Phys. 03 (2008) 038.

[29] S. Dulat *et al.*, New parton distribution functions from a global analysis of quantum chromodynamics, Phys. Rev. D **93,** 033006 (2016).

[30] H.-L. Lai *et al.*, New parton distributions for collider physics, Phys. Rev. D **82,** 074024 (2010).

[31] G. S. Chahal and F. Krauss, Cluster hadronisation in SHERPA, SciPost Phys. **13,** 019 (2022).

[32] ATLAS Collaboration, Dependence of the jet energy scale on the particle content of hadronic jets in the ATLAS detector simulation, ATL-PHYS-PUB-2022-021, 2022, https://cds.cern.ch/record/2808016.

[33] M. Bähr *et al.*, HERWIG++ physics and manual, Eur. Phys. J. C **58,** 639 (2008).

[34] J. Bellm *et al.*, HERWIG7.0/HERWIG++3.0 release note, Eur. Phys. J. C **76,** 196 (2016).

[35] J. Bellm *et al.*, HERWIG7.1 Release Note, arXiv:1705.06919.

[36] P. Nason, A new method for combining NLO QCD with shower Monte Carlo algorithms, J. High Energy Phys. 11 (2004) 040.

[37] S. Frixione, P. Nason, and C. Oleari, Matching NLO QCD computations with parton shower simulations: The POWHEG method, J. High Energy Phys. 11 (2007) 070.

[38] S. Alioli, K. Hamilton, P. Nason, C. Oleari, and E. Re, Jet pair production in POWHEG, J. High Energy Phys. 04 (2011) 081.

[39] S. Alioli, P. Nason, C. Oleari, and E. Re, A general framework for implementing NLO calculations in shower Monte Carlo programs: The POWHEG BOX, J. High Energy Phys. 06 (2010) 043.

[40] R. D. Ball *et al.* (NNPDF Collaboration), Parton distributions for the LHC run II, J. High Energy Phys. 04 (2015) 040.

[41] ATLAS Collaboration, The ATLAS simulation infrastructure, Eur. Phys. J. C **70,** 823 (2010).

[42] S. Agostinelli *et al.*, GEANT4—a simulation toolkit, Nucl. Instrum. Methods Phys. Res., Sect. A **506,** 250 (2003).

[43] ATLAS Collaboration, The PYTHIA8 A3 tune description of ATLAS minimum bias and inelastic measurements incorporating the Donnachie-Landshoff diffractive model, Report No. ATL-PHYS-PUB-2016-017, 2016, https://cds.cern.ch/record/2206965.

[44] ATLAS Collaboration, Multijet simulation for 13 TeV ATLAS Analyses, Report No. ATL-PHYS-PUB-2019-017, 2019, https://cds.cern.ch/record/2672252.

[45] M. Cacciari, G. P. Salam, and G. Soyez, The anti-k_t jet clustering algorithm, J. High Energy Phys. 04 (2008) 063.

[46] M. Cacciari, G. P. Salam, and G. Soyez, FASTJET user manual, Eur. Phys. J. C **72,** 1896 (2012).

[47] ATLAS Collaboration, Jet reconstruction and performance using particle flow with the ATLAS detector, Eur. Phys. J. C **77,** 466 (2017).

[48] ATLAS Collaboration, Topological cell clustering in the ATLAS calorimeters and its performance in LHC Run 1, Eur. Phys. J. C **77,** 490 (2017).

[49] ATLAS Collaboration, Jet energy scale and resolution measured in proton-proton collisions at $\sqrt{s} = 13$ TeV with the ATLAS detector, Eur. Phys. J. C **81,** 689 (2021).

[50] ATLAS Collaboration, Selection of jets produced in 13 TeV proton-proton collisions with the ATLAS detector, Report No. ATLAS-CONF-2015-029, 2015, https://cds.cern.ch/record/2037702.

[51] ATLAS Collaboration, Performance of pile-up mitigation techniques for jets in pp collisions at $\sqrt{s} = 8$ TeV using the ATLAS detector, Eur. Phys. J. C **76,** 581 (2016).

[52] ATLAS Collaboration, Identification and rejection of pile-up jets at high pseudorapidity with the ATLAS detector, Eur. Phys. J. C **77,** 580 (2017); **77,** 712(E) (2017).

[53] ATLAS Collaboration, The performance of the jet trigger for the ATLAS detector during 2011 data taking, Eur. Phys. J. C **76,** 526 (2016).

[54] G. P. Salam and E. Slade, Cuts for two-body decays at colliders, J. High Energy Phys. 11 (2021) 220.

[55] S. Frixione and G. Ridolfi, Jet photoproduction at HERA, Nucl. Phys. **B507,** 315 (1997).

[56] V. Lendermann *et al.*, Combining triggers in HEP data analysis, Nucl. Instrum. Methods Phys. Res., Sect. A **604,** 707 (2009).

[57] CMS Collaboration, Measurement of the triple-differential dijet cross section in proton-proton collisions at $\sqrt{s} = 8$ TeV and constraints on parton distribution functions, Eur. Phys. J. C **77,** 746 (2017).

[58] G. D'Agostini, A multidimensional unfolding method based on Bayes' theorem, Nucl. Instrum. Methods Phys. Res., Sect. A **362,** 487 (1995).

[59] T. Adye, Unfolding algorithms and tests using ROOUN-FOLD, *Proceedings, 2011 Workshop on Statistical Issues Related to Discovery Claims in Search Experiments and Unfolding (PHYSTAT 2011)* (CERN, Geneva, Switzerland, 2011), 313; arXiv:1105.1160.

[60] ATLAS Collaboration, Jet energy measurement and its systematic uncertainty in proton-proton collisions at

$\sqrt{s} = 7$ TeV with the ATLAS detector, Eur. Phys. J. C **75,** 17 (2015).

[61] ATLAS Collaboration, A measurement of the calorimeter response to single hadrons and determination of the jet energy scale uncertainty using LHC Run-1 pp-collision data with the ATLAS detector, Eur. Phys. J. C **77,** 26 (2017).

[62] ATLAS Collaboration, Measurement of the energy response of the ATLAS calorimeter to charged pions from $W^{\pm} \to \tau^{\pm}(\to \pi^{\pm}\nu_{\tau})\nu_{\tau}$ events in run 2 data, Eur. Phys. J. C **82,** 223 (2022).

[63] P. Gras et al., Systematics of quark/gluon tagging, J. High Energy Phys. 07 (2017) 091.

[64] P. T. Komiske, E. M. Metodiev, and J. Thaler, An operational definition of quark and gluon jets, J. High Energy Phys. 11 (2018) 059.

[65] M. Cacciari and G. P. Salam, Pileup subtraction using jet areas, Phys. Lett. B **659,** 119 (2008).

[66] ATLAS Collaboration, Light-quark and gluon jet discrimination in pp collisions at $\sqrt{s} = 7$ TeV with the ATLAS detector, Eur. Phys. J. C **74,** 3023 (2014).

[67] ATLAS Collaboration, Properties of jet fragmentation using charged particles measured with the ATLAS detector in pp collisions at $\sqrt{s} = 13$ TeV, Phys. Rev. D **100,** 052011 (2019).

[68] P. Adragna et al., Measurement of pion and proton response and longitudinal shower profiles up to 20 nuclear interaction lengths with the ATLAS tile calorimeter, Nucl. Instrum. Methods Phys. Res., Sect. A **615,** 158 (2010).

[69] J. Abdallah et al., Study of energy response and resolution of the ATLAS tile calorimeter to hadrons of energies from 16 to 30 GeV, Eur. Phys. J. C **81,** 549 (2021).

[70] J. R. Christiansen and P. Z. Skands, String formation beyond leading colour, J. High Energy Phys. 08 (2015) 003.

[71] S. Gieseke, P. Kirchgaeßer, and S. Plätzer, Baryon production from cluster hadronisation, Eur. Phys. J. C **78,** 99 (2018).

[72] S. Gieseke, P. Kirchgaeßer, S. Plätzer, and A. Siodmok, Colour reconnection from soft gluon evolution, J. High Energy Phys. 11 (2018) 149.

[73] UA1 Collaboration, Analysis of the fragmentation properties of quark and gluon jets at the CERN SPS $p\bar{p}$ collider, Nucl. Phys. **B276,** 253 (1986).

[74] UA2 Collaboration, Measurement of jet fragmentation properties at the CERN $p\bar{p}$ collider, Phys. Lett. **144B,** 291 (1984).

[75] UA2 Collaboration, Measurement of production and properties of jets at the CERN $\bar{p}p$ collider, Z. Phys. C **20,** 117 (1983).

[76] OPAL Collaboration, A direct observation of quark-gluon jet differences at LEP, Phys. Lett. B **265,** 462 (1991).

[77] OPAL Collaboration, A study of differences between quark and gluon jets using vertex tagging of quark jets, Z. Phys. C **58,** 387 (1993).

[78] OPAL Collaboration, A model independent measurement of quark and gluon jet properties and differences, Z. Phys. C **68,** 179 (1995).

[79] ALEPH Collaboration, Study of the subjet structure of quark and gluon jets, Phys. Lett. B **346,** 389 (1995).

[80] OPAL Collaboration, Test of QCD analytic predictions for the multiplicity ratio between gluon and quark jets, Phys. Lett. B **388,** 659 (1996).

[81] ALEPH Collaboration, Quark and gluon jet properties in symmetric three-jet events, Phys. Lett. B **384,** 353 (1996).

[82] DELPHI Collaboration, Energy dependence of the differences between the quark and gluon jet fragmentation, Z. Phys. C **70,** 179 (1996).

[83] OPAL Collaboration, Multiplicity distributions of gluon and quark jets and tests of QCD analytic predictions, Eur. Phys. J. C **1,** 479 (1998).

[84] DELPHI Collaboration, The scale dependence of the hadron multiplicity in quark and gluon jets and a precise determination of C_A/C_F, Phys. Lett. B **449,** 383 (1999).

[85] OPAL Collaboration, Experimental properties of gluon and quark jets from a point source, Eur. Phys. J. C **11,** 217 (1999).

[86] OPAL Collaboration, A study of coherence of soft gluons in hadron jets, Phys. Lett. B **247,** 617 (1990).

[87] OPAL Collaboration, Scaling violations of quark and gluon jet fragmentation functions in e^+e^- annihilations at $\sqrt{s} = 91.2$ and 183–209 GeV, Eur. Phys. J. C **37,** 25 (2004).

[88] ATLAS Collaboration, Study of jet shapes in inclusive jet production in pp collisions at $\sqrt{s} = 7$ TeV using the ATLAS detector, Phys. Rev. D **83,** 052003 (2011).

[89] ATLAS Collaboration, ATLAS measurements of the properties of jets for boosted particle searches, Phys. Rev. D **86,** 072006 (2012).

[90] ATLAS Collaboration, Measurement of the soft-drop jet mass in pp collisions at $\sqrt{s} = 13$ TeV with the ATLAS detector, Phys. Rev. Lett. **121,** 092001 (2018).

[91] ATLAS Collaboration, Measurement of the Lund jet plane using charged particles in 13 TeV proton-proton collisions with the ATLAS detector, Phys. Rev. Lett. **124,** 222002 (2020).

[92] ATLAS Collaboration, Measurements of Lund subjet multiplicities in 13 TeV proton-proton collisions with the ATLAS detector, arXiv:2402.13052.

[93] CMS Collaboration, Measurements of the differential jet cross section as a function of the jet mass in dijet events from proton-proton collisions at $\sqrt{s} = 13$ TeV, J. High Energy Phys. 11 (2018) 113.

[94] CMS Collaboration, Study of quark and gluon jet substructure in $Z +$ jet and dijet events from pp collisions, J. High Energy Phys. 01 (**2022**) 188.

[95] CMS Collaboration, Measurement of the primary Lund jet plane density in proton-proton collisions at $\sqrt{s} = 13$ TeV, J. High Energy Phys. 05 (2024) 116.

[96] CDF Collaboration, Charged-particle multiplicity in $p\bar{p}$ collisions at $\sqrt{s} = 1.8$ TeV, Phys. Rev. Lett. **87,** 211804 (2001).

[97] CDF Collaboration, Momentum distribution of charged particles in jets in dijet events in $p\bar{p}$ collisions at $\sqrt{s} = 1.8$ TeV and comparisons to perturbative QCD predictions, Phys. Rev. D **68,** 012003 (2003).

[98] CDF Collaboration, Two-particle momentum correlations in jets produced in $p\bar{p}$ collisions at $\sqrt{s} = 1.96$ TeV, Phys. Rev. D **77,** 092001 (2008).

[99] CDF Collaboration, Measurement of the k_T distribution of particles in jets produced in $p\bar{p}$ collisions at $\sqrt{s} = 1.96$ TeV, Phys. Rev. Lett. **102**, 232002 (2009).

[100] JADE Collabortion, Experimental evidence for differences in $\langle p_\perp \rangle$ between quark jets and gluon jets, Phys. Lett. **123B**, 460 (1983).

[101] TASSO Collaboration, Charged multiplicity distributions and correlations in e^+e^- annihilation at PETRA energies, Z. Phys. C **45**, 193 (1989).

[102] HRS Collaboration, Comparison of charged particle multiplicities in quark and gluon jets produced in e^+e^- annihilation at 29 GeV, Phys. Lett. **165B**, 449 (1985).

[103] MARK II Collaboration, Inclusive charged-particle distribution in nearly threefold-symmetric three-jet events at $E_{\text{c.m.}} = 29$ GeV, Phys. Rev. Lett. **55**, 1954 (1985).

[104] SLD Collaboration, Measurement of the charged multiplicity of $Z^0 \to b\bar{b}$ events, Phys. Rev. Lett. **72**, 3145 (1994).

[105] SLD Collaboration, Measurement of the charged multiplicities in b, c and light quark events from Z^0 decays, Phys. Lett. B **386**, 475 (1996).

[106] AMY Collaboration, Comparison of quark and gluon jets produced in high-energy e^+e^- annihilations, Phys. Rev. Lett. **63**, 1772 (1989).

[107] CLEO Collaboration, Study of gluon versus quark fragmentation in $\Upsilon \to gg\gamma$ and $e^+e^- \to q\bar{q}\gamma$ events at $\sqrt{s} = 10$ GeV, Phys. Rev. D **56**, 17 (1997).

[108] H1 Collaboration, A study of the fragmentation of quarks in e–p collisions at HERA, Nucl. Phys. **B445**, 3 (1995).

[109] ZEUS Collaboration, Measurement of multiplicity and momentum spectra in the current fragmentation region of the Breit frame at HERA, Z. Phys. C **67**, 93 (1995).

[110] H1 Collaboration, Unbinned deep learning jet substructure measurement in high $Q^2 ep$ collisions at HERA, Phys. Lett. B **844**, 138101 (2023).

[111] ALICE Collaboration, Measurement of the production of charm jets tagged with D^0 mesons in pp collisions at $\sqrt{s} = 7$ TeV, J. High Energy Phys. 08 (2019) 133.

[112] ALICE Collaboration, Direct observation of the dead-cone effect in quantum chromodynamics, Nature (London) **605**, 440 (2022); **607**, E22 (2017).

[113] ALICE Collaboration, Measurements of groomed-jet substructure of charm jets tagged by D^0 mesons in proton-proton collisions at s = 13 TeV, Phys. Rev. Lett. **131**, 192301 (2023).

[114] ATLAS Collaboration, Single hadron response measurement and calorimeter jet energy scale uncertainty with the ATLAS detector at the LHC, Eur. Phys. J. C **73**, 2305 (2013).

[115] ATLAS Collaboration, Electron and photon performance measurements with the ATLAS detector using the 2015–2017 LHC proton-proton collision data, J. Instrum. **14**, P12006 (2019).

[116] ATLAS Collaboration, Evaluating statistical uncertainties and correlations using the bootstrap method, Report No. ATL-PHYS-PUB-2021-011, 2021, https://cds.cern.ch/record/2759945.

[117] B. Malaescu, An iterative, dynamically stabilized method of data unfolding, arXiv:0907.3791.

[118] Z. Nagy, Three-jet cross sections in hadron-hadron collisions at next-to-leading-order, Phys. Rev. Lett. **88**, 122003 (2002).

[119] Z. Nagy, Next-to-leading order calculation of three-jet observables in hadron-hadron collisions, Phys. Rev. D **68**, 094002 (2003).

[120] A. Buckley *et al.*, LHAPDF6: Parton density access in the LHC precision era, Eur. Phys. J. C **75**, 132 (2015).

[121] T.-J. Hou *et al.*, New CTEQ global analysis of quantum chromodynamics with high-precision data from the LHC, Phys. Rev. D **103**, 014013 (2021).

[122] R. D. Ball *et al.* (NNPDF Collaboration), The path to proton structure at 1% accuracy, Eur. Phys. J. C **82**, 428 (2022).

[123] S. Bailey, T. Cridge, L. A. Harland-Lang, A. D. Martin, and R. S. Thorne, Parton distributions from LHC, HERA, Tevatron and fixed target data: MSHT20 PDFs, Eur. Phys. J. C **81**, 341 (2021).

[124] ATLAS Collaboration, Determination of the parton distribution functions of the proton using diverse ATLAS data from pp collisions at $\sqrt{s} = 7$, 8 and 13 TeV, Eur. Phys. J. C **82**, 438 (2022).

[125] J. Currie *et al.*, Infrared sensitivity of single jet inclusive production at hadron colliders, J. High Energy Phys. 10 (2018) 155.

[126] M. Czakon and D. Heymes, Four-dimensional formulation of the sector-improved residue subtraction scheme, Nucl. Phys. **B890**, 152 (2014).

[127] M. Czakon, A. van Hameren, A. Mitov, and R. Poncelet, Single-jet inclusive rates with exact color at $\mathcal{O}(\alpha_s^4)$, J. High Energy Phys. 10 (2019) 262.

[128] M. Alvarez *et al.*, NNLO QCD corrections to event shapes at the LHC, J. High Energy Phys. 03 (2023) 129.

[129] M. Bury and A. van Hameren, Numerical evaluation of multi-gluon amplitudes for high energy factorization, Comput. Phys. Commun. **196**, 592 (2015).

[130] F. Buccioni *et al.*, OpenLoops 2, Eur. Phys. J. C **79**, 866 (2019).

[131] S. Abreu, F. Febres Cordero, H. Ita, B. Page, and V. Sotnikov, Leading-color two-loop QCD corrections for three-jet production at hadron colliders, J. High Energy Phys. 07 (2021) 095.

[132] D. Chicherin and V. Sotnikov, Pentagon functions for scattering of five massless particles, J. High Energy Phys. 12 (2020) 167.

[133] P. Skands, S. Carrazza, and J. Rojo, Tuning PYTHIA8.1: The MONASH 2013 tune, Eur. Phys. J. C **74**, 3024 (2014).

[134] J. R. Andersen and J. M. Smillie, Constructing all-order corrections to multi-jet rates, J. High Energy Phys. 01 (2010) 039.

[135] J. R. Andersen and J. M. Smillie, Multiple jets at the LHC with high energy jets, J. High Energy Phys. 06 (2011) 010.

[136] J. R. Andersen *et al.*, Combined subleading high-energy logarithms and NLO accuracy for W production in association with multiple jets, J. High Energy Phys. 04 (2021) 105.

[137] ATLAS Collaboration, Measurement of hadronic event shapes in high-p_T multijet final states at $\sqrt{s} = 13$ TeV with the ATLAS detector, J. High Energy Phys. 01 (2021) 188; 12 (2021) 53.

[138] ATLAS Collaboration, Measurements of multijet event isotropies using optimal transport with the ATLAS detector, J. High Energy Phys. 10 (2023) 060.

[139] A. Buckley *et al.*, RIVET user manual, Comput. Phys. Commun. **184**, 2803 (2013).

[140] ATLAS Collaboration, HEPData (collection), 10.17182/hepdata.105630, 2024.

[141] ATLAS Collaboration, ATLAS computing acknowledgements, Report No. ATL-SOFT-PUB-2023-001, 2023, https://cds.cern.ch/record/2869272.

G. Aad[103] E. Aakvaag[16] B. Abbott[121] K. Abeling[55] N. J. Abicht[49] S. H. Abidi[29] M. Aboelela[44] A. Aboulhorma[35e] H. Abramowicz[152] H. Abreu[151] Y. Abulaiti[118] B. S. Acharya[69a,69b,b] A. Ackermann[63a] C. Adam Bourdarios[4] L. Adamczyk[86a] S. V. Addepalli[26] M. J. Addison[102] J. Adelman[116] A. Adiguzel[21c] T. Adye[135] A. A. Affolder[137] Y. Afik[39] M. N. Agaras[13] J. Agarwala[73a,73b] A. Aggarwal[101] C. Agheorghiesei[27c] A. Ahmad[36] F. Ahmadov[38,c] W. S. Ahmed[105] S. Ahuja[96] X. Ai[62e] G. Aielli[76a,76b] A. Aikot[164] M. Ait Tamlihat[35e] B. Aitbenchikh[35a] I. Aizenberg[170] M. Akbiyik[101] T. P. A. Åkesson[99] A. V. Akimov[37] D. Akiyama[169] N. N. Akolkar[24] S. Aktas[21a] K. Al Khoury[41] G. L. Alberghi[23b] J. Albert[166] P. Albicocco[53] G. L. Albouy[60] S. Alderweireldt[52] Z. L. Alegria[122] M. Aleksa[36] I. N. Aleksandrov[38] C. Alexa[27b] T. Alexopoulos[10] F. Alfonsi[23b] M. Algren[56] M. Alhroob[142] B. Ali[133] H. M. J. Ali[92] S. Ali[149] S. W. Alibocus[93] M. Aliev[33c] G. Alimonti[71a] W. Alkakhi[55] C. Allaire[66] B. M. M. Allbrooke[147] J. F. Allen[52] C. A. Allendes Flores[138f] P. P. Allport[20] A. Aloisio[72a,72b] F. Alonso[91] C. Alpigiani[139] M. Alvarez Estevez[100] A. Alvarez Fernandez[101] M. Alves Cardoso[56] M. G. Alviggi[72a,72b] M. Aly[102] Y. Amaral Coutinho[83b] A. Ambler[105] C. Amelung,[36] M. Amerl[102] C. G. Ames[110] D. Amidei[107] K. J. Amirie[156] S. P. Amor Dos Santos[131a] K. R. Amos[164] S. An,[84] V. Ananiev[126] C. Anastopoulos[140] T. Andeen[11] J. K. Anders[36] S. Y. Andrean[47a,47b] A. Andreazza[71a,71b] S. Angelidakis[9] A. Angerami[41,d] A. V. Anisenkov[37] A. Annovi[74a] C. Antel[56] M. T. Anthony[140] E. Antipov[146] M. Antonelli[53] F. Anulli[75a] M. Aoki[84] T. Aoki[154] J. A. Aparisi Pozo[164] M. A. Aparo[147] L. Aperio Bella[48] C. Appelt[18] A. Apyan[26] S. J. Arbiol Val[87] C. Arcangeletti[53] A. T. H. Arce[51] E. Arena[93] J-F. Arguin[109] S. Argyropoulos[54] J.-H. Arling[48] O. Arnaez[4] H. Arnold[115] G. Artoni[75a,75b] H. Asada[112] K. Asai[119] S. Asai[154] N. A. Asbah[36] K. Assamagan[29] R. Astalos[28a] K. S. V. Astrand[99] S. Atashi[160] R. J. Atkin[33a] M. Atkinson,[163] H. Atmani[35f] P. A. Atmasiddha[129] K. Augsten[133] S. Auricchio[72a,72b] A. D. Auriol[20] V. A. Austrup[102] G. Avolio[36] K. Axiotis[56] G. Azuelos[109,e] D. Babal[28b] H. Bachacou[136] K. Bachas[153,f] A. Bachiu[34] F. Backman[47a,47b] A. Badea[39] T. M. Baer[107] P. Bagnaia[75a,75b] M. Bahmani[18] D. Bahner[54] K. Bai[124] J. T. Baines[135] L. Baines[95] O. K. Baker[173] E. Bakos[15] D. Bakshi Gupta[8] V. Balakrishnan[121] R. Balasubramanian[115] E. M. Baldin[37] P. Balek[86a] E. Ballabene[23b,23a] F. Balli[136] L. M. Baltes[63a] W. K. Balunas[32] J. Balz[101] E. Banas[87] M. Bandieramonte[130] A. Bandyopadhyay[24] S. Bansal[24] L. Barak[152] M. Barakat[48] E. L. Barberio[106] D. Barberis[57b,57a] M. Barbero[103] M. Z. Barel[115] K. N. Barends[33a] T. Barillari[111] M-S. Barisits[36] T. Barklow[144] P. Baron[123] D. A. Baron Moreno[102] A. Baroncelli[62a] G. Barone[29] A. J. Barr[127] J. D. Barr[97] F. Barreiro[100] J. Barreiro Guimarães da Costa[14a] U. Barron[152] M. G. Barros Teixeira[131a] S. Barsov[37] F. Bartels[63a] R. Bartoldus[144] A. E. Barton[92] P. Bartos[28a] A. Basan[101] M. Baselga[49] A. Bassalat[66,g] M. J. Basso[157a] R. Bate[165] R. L. Bates[59] S. Batlamous,[100] B. Batool[142] M. Battaglia[137] D. Battulga[18] M. Bauce[75a,75b] M. Bauer[36] P. Bauer[24] L. T. Bazzano Hurrell[30] J. B. Beacham[51] T. Beau[128] J. Y. Beaucamp[91] P. H. Beauchemin[159] P. Bechtle[24] H. P. Beck[19,h] K. Becker[168] A. J. Beddall[82] V. A. Bednyakov[38] C. P. Bee[146] L. J. Beemster[15] T. A. Beermann[36] M. Begalli[83d] M. Begel[29] A. Behera[146] J. K. Behr[48] J. F. Beirer[36] F. Beisiegel[24] M. Belfkir[117b] G. Bella[152] L. Bellagamba[23b] A. Bellerive[34] P. Bellos[20] K. Beloborodov[37] D. Benchekroun[35a] F. Bendebba[35a] Y. Benhammou[152] K. C. Benkendorfer[61] L. Beresford[48] M. Beretta[53] E. Bergeaas Kuutmann[162] N. Berger[4] B. Bergmann[133] J. Beringer[17a] G. Bernardi[5] C. Bernius[144] F. U. Bernlochner[24] F. Bernon[36,103] A. Berrocal Guardia[13] T. Berry[96] P. Berta[134] A. Berthold[50] S. Bethke[111] A. Betti[75a,75b] A. J. Bevan[95] N. K. Bhalla[54] M. Bhamjee[33c] S. Bhatta[146] D. S. Bhattacharya[167] P. Bhattarai[144] K. D. Bhide[54] V. S. Bhopatkar[122] R. M. Bianchi[130] G. Bianco[23b,23a] O. Biebel[110] R. Bielski[124] M. Biglietti[77a] C. S. Billingsley,[44] M. Bindi[55] A. Bingul[21b] C. Bini[75a,75b] A. Biondini[93] C. J. Birch-sykes[102] G. A. Bird[32] M. Birman[170] M. Biros[134] S. Biryukov[147] T. Bisanz[49]

E. Bisceglie[43b,43a] J. P. Biswal[135] D. Biswas[142] I. Bloch[48] A. Blue[59] U. Blumenschein[95] J. Blumenthal[101] V. S. Bobrovnikov[37] M. Boehler[54] B. Boehm[167] D. Bogavac[36] A. G. Bogdanchikov[37] C. Bohm[47a] V. Boisvert[96] P. Bokan[36] T. Bold[86a] M. Bomben[5] M. Bona[95] M. Boonekamp[136] C. D. Booth[96] A. G. Borbély[59] I. S. Bordulev[37] H. M. Borecka-Bielska[109] G. Borissov[92] D. Bortoletto[127] D. Boscherini[23b] M. Bosman[13] J. D. Bossio Sola[36] K. Bouaouda[35a] N. Bouchhar[164] J. Boudreau[130] E. V. Bouhova-Thacker[92] D. Boumediene[40] R. Bouquet[57b,57a] A. Boveia[120] J. Boyd[36] D. Boye[29] I. R. Boyko[38] J. Bracinik[20] N. Brahimi[4] G. Brandt[172] O. Brandt[32] F. Braren[48] B. Brau[104] J. E. Brau[124] R. Brener[170] L. Brenner[115] R. Brenner[162] S. Bressler[170] D. Britton[59] D. Britzger[111] I. Brock[24] G. Brooijmans[41] E. Brost[29] L. M. Brown[166] L. E. Bruce[61] T. L. Bruckler[127] P. A. Bruckman de Renstrom[87] B. Brüers[48] A. Bruni[23b] G. Bruni[23b] M. Bruschi[23b] N. Bruscino[75a,75b] T. Buanes[16] Q. Buat[139] D. Buchin[111] A. G. Buckley[59] O. Bulekov[37] B. A. Bullard[144] S. Burdin[93] C. D. Burgard[49] A. M. Burger[36] B. Burghgrave[8] O. Burlayenko[54] J. T. P. Burr[32] C. D. Burton[11] J. C. Burzynski[143] E. L. Busch[41] V. Büscher[101] P. J. Bussey[59] J. M. Butler[25] C. M. Buttar[59] J. M. Butterworth[97] W. Buttinger[135] C. J. Buxo Vazquez[108] A. R. Buzykaev[37] S. Cabrera Urbán[164] L. Cadamuro[66] D. Caforio[58] H. Cai[130] Y. Cai[14a,14e] Y. Cai[14c] V. M. M. Cairo[36] O. Cakir[3a] N. Calace[36] P. Calafiura[17a] G. Calderini[128] P. Calfayan[68] G. Callea[59] L. P. Caloba[83b] D. Calvet[40] S. Calvet[40] M. Calvetti[74a,74b] R. Camacho Toro[128] S. Camarda[36] D. Camarero Munoz[26] P. Camarri[76a,76b] M. T. Camerlingo[72a,72b] D. Cameron[36] C. Camincher[166] M. Campanelli[97] A. Camplani[42] V. Canale[72a,72b] A. C. Canbay[3a] E. Canonero[96] J. Cantero[164] Y. Cao[163] F. Capocasa[26] M. Capua[43b,43a] A. Carbone[71a,71b] R. Cardarelli[76a] J. C. J. Cardenas[8] F. Cardillo[164] G. Carducci[43b,43a] T. Carli[36] G. Carlino[72a] J. I. Carlotto[13] B. T. Carlson[130,i] E. M. Carlson[166,157a] J. Carmignani[93] L. Carminati[71a,71b] A. Carnelli[136] M. Carnesale[75a,75b] S. Caron[114] E. Carquin[138f] S. Carrá[71a] G. Carratta[23b,23a] A. M. Carroll[124] T. M. Carter[52] M. P. Casado[13,j] M. Caspar[48] F. L. Castillo[4] L. Castillo Garcia[13] V. Castillo Gimenez[164] N. F. Castro[131a,131e] A. Catinaccio[36] J. R. Catmore[126] T. Cavaliere[4] V. Cavaliere[29] N. Cavalli[23b,23a] Y. C. Cekmecelioglu[48] E. Celebi[21a] S. Cella[36] F. Celli[127] M. S. Centonze[70a,70b] V. Cepaitis[56] K. Cerny[123] A. S. Cerqueira[83a] A. Cerri[147] L. Cerrito[76a,76b] F. Cerutti[17a] B. Cervato[142] A. Cervelli[23b] G. Cesarini[53] S. A. Cetin[82] D. Chakraborty[116] J. Chan[17a] W. Y. Chan[154] J. D. Chapman[32] E. Chapon[136] B. Chargeishvili[150b] D. G. Charlton[20] M. Chatterjee[19] C. Chauhan[134] Y. Che[14c] S. Chekanov[6] S. V. Chekulaev[157a] G. A. Chelkov[38,k] A. Chen[107] B. Chen[152] B. Chen[166] H. Chen[14c] H. Chen[29] J. Chen[62c] J. Chen[143] M. Chen[127] S. Chen[154] S. J. Chen[14c] X. Chen[62c,136] X. Chen[14b,l] Y. Chen[62a] C. L. Cheng[171] H. C. Cheng[64a] S. Cheong[144] A. Cheplakov[38] E. Cheremushkina[48] E. Cherepanova[115] R. Cherkaoui El Moursli[35e] E. Cheu[7] K. Cheung[65] L. Chevalier[136] V. Chiarella[53] G. Chiarelli[74a] N. Chiedde[103] G. Chiodini[70a] A. S. Chisholm[20] A. Chitan[27b] M. Chitishvili[164] M. V. Chizhov[38] K. Choi[11] Y. Chou[139] E. Y. S. Chow[114] K. L. Chu[170] M. C. Chu[64a] X. Chu[14a,14e] J. Chudoba[132] J. J. Chwastowski[87] D. Cieri[111] K. M. Ciesla[86a] V. Cindro[94] A. Ciocio[17a] F. Cirotto[72a,72b] Z. H. Citron[170] M. Citterio[71a] D. A. Ciubotaru[27b] A. Clark[56] P. J. Clark[52] C. Clarry[156] J. M. Clavijo Columbie[48] S. E. Clawson[48] C. Clement[47a,47b] J. Clercx[48] Y. Coadou[103] M. Cobal[69a,69c] A. Coccaro[57b] R. F. Coelho Barrue[131a] R. Coelho Lopes De Sa[104] S. Coelli[71a] B. Cole[41] J. Collot[60] P. Conde Muiño[131a,131g] M. P. Connell[33c] S. H. Connell[33c] E. I. Conroy[127] F. Conventi[72a,m] H. G. Cooke[20] A. M. Cooper-Sarkar[127] F. A. Corchia[23b,23a] A. Cordeiro Oudot Choi[128] L. D. Corpe[40] M. Corradi[75a,75b] F. Corriveau[105,n] A. Cortes-Gonzalez[18] M. J. Costa[164] F. Costanza[4] D. Costanzo[140] B. M. Cote[120] G. Cowan[96] K. Cranmer[171] D. Cremonini[23b,23a] S. Crépé-Renaudin[60] F. Crescioli[128] M. Cristinziani[142] M. Cristoforetti[78a,78b] V. Croft[115] J. E. Crosby[122] G. Crosetti[43b,43a] A. Cueto[100] H. Cui[14a,14e] Z. Cui[7] W. R. Cunningham[59] F. Curcio[164] J. R. Curran[52] P. Czodrowski[36] M. M. Czurylo[36] M. J. Da Cunha Sargedas De Sousa[57b,57a] J. V. Da Fonseca Pinto[83b] C. Da Via[102] W. Dabrowski[86a] T. Dado[49] S. Dahbi[149] T. Dai[107] D. Dal Santo[19] C. Dallapiccola[104] M. Dam[42] G. D'amen[29] V. D'Amico[110] J. Damp[101] J. R. Dandoy[34] M. Danninger[143] V. Dao[36] G. Darbo[57b] S. J. Das[29,o] F. Dattola[48] S. D'Auria[71a,71b] A. D'avanzo[72a,72b] C. David[33a] T. Davidek[134] B. Davis-Purcell[34] I. Dawson[95] H. A. Day-hall[133] K. De[8] R. De Asmundis[72a] N. De Biase[48] S. De Castro[23b,23a] N. De Groot[114] P. de Jong[115] H. De la Torre[116] A. De Maria[14c] A. De Salvo[75a] U. De Sanctis[76a,76b] F. De Santis[70a,70b] A. De Santo[147] J. B. De Vivie De Regie[60] D. V. Dedovich[38] J. Degens[93] A. M. Deiana[44] F. Del Corso[23b,23a] J. Del Peso[100]

F. Del Rio[63a] L. Delagrange[128] F. Deliot[136] C. M. Delitzsch[49] M. Della Pietra[72a,72b] D. Della Volpe[56] A. Dell'Acqua[36] L. Dell'Asta[71a,71b] M. Delmastro[4] P. A. Delsart[60] S. Demers[173] M. Demichev[38] S. P. Denisov[37] L. D'Eramo[40] D. Derendarz[87] F. Derue[128] P. Dervan[93] K. Desch[24] C. Deutsch[24] F. A. Di Bello[57b,57a] A. Di Ciaccio[76a,76b] L. Di Ciaccio[4] A. Di Domenico[75a,75b] C. Di Donato[72a,72b] A. Di Girolamo[36] G. Di Gregorio[36] A. Di Luca[78a,78b] B. Di Micco[77a,77b] R. Di Nardo[77a,77b] M. Diamantopoulou[34] F. A. Dias[115] T. Dias Do Vale[143] M. A. Diaz[138a,138b] F. G. Diaz Capriles[24] M. Didenko[164] E. B. Diehl[107] S. Díez Cornell[48] C. Diez Pardos[142] C. Dimitriadi[162,24] A. Dimitrievska[20] J. Dingfelder[24] I-M. Dinu[27b] S. J. Dittmeier[63b] F. Dittus[36] M. Divisek[134] F. Djama[103] T. Djobava[150b] C. Doglioni[102,99] A. Dohnalova[28a] J. Dolejsi[134] Z. Dolezal[134] K. M. Dona[39] M. Donadelli[83c] B. Dong[108] J. Donini[40] A. D'Onofrio[72a,72b] M. D'Onofrio[93] J. Dopke[135] A. Doria[72a] N. Dos Santos Fernandes[131a] P. Dougan[102] M. T. Dova[91] A. T. Doyle[59] M. A. Draguet[127] E. Dreyer[170] I. Drivas-koulouris[10] M. Drnevich[118] M. Drozdova[56] D. Du[62a] T. A. du Pree[115] F. Dubinin[37] M. Dubovsky[28a] E. Duchovni[170] G. Duckeck[110] O. A. Ducu[27b] D. Duda[52] A. Dudarev[36] E. R. Duden[26] M. D'uffizi[102] L. Duflot[66] M. Dührssen[36] I. Duminica[27g] A. E. Dumitriu[27b] M. Dunford[63a] S. Dungs[49] K. Dunne[47a,47b] A. Duperrin[103] H. Duran Yildiz[3a] M. Düren[58] A. Durglishvili[150b] B. L. Dwyer[116] G. I. Dyckes[17a] M. Dyndal[86a] B. S. Dziedzic[87] Z. O. Earnshaw[147] G. H. Eberwein[127] B. Eckerova[28a] S. Eggebrecht[55] E. Egidio Purcino De Souza[128] L. F. Ehrke[56] G. Eigen[16] K. Einsweiler[17a] T. Ekelof[162] P. A. Ekman[99] S. El Farkh[35b] Y. El Ghazali[35b] H. El Jarrari[36] A. El Moussaouy[109] V. Ellajosyula[162] M. Ellert[162] F. Ellinghaus[172] N. Ellis[36] J. Elmsheuser[29] M. Elsawy[117a] M. Elsing[36] D. Emeliyanov[135] Y. Enari[154] I. Ene[17a] S. Epari[13] P. A. Erland[87] M. Errenst[172] M. Escalier[66] C. Escobar[164] E. Etzion[152] G. Evans[131a] H. Evans[68] L. S. Evans[96] A. Ezhilov[37] S. Ezzarqtouni[35a] F. Fabbri[23b,23a] L. Fabbri[23b,23a] G. Facini[97] V. Fadeyev[137] R. M. Fakhrutdinov[37] D. Fakoudis[101] S. Falciano[75a] L. F. Falda Ulhoa Coelho[36] P. J. Falke[24] F. Fallavollita[111] J. Faltova[134] C. Fan[163] Y. Fan[14a] Y. Fang[14a,14e] M. Fanti[71a,71b] M. Faraj[69a,69b] Z. Farazpay[98] A. Farbin[8] A. Farilla[77a] T. Farooque[108] S. M. Farrington[52] F. Fassi[35e] D. Fassouliotis[9] M. Faucci Giannelli[76a,76b] W. J. Fawcett[32] L. Fayard[66] P. Federic[134] P. Federicova[132] O. L. Fedin[37,k] M. Feickert[171] L. Feligioni[103] D. E. Fellers[124] C. Feng[62b] M. Feng[14b] Z. Feng[115] M. J. Fenton[160] L. Ferencz[48] R. A. M. Ferguson[92] S. I. Fernandez Luengo[138f] P. Fernandez Martinez[13] M. J. V. Fernoux[103] J. Ferrando[92] A. Ferrari[162] P. Ferrari[115,114] R. Ferrari[73a] D. Ferrere[56] C. Ferretti[107] F. Fiedler[101] P. Fiedler[133] A. Filipčič[94] E. K. Filmer[1] F. Filthaut[114] M. C. N. Fiolhais[131a,131c,p] L. Fiorini[164] W. C. Fisher[108] T. Fitschen[102] P. M. Fitzhugh[136] I. Fleck[142] P. Fleischmann[107] T. Flick[172] M. Flores[33d,q] L. R. Flores Castillo[64a] L. Flores Sanz De Acedo[36] F. M. Follega[78a,78b] N. Fomin[16] J. H. Foo[156] A. Formica[136] A. C. Forti[102] E. Fortin[36] A. W. Fortman[17a] M. G. Foti[17a] L. Fountas[9,r] D. Fournier[66] H. Fox[92] P. Francavilla[74a,74b] S. Francescato[61] S. Franchellucci[56] M. Franchini[23b,23a] S. Franchino[63a] D. Francis[36] L. Franco[114] V. Franco Lima[36] L. Franconi[48] M. Franklin[61] G. Frattari[26] W. S. Freund[83b] Y. Y. Frid[152] J. Friend[59] N. Fritzsche[50] A. Froch[54] D. Froidevaux[36] J. A. Frost[127] Y. Fu[62a] S. Fuenzalida Garrido[138f] M. Fujimoto[103] K. Y. Fung[64a] E. Furtado De Simas Filho[83e] M. Furukawa[154] J. Fuster[164] A. Gabrielli[23b,23a] A. Gabrielli[156] P. Gadow[36] G. Gagliardi[57b,57a] L. G. Gagnon[17a] S. Gaid[161] S. Galantzan[152] E. J. Gallas[127] B. J. Gallop[135] K. K. Gan[120] S. Ganguly[154] Y. Gao[52] F. M. Garay Walls[138a,138b] B. Garcia[29] C. García[164] A. Garcia Alonso[115] A. G. Garcia Caffaro[173] J. E. García Navarro[164] M. Garcia-Sciveres[17a] G. L. Gardner[129] R. W. Gardner[39] N. Garelli[159] D. Garg[80] R. B. Garg[144,s] J. M. Gargan[52] C. A. Garner[156] C. M. Garvey[33a] P. Gaspar[83b] V. K. Gassmann[159] G. Gaudio[73a] V. Gautam[13] P. Gauzzi[75a,75b] I. L. Gavrilenko[37] A. Gavrilyuk[37] C. Gay[165] G. Gaycken[48] E. N. Gazis[10] A. A. Geanta[27b] C. M. Gee[137] A. Gekow[120] C. Gemme[57b] M. H. Genest[60] A. D. Gentry[113] S. George[96] W. F. George[20] T. Geralis[46] P. Gessinger-Befurt[36] M. E. Geyik[172] M. Ghani[168] K. Ghorbanian[95] A. Ghosal[142] A. Ghosh[160] A. Ghosh[7] B. Giacobbe[23b] S. Giagu[75a,75b] T. Giani[115] P. Giannetti[74a] A. Giannini[62a] S. M. Gibson[96] M. Gignac[137] D. T. Gil[86b] A. K. Gilbert[86a] B. J. Gilbert[41] D. Gillberg[34] G. Gilles[115] L. Ginabat[128] D. M. Gingrich[2,e] M. P. Giordani[69a,69c] P. F. Giraud[136] G. Giugliarelli[69a,69c] D. Giugni[71a] F. Giuli[36] I. Gkialas[9,r] L. K. Gladilin[37] C. Glasman[100] G. R. Gledhill[124] G. Glemža[48] M. Glisic[124] I. Gnesi[43b,t] Y. Go[29] M. Goblirsch-Kolb[36] B. Gocke[49] D. Godin[109] B. Gokturk[21a] S. Goldfarb[106] T. Golling[56] M. G. D. Gololo[33g]

D. Golubkov[37] J. P. Gombas[108] A. Gomes[131a,131b] G. Gomes Da Silva[142] A. J. Gomez Delegido[164]
R. Gonçalo[131a,131c] L. Gonella[20] A. Gongadze[150c] F. Gonnella[20] J. L. Gonski[144] R. Y. González Andana[52]
S. González de la Hoz[164] R. Gonzalez Lopez[93] C. Gonzalez Renteria[17a] M. V. Gonzalez Rodrigues[48]
R. Gonzalez Suarez[162] S. Gonzalez-Sevilla[56] L. Goossens[36] B. Gorini[36] E. Gorini[70a,70b] A. Gorišek[94]
T. C. Gosart[129] A. T. Goshaw[51] M. I. Gostkin[38] S. Goswami[122] C. A. Gottardo[36] S. A. Gotz[110]
M. Gouighri[35b] V. Goumarre[48] A. G. Goussiou[139] N. Govender[33c] I. Grabowska-Bold[86a] K. Graham[34]
E. Gramstad[126] S. Grancagnolo[70a,70b] C. M. Grant[1,136] P. M. Gravila[27f] F. G. Gravili[70a,70b] H. M. Gray[17a]
M. Greco[70a,70b] C. Grefe[24] I. M. Gregor[48] K. T. Greif[160] P. Grenier[144] S. G. Grewe,[111] A. A. Grillo[137]
K. Grimm[31] S. Grinstein[13,u] J.-F. Grivaz[66] E. Gross[170] J. Grosse-Knetter[55] J. C. Grundy[127] L. Guan[107]
C. Gubbels[165] J. G. R. Guerrero Rojas[164] G. Guerrieri[69a,69c] F. Guescini[111] R. Gugel[101] J. A. M. Guhit[107]
A. Guida[18] E. Guilloton[168] S. Guindon[36] F. Guo[14a,14e] J. Guo[62c] L. Guo[48] Y. Guo[107] R. Gupta[48]
R. Gupta[130] S. Gurbuz[24] S. S. Gurdasani[54] G. Gustavino[36] M. Guth[56] P. Gutierrez[121]
L. F. Gutierrez Zagazeta[129] M. Gutsche[50] C. Gutschow[97] C. Gwenlan[127] C. B. Gwilliam[93] E. S. Haaland[126]
A. Haas[118] M. Habedank[48] C. Haber[17a] H. K. Hadavand[8] A. Hadef[50] S. Hadzic[111] A. I. Hagan[92]
J. J. Hahn[142] E. H. Haines[97] M. Haleem[167] J. Haley[122] J. J. Hall[140] G. D. Hallewell[103] L. Halser[19]
K. Hamano[166] M. Hamer[24] G. N. Hamity[52] E. J. Hampshire[96] J. Han[62b] K. Han[62a] L. Han[14c] L. Han[62a]
S. Han[17a] Y. F. Han[156] K. Hanagaki[84] M. Hance[137] D. A. Hangal[41] H. Hanif[143] M. D. Hank[129]
J. B. Hansen[42] P. H. Hansen[42] K. Hara[158] D. Harada[56] T. Harenberg[172] S. Harkusha[37] M. L. Harris[104]
Y. T. Harris[127] J. Harrison[13] N. M. Harrison[120] P. F. Harrison,[168] N. M. Hartman[111] N. M. Hartmann[110]
R. Z. Hasan[96,135] Y. Hasegawa[141] S. Hassan[16] R. Hauser[108] C. M. Hawkes[20] R. J. Hawkings[36] Y. Hayashi[154]
S. Hayashida[112] D. Hayden[108] C. Hayes[107] R. L. Hayes[115] C. P. Hays[127] J. M. Hays[95] H. S. Hayward[93]
F. He[62a] M. He[14a,14e] Y. He[155] Y. He[48] Y. He[97] N. B. Heatley[95] V. Hedberg[99] A. L. Heggelund[126]
N. D. Hehir[95,a] C. Heidegger[54] K. K. Heidegger[54] W. D. Heidorn[81] J. Heilman[34] S. Heim[48] T. Heim[17a]
J. G. Heinlein[129] J. J. Heinrich[124] L. Heinrich,[111,v] J. Hejbal[132] A. Held[171] S. Hellesund[16] C. M. Helling[165]
S. Hellman[47a,47b] R. C. W. Henderson,[92] L. Henkelmann[32] A. M. Henriques Correia,[36] H. Herde[99]
Y. Hernández Jiménez[146] L. M. Herrmann[24] T. Herrmann[50] G. Herten[54] R. Hertenberger[110] L. Hervas[36]
M. E. Hesping[101] N. P. Hessey[157a] M. Hidaoui[35b] E. Hill[156] S. J. Hillier[20] J. R. Hinds[108] F. Hinterkeuser[24]
M. Hirose[125] S. Hirose[158] D. Hirschbuehl[172] T. G. Hitchings[102] B. Hiti[94] J. Hobbs[146] R. Hobincu[27e]
N. Hod[170] M. C. Hodgkinson[140] B. H. Hodkinson[127] A. Hoecker[36] D. D. Hofer[107] J. Hofer[48] T. Holm[24]
M. Holzbock[111] L. B. A. H. Hommels[32] B. P. Honan[102] J. Hong[62c] T. M. Hong[130] B. H. Hooberman[163]
W. H. Hopkins[6] Y. Horii[112] S. Hou[149] A. S. Howard[94] J. Howarth[59] J. Hoya[6] M. Hrabovsky[123]
A. Hrynevich[48] T. Hryn'ova[4] P. J. Hsu[65] S.-C. Hsu[139] T. Hsu[66] M. Hu[17a] Q. Hu[62a] S. Huang[64b]
X. Huang[14a,14e] Y. Huang[140] Y. Huang[101] Y. Huang[14a] Z. Huang[102] Z. Hubacek[133] M. Huebner[24]
F. Huegging[24] T. B. Huffman[127] C. A. Hugli[48] M. Huhtinen[36] S. K. Huiberts[16] R. Hulsken[105]
N. Huseynov[12] J. Huston[108] J. Huth[61] R. Hyneman[144] G. Iacobucci[56] G. Iakovidis[29] I. Ibragimov[142]
L. Iconomidou-Fayard[66] J. P. Iddon[36] P. Iengo[72a,72b] R. Iguchi[154] T. Iizawa[127] Y. Ikegami[84] N. Ilic[156]
H. Imam[35a] M. Ince Lezki[56] T. Ingebretsen Carlson[47a,47b] G. Introzzi[73a,73b] M. Iodice[77a] V. Ippolito[75a,75b]
R. K. Irwin[93] M. Ishino[154] W. Islam[171] C. Issever[18,48] S. Istin[21a,w] H. Ito[169] R. Iuppa[78a,78b] A. Ivina[170]
J. M. Izen[45] V. Izzo[72a] P. Jacka[132,133] P. Jackson[1] B. P. Jaeger[143] C. S. Jagfeld[110] G. Jain[157a] P. Jain[54]
K. Jakobs[54] T. Jakoubek[170] J. Jamieson[59] K. W. Janas[86a] M. Javurkova[104] L. Jeanty[124] J. Jejelava[150a,x]
P. Jenni[54,y] C. E. Jessiman[34] C. Jia,[62b] J. Jia[146] X. Jia[61] X. Jia[14a,14e] Z. Jia[14c] C. Jiang[52] S. Jiggins[48]
J. Jimenez Pena[13] S. Jin[14c] A. Jinaru[27b] O. Jinnouchi[155] P. Johansson[140] K. A. Johns[7] J. W. Johnson[137]
D. M. Jones[147] E. Jones[48] P. Jones[32] R. W. L. Jones[92] T. J. Jones[93] H. L. Joos[55,36] R. Joshi[120]
J. Jovicevic[15] X. Ju[17a] J. J. Junggeburth[104] T. Junkermann[63a] A. Juste Rozas[13,u] M. K. Juzek[87] S. Kabana[138e]
A. Kaczmarska[87] M. Kado[111] H. Kagan[120] M. Kagan[144] A. Kahn,[41] A. Kahn[129] C. Kahra[101] T. Kaji[154]
E. Kajomovitz[151] N. Kakati[170] I. Kalaitzidou[54] C. W. Kalderon[29] N. J. Kang[137] D. Kar[33g] K. Karava[127]
M. J. Kareem[157b] E. Karentzos[54] I. Karkanias[153] O. Karkout[115] S. N. Karpov[38] Z. M. Karpova[38]
V. Kartvelishvili[92] A. N. Karyukhin[37] E. Kasimi[153] J. Katzy[48] S. Kaur[34] K. Kawade[141] M. P. Kawale[121]
C. Kawamoto[88] T. Kawamoto[62a] E. F. Kay[36] F. I. Kaya[159] S. Kazakos[108] V. F. Kazanin[37] Y. Ke[146]

J. M. Keaveney[33a] R. Keeler[166] G. V. Kehris[61] J. S. Keller[34] A. S. Kelly[97] J. J. Kempster[147] P. D. Kennedy[101] O. Kepka[132] B. P. Kerridge[135] S. Kersten[172] B. P. Kerševan[94] L. Keszeghova[28a] S. Ketabchi Haghighat[156] R. A. Khan[130] A. Khanov[122] A. G. Kharlamov[37] T. Kharlamova[37] E. E. Khoda[139] M. Kholodenko[37] T. J. Khoo[18] G. Khoriauli[167] J. Khubua[150b] Y. A. R. Khwaira[66] B. Kibirige[33g] A. Kilgallon[124] D. W. Kim[47a,47b] Y. K. Kim[39] N. Kimura[97] M. K. Kingston[55] A. Kirchhoff[55] C. Kirfel[24] F. Kirfel[24] J. Kirk[135] A. E. Kiryunin[111] C. Kitsaki[10] O. Kivernyk[24] M. Klassen[159] C. Klein[34] L. Klein[167] M. H. Klein[44] S. B. Klein[56] U. Klein[93] P. Klimek[36] A. Klimentov[29] T. Klioutchnikova[36] P. Kluit[115] S. Kluth[111] E. Kneringer[79] T. M. Knight[156] A. Knue[49] R. Kobayashi[88] D. Kobylianskii[170] S. F. Koch[127] M. Kocian[144] P. Kodyš[134] D. M. Koeck[124] P. T. Koenig[24] T. Koffas[34] O. Kolay[50] I. Koletsou[4] T. Komarek[123] K. Köneke[54] A. X. Y. Kong[1] T. Kono[119] N. Konstantinidis[97] P. Kontaxakis[56] B. Konya[99] R. Kopeliansky[41] S. Koperny[86a] K. Korcyl[87] K. Kordas[153,z] A. Korn[97] S. Korn[55] I. Korolkov[13] N. Korotkova[37] B. Kortman[115] O. Kortner[111] S. Kortner[111] W. H. Kostecka[116] V. V. Kostyukhin[142] A. Kotsokechagia[136] A. Kotwal[51] A. Koulouris[36] A. Kourkoumeli-Charalampidi[73a,73b] C. Kourkoumelis[9] E. Kourlitis[111,v] O. Kovanda[124] R. Kowalewski[166] W. Kozanecki[136] A. S. Kozhin[37] V. A. Kramarenko[37] G. Kramberger[94] P. Kramer[101] M. W. Krasny[128] A. Krasznahorkay[36] J. W. Kraus[172] J. A. Kremer[48] T. Kresse[50] J. Kretzschmar[93] K. Kreul[18] P. Krieger[156] S. Krishnamurthy[104] M. Krivos[134] K. Krizka[20] K. Kroeninger[49] H. Kroha[111] J. Kroll[132] J. Kroll[129] K. S. Krowpman[108] U. Kruchonak[38] H. Krüger[24] N. Krumnack[81] M. C. Kruse[51] O. Kuchinskaia[37] S. Kuday[3a] S. Kuehn[36] R. Kuesters[54] T. Kuhl[48] V. Kukhtin[38] Y. Kulchitsky[37,k] S. Kuleshov[138d,138b] M. Kumar[33g] N. Kumari[48] P. Kumari[157b] A. Kupco[132] T. Kupfer[49] A. Kupich[37] O. Kuprash[54] H. Kurashige[85] L. L. Kurchaninov[157a] O. Kurdysh[66] Y. A. Kurochkin[37] A. Kurova[37] M. Kuze[155] A. K. Kvam[104] J. Kvita[123] T. Kwan[105] N. G. Kyriacou[107] L. A. O. Laatu[103] C. Lacasta[164] F. Lacava[75a,75b] H. Lacker[18] D. Lacour[128] N. N. Lad[97] E. Ladygin[38] A. Lafarge[40] B. Laforge[128] T. Lagouri[173] F. Z. Lahbabi[35a] S. Lai[55] I. K. Lakomiec[86a] J. E. Lambert[166] S. Lammers[68] W. Lampl[7] C. Lampoudis[153,z] G. Lamprinoudis[101] A. N. Lancaster[116] E. Lançon[29] U. Landgraf[54] M. P. J. Landon[95] V. S. Lang[54] O. K. B. Langrekken[126] A. J. Lankford[160] F. Lanni[36] K. Lantzsch[24] A. Lanza[73a] A. Lapertosa[57b,57a] J. F. Laporte[136] T. Lari[71a] F. Lasagni Manghi[23b] M. Lassnig[36] V. Latonova[132] A. Laudrain[101] A. Laurier[151] S. D. Lawlor[140] Z. Lawrence[102] R. Lazaridou[168] M. Lazzaroni[71a,71b] B. Le[102] E. M. Le Boulicaut[51] L. T. Le Pottier[17a] B. Leban[23b,23a] A. Lebedev[81] M. LeBlanc[102] F. Ledroit-Guillon[60] S. C. Lee[149] S. Lee[47a,47b] T. F. Lee[93] L. L. Leeuw[33c] H. P. Lefebvre[96] M. Lefebvre[166] C. Leggett[17a] G. Lehmann Miotto[36] M. Leigh[56] W. A. Leight[104] W. Leinonen[114] A. Leisos[153,aa] M. A. L. Leite[83c] C. E. Leitgeb[18] R. Leitner[134] K. J. C. Leney[44] T. Lenz[24] S. Leone[74a] C. Leonidopoulos[52] A. Leopold[145] C. Leroy[109] R. Les[108] C. G. Lester[32] M. Levchenko[37] J. Levêque[4] L. J. Levinson[170] G. Levrini[23b,23a] M. P. Lewicki[87] C. Lewis[139] D. J. Lewis[4] A. Li[5] B. Li[62b] C. Li[62a] C-Q. Li[111] H. Li[62a] H. Li[62b] H. Li[14c] H. Li[14b] H. Li[62b] J. Li[62c] K. Li[139] L. Li[62c] M. Li[14a,14e] Q. Y. Li[62a] S. Li[14a,14e] S. Li[62d,62c,bb] T. Li[5] X. Li[105] Z. Li[127] Z. Li[154] Z. Li[14a,14e] S. Liang[14a,14e] Z. Liang[14a] M. Liberatore[136] B. Liberti[76a] K. Lie[64c] J. Lieber Marin[83e] H. Lien[68] K. Lin[108] R. E. Lindley[7] J. H. Lindon[2] E. Lipeles[129] A. Lipniacka[16] A. Lister[165] J. D. Little[4] B. Liu[14a] B. X. Liu[143] D. Liu[62d,62c] E. H. L. Liu[20] J. B. Liu[62a] J. K. K. Liu[32] K. Liu[62d] K. Liu[62d,62c] M. Liu[62a] M. Y. Liu[62a] P. Liu[14a] Q. Liu[62d,139,62c] X. Liu[62a] X. Liu[62b] Y. Liu[14d,14e] Y. L. Liu[62b] Y. W. Liu[62a] J. Llorente Merino[143] S. L. Lloyd[95] E. M. Lobodzinska[48] P. Loch[7] T. Lohse[18] K. Lohwasser[140] E. Loiacono[48] M. Lokajicek[132,a] J. D. Lomas[20] J. D. Long[163] I. Longarini[160] L. Longo[70a,70b] R. Longo[163] I. Lopez Paz[67] A. Lopez Solis[48] N. Lorenzo Martinez[4] A. M. Lory[110] G. Löschcke Centeno[147] O. Loseva[37] X. Lou[47a,47b] X. Lou[14a,14e] A. Lounis[66] P. A. Love[92] G. Lu[14a,14e] M. Lu[66] S. Lu[129] Y. J. Lu[65] H. J. Lubatti[139] C. Luci[75a,75b] F. L. Lucio Alves[14c] F. Luehring[68] I. Luise[146] O. Lukianchuk[66] O. Lundberg[145] B. Lund-Jensen[145,a] N. A. Luongo[6] M. S. Lutz[36] A. B. Lux[25] D. Lynn[29] R. Lysak[132] E. Lytken[99] V. Lyubushkin[38] T. Lyubushkina[38] M. M. Lyukova[146] M. Firdaus M. Soberi[52] H. Ma[29] K. Ma[62a] L. L. Ma[62b] W. Ma[62a] Y. Ma[122] D. M. Mac Donell[166] G. Maccarrone[53] J. C. MacDonald[101] P. C. Machado De Abreu Farias[83e] R. Madar[40] T. Madula[97] J. Maeda[85] T. Maeno[29] H. Maguire[140] V. Maiboroda[136] A. Maio[131a,131b,131d] K. Maj[86a] O. Majersky[48] S. Majewski[124] N. Makovec[66] V. Maksimovic[15] B. Malaescu[128] Pa. Malecki[87] V. P. Maleev[37] F. Malek[60,cc] M. Mali[94] D. Malito[96]

U. Mallik[80], S. Maltezos[10], S. Malyukov[38], J. Mamuzic[13], G. Mancini[53], M. N. Mancini[26], G. Manco[73a,73b],
J. P. Mandalia[95], I. Mandić[94], L. Manhaes de Andrade Filho[83a], I. M. Maniatis[170], J. Manjarres Ramos[90],
D. C. Mankad[170], A. Mann[110], S. Manzoni[36], L. Mao[62c], X. Mapekula[33c], A. Marantis[153,aa], G. Marchiori[5],
M. Marcisovsky[132], C. Marcon[71a], M. Marinescu[20], S. Marium[48], M. Marjanovic[121], A. Markhoos[54],
M. Markovitch[66], E. J. Marshall[92], Z. Marshall[17a], S. Marti-Garcia[164], T. A. Martin[168], V. J. Martin[52],
B. Martin dit Latour[16], L. Martinelli[75a,75b], M. Martinez[13,u], P. Martinez Agullo[164], V. I. Martinez Outschoorn[104],
P. Martinez Suarez[13], S. Martin-Haugh[135], G. Martinovicova[134], V. S. Martoiu[27b], A. C. Martyniuk[97],
A. Marzin[36], D. Mascione[78a,78b], L. Masetti[101], T. Mashimo[154], J. Masik[102], A. L. Maslennikov[37],
P. Massarotti[72a,72b], P. Mastrandrea[74a,74b], A. Mastroberardino[43b,43a], T. Masubuchi[154], T. Mathisen[162],
J. Matousek[134], N. Matsuzawa[154], J. Maurer[27b], A. J. Maury[66], B. Maček[94], D. A. Maximov[37], A. E. May[102],
R. Mazini[149], I. Maznas[116], M. Mazza[108], S. M. Mazza[137], E. Mazzeo[71a,71b], C. Mc Ginn[29], J. P. Mc Gowan[166],
S. P. Mc Kee[107], C. C. McCracken[165], E. F. McDonald[106], A. E. McDougall[115], J. A. Mcfayden[147],
R. P. McGovern[129], G. Mchedlidze[150b], R. P. Mckenzie[33g], T. C. Mclachlan[48], D. J. Mclaughlin[97],
S. J. McMahon[135], C. M. Mcpartland[93], R. A. McPherson[166,n], S. Mehlhase[110], A. Mehta[93], D. Melini[164],
B. R. Mellado Garcia[33g], A. H. Melo[55], F. Meloni[48], A. M. Mendes Jacques Da Costa[102], H. Y. Meng[156],
L. Meng[92], S. Menke[111], M. Mentink[36], E. Meoni[43b,43a], G. Mercado[116], C. Merlassino[69a,69c], L. Merola[72a,72b],
C. Meroni[71a,71b], J. Metcalfe[6], A. S. Mete[6], C. Meyer[68], J-P. Meyer[136], R. P. Middleton[135], L. Mijović[52],
G. Mikenberg[170], M. Mikestikova[132], M. Mikuž[94], H. Mildner[101], A. Milic[36], D. W. Miller[39], E. H. Miller[144],
L. S. Miller[34], A. Milov[170], D. A. Milstead[47a,47b], T. Min[14c], A. A. Minaenko[37], I. A. Minashvili[150b], L. Mince[59],
A. I. Mincer[118], B. Mindur[86a], M. Mineev[38], Y. Mino[88], L. M. Mir[13], M. Miralles Lopez[59], M. Mironova[17a],
A. Mishima[154], M. C. Missio[114], A. Mitra[168], V. A. Mitsou[164], Y. Mitsumori[112], O. Miu[156], P. S. Miyagawa[95],
T. Mkrtchyan[63a], M. Mlinarevic[97], T. Mlinarevic[97], M. Mlynarikova[36], S. Mobius[19], P. Mogg[110],
M. H. Mohamed Farook[113], A. F. Mohammed[14a,14e], S. Mohapatra[41], G. Mokgatitswane[33g], L. Moleri[170],
B. Mondal[142], S. Mondal[133], K. Mönig[48], E. Monnier[103], L. Monsonis Romero[164], J. Montejo Berlingen[13],
M. Montella[120], F. Montereali[77a,77b], F. Monticelli[91], S. Monzani[69a,69c], N. Morange[66],
A. L. Moreira De Carvalho[48], M. Moreno Llácer[164], C. Moreno Martinez[56], P. Morettini[57b], S. Morgenstern[36],
M. Morii[61], M. Morinaga[154], F. Morodei[75a,75b], L. Morvaj[36], P. Moschovakos[36], B. Moser[36], M. Mosidze[150b],
T. Moskalets[54], P. Moskvitina[114], J. Moss[31,dd], P. Moszkowicz[86a], A. Moussa[35d], E. J. W. Moyse[104],
O. Mtintsilana[33g], S. Muanza[103], J. Mueller[130], D. Muenstermann[92], R. Müller[19], G. A. Mullier[162], A. J. Mullin[32],
J. J. Mullin[129], D. P. Mungo[156], D. Munoz Perez[164], F. J. Munoz Sanchez[102], M. Murin[102], W. J. Murray[168,135],
M. Muškinja[94], C. Mwewa[29], A. G. Myagkov[37,k], A. J. Myers[8], G. Myers[107], M. Myska[133], B. P. Nachman[17a],
O. Nackenhorst[49], K. Nagai[127], K. Nagano[84], J. L. Nagle[29,o], E. Nagy[103], A. M. Nairz[36], Y. Nakahama[84],
K. Nakamura[84], K. Nakkalil[5], H. Nanjo[125], R. Narayan[44], E. A. Narayanan[113], I. Naryshkin[37], M. Naseri[34],
S. Nasri[117b], C. Nass[24], G. Navarro[22a], J. Navarro-Gonzalez[164], R. Nayak[152], A. Nayaz[18], P. Y. Nechaeva[37],
S. Nechaeva[23b,23a], F. Nechansky[48], L. Nedic[127], T. J. Neep[20], A. Negri[73a,73b], M. Negrini[23b], C. Nellist[115],
C. Nelson[105], K. Nelson[107], S. Nemecek[132], M. Nessi[36,ee], M. S. Neubauer[163], F. Neuhaus[101], J. Neundorf[48],
R. Newhouse[165], P. R. Newman[20], C. W. Ng[130], Y. W. Y. Ng[48], B. Ngair[117a], H. D. N. Nguyen[109],
R. B. Nickerson[127], R. Nicolaidou[136], J. Nielsen[137], M. Niemeyer[55], J. Niermann[55], N. Nikiforou[36],
V. Nikolaenko[37,k], I. Nikolic-Audit[128], K. Nikolopoulos[20], P. Nilsson[29], I. Ninca[48], H. R. Nindhito[56],
G. Ninio[152], A. Nisati[75a], N. Nishu[2], R. Nisius[111], J-E. Nitschke[50], E. K. Nkadimeng[33g], T. Nobe[154],
D. L. Noel[32], T. Nommensen[148], M. B. Norfolk[140], R. R. B. Norisam[97], B. J. Norman[34], M. Noury[35a],
J. Novak[94], T. Novak[48], L. Novotny[133], R. Novotny[113], L. Nozka[123], K. Ntekas[160],
N. M. J. Nunes De Moura Junior[83b], J. Ocariz[128], A. Ochi[85], I. Ochoa[131a], S. Oerdek[48,ff], J. T. Offermann[39],
A. Ogrodnik[134], A. Oh[102], C. C. Ohm[145], H. Oide[84], R. Oishi[154], M. L. Ojeda[48], Y. Okumura[154],
L. F. Oleiro Seabra[131a], S. A. Olivares Pino[138d], G. Oliveira Correa[13], D. Oliveira Damazio[29],
D. Oliveira Goncalves[83a], J. L. Oliver[160], Ö. O. Öncel[54], A. P. O'Neill[19], A. Onofre[131a,131e], P. U. E. Onyisi[11],
M. J. Oreglia[39], G. E. Orellana[91], D. Orestano[77a,77b], N. Orlando[13], R. S. Orr[156], V. O'Shea[59], L. M. Osojnak[129],
R. Ospanov[62a], G. Otero y Garzon[30], H. Otono[89], P. S. Ott[63a], G. J. Ottino[17a], M. Ouchrif[35d], F. Ould-Saada[126],
T. Ovsiannikova[139], M. Owen[59], R. E. Owen[135], K. Y. Oyulmaz[21a], V. E. Ozcan[21a], F. Ozturk[87], N. Ozturk[8],

S. Ozturk,[82] H. A. Pacey,[127] A. Pacheco Pages,[13] C. Padilla Aranda,[13] G. Padovano,[75a,75b] S. Pagan Griso,[17a] G. Palacino,[68] A. Palazzo,[70a,70b] J. Pampel,[24] J. Pan,[173] T. Pan,[64a] D. K. Panchal,[11] C. E. Pandini,[115] J. G. Panduro Vazquez,[96] H. D. Pandya,[1] H. Pang,[14b] P. Pani,[48] G. Panizzo,[69a,69c] L. Panwar,[128] L. Paolozzi,[56] S. Parajuli,[163] A. Paramonov,[6] C. Paraskevopoulos,[53] D. Paredes Hernandez,[64b] A. Pareti,[73a,73b] K. R. Park,[41] T. H. Park,[156] M. A. Parker,[32] F. Parodi,[57b,57a] E. W. Parrish,[116] V. A. Parrish,[52] J. A. Parsons,[41] U. Parzefall,[54] B. Pascual Dias,[109] L. Pascual Dominguez,[152] E. Pasqualucci,[75a] S. Passaggio,[57b] F. Pastore,[96] P. Patel,[87] U. M. Patel,[51] J. R. Pater,[102] T. Pauly,[36] C. I. Pazos,[159] J. Pearkes,[144] M. Pedersen,[126] R. Pedro,[131a] S. V. Peleganchuk,[37] O. Penc,[36] E. A. Pender,[52] G. D. Penn,[173] K. E. Penski,[110] M. Penzin,[37] B. S. Peralva,[83d] A. P. Pereira Peixoto,[139] L. Pereira Sanchez,[144] D. V. Perepelitsa,[29,o] E. Perez Codina,[157a] M. Perganti,[10] H. Pernegger,[36] O. Perrin,[40] K. Peters,[48] R. F. Y. Peters,[102] B. A. Petersen,[36] T. C. Petersen,[42] E. Petit,[103] V. Petousis,[133] C. Petridou,[153,z] T. Petru,[134] A. Petrukhin,[142] M. Pettee,[17a] N. E. Pettersson,[36] A. Petukhov,[37] K. Petukhova,[134] R. Pezoa,[138f] L. Pezzotti,[36] G. Pezzullo,[173] T. M. Pham,[171] T. Pham,[106] P. W. Phillips,[135] G. Piacquadio,[146] E. Pianori,[17a] F. Piazza,[124] R. Piegaia,[30] D. Pietreanu,[27b] A. D. Pilkington,[102] M. Pinamonti,[69a,69c] J. L. Pinfold,[2] B. C. Pinheiro Pereira,[131a] A. E. Pinto Pinoargote,[101,136] L. Pintucci,[69a,69c] K. M. Piper,[147] A. Pirttikoski,[56] D. A. Pizzi,[34] L. Pizzimento,[64b] A. Pizzini,[115] M.-A. Pleier,[29] V. Plesanovs,[54] V. Pleskot,[134] E. Plotnikova,[38] G. Poddar,[95] R. Poettgen,[99] L. Poggioli,[128] I. Pokharel,[55] S. Polacek,[134] G. Polesello,[73a] A. Poley,[143,157a] A. Polini,[23b] C. S. Pollard,[168] Z. B. Pollock,[120] E. Pompa Pacchi,[75a,75b] D. Ponomarenko,[114] L. Pontecorvo,[36] S. Popa,[27a] G. A. Popeneciu,[27d] A. Poreba,[36] D. M. Portillo Quintero,[157a] S. Pospisil,[133] M. A. Postill,[140] P. Postolache,[27c] K. Potamianos,[168] P. A. Potepa,[86a] I. N. Potrap,[38] C. J. Potter,[32] H. Potti,[1] J. Poveda,[164] M. E. Pozo Astigarraga,[36] A. Prades Ibanez,[164] J. Pretel,[54] D. Price,[102] M. Primavera,[70a] M. A. Principe Martin,[100] R. Privara,[123] T. Procter,[59] M. L. Proffitt,[139] N. Proklova,[129] K. Prokofiev,[64c] G. Proto,[111] J. Proudfoot,[6] M. Przybycien,[86a] W. W. Przygoda,[86b] A. Psallidas,[46] J. E. Puddefoot,[140] D. Pudzha,[37] D. Pyatiizbyantseva,[37] J. Qian,[107] D. Qichen,[102] Y. Qin,[13] T. Qiu,[52] A. Quadt,[55] M. Queitsch-Maitland,[102] G. Quetant,[56] R. P. Quinn,[165] G. Rabanal Bolanos,[61] D. Rafanoharana,[54] F. Ragusa,[71a,71b] J. L. Rainbolt,[39] J. A. Raine,[56] S. Rajagopalan,[29] E. Ramakoti,[37] I. A. Ramirez-Berend,[34] K. Ran,[48,14e] N. P. Rapheeha,[33g] H. Rasheed,[27b] V. Raskina,[128] D. F. Rassloff,[63a] A. Rastogi,[17a] S. Rave,[101] B. Ravina,[55] I. Ravinovich,[170] M. Raymond,[36] A. L. Read,[126] N. P. Readioff,[140] D. M. Rebuzzi,[73a,73b] G. Redlinger,[29] A. S. Reed,[111] K. Reeves,[26] J. A. Reidelsturz,[172] D. Reikher,[152] A. Rej,[49] C. Rembser,[36] M. Renda,[27b] M. B. Rendel,[111] F. Renner,[48] A. G. Rennie,[160] A. L. Rescia,[48] S. Resconi,[71a] M. Ressegotti,[57b,57a] S. Rettie,[36] J. G. Reyes Rivera,[108] E. Reynolds,[17a] O. L. Rezanova,[37] P. Reznicek,[134] H. Riani,[35d] N. Ribaric,[92] E. Ricci,[78a,78b] R. Richter,[111] S. Richter,[47a,47b] E. Richter-Was,[86b] M. Ridel,[128] S. Ridouani,[35d] P. Rieck,[118] P. Riedler,[36] E. M. Riefel,[47a,47b] J. O. Rieger,[115] M. Rijssenbeek,[146] M. Rimoldi,[36] L. Rinaldi,[23b,23a] T. T. Rinn,[29] M. P. Rinnagel,[110] G. Ripellino,[162] I. Riu,[13] J. C. Rivera Vergara,[166] F. Rizatdinova,[122] E. Rizvi,[95] B. R. Roberts,[17a] S. H. Robertson,[105,n] D. Robinson,[32] C. M. Robles Gajardo,[138f] M. Robles Manzano,[101] A. Robson,[59] A. Rocchi,[76a,76b] C. Roda,[74a,74b] S. Rodriguez Bosca,[36] Y. Rodriguez Garcia,[22a] A. Rodriguez Rodriguez,[54] A. M. Rodríguez Vera,[116] S. Roe,[36] J. T. Roemer,[160] A. R. Roepe-Gier,[137] J. Roggel,[172] O. Røhne,[126] R. A. Rojas,[104] C. P. A. Roland,[128] J. Roloff,[29] A. Romaniouk,[37] E. Romano,[73a,73b] M. Romano,[23b] A. C. Romero Hernandez,[163] N. Rompotis,[93] L. Roos,[128] S. Rosati,[75a] B. J. Rosser,[39] E. Rossi,[127] E. Rossi,[72a,72b] L. P. Rossi,[61] L. Rossini,[54] R. Rosten,[120] M. Rotaru,[27b] B. Rottler,[54] C. Rougier,[90] D. Rousseau,[66] D. Rousso,[48] A. Roy,[163] S. Roy-Garand,[156] A. Rozanov,[103] Z. M. A. Rozario,[59] Y. Rozen,[151] A. Rubio Jimenez,[164] A. J. Ruby,[93] V. H. Ruelas Rivera,[18] T. A. Ruggeri,[1] A. Ruggiero,[127] A. Ruiz-Martinez,[164] A. Rummler,[36] Z. Rurikova,[54] N. A. Rusakovich,[38] H. L. Russell,[166] G. Russo,[75a,75b] J. P. Rutherfoord,[7] S. Rutherford Colmenares,[32] K. Rybacki,[92] M. Rybar,[134] E. B. Rye,[126] A. Ryzhov,[44] J. A. Sabater Iglesias,[56] P. Sabatini,[164] H. F-W. Sadrozinski,[137] F. Safai Tehrani,[75a] B. Safarzadeh Samani,[135] S. Saha,[1] M. Sahinsoy,[111] A. Saibel,[164] M. Saimpert,[136] M. Saito,[154] T. Saito,[154] A. Sala,[71a,71b] D. Salamani,[36] A. Salnikov,[144] J. Salt,[164] A. Salvador Salas,[152] D. Salvatore,[43b,43a] F. Salvatore,[147] A. Salzburger,[36] D. Sammel,[54] E. Sampson,[92] D. Sampsonidis,[153,z] D. Sampsonidou,[124] J. Sánchez,[164] V. Sanchez Sebastian,[164] H. Sandaker,[126] C. O. Sander,[48] J. A. Sandesara,[104] M. Sandhoff,[172] C. Sandoval,[22b] D. P. C. Sankey,[135] T. Sano,[88] A. Sansoni,[53] L. Santi,[75a,75b] C. Santoni,[40] H. Santos,[131a,131b] A. Santra,[170] E. Sanzani,[23b,23a] K. A. Saoucha,[161] J. G. Saraiva,[131a,131d]

J. Sardain[7] O. Sasaki[84] K. Sato[158] C. Sauer,[63b] F. Sauerburger[54] E. Sauvan[4] P. Savard,[156,e] R. Sawada,[154] C. Sawyer[135] L. Sawyer[98] I. Sayago Galvan,[164] C. Sbarra[23b] A. Sbrizzi[23b,23a] T. Scanlon[97] J. Schaarschmidt[139] U. Schäfer[101] A. C. Schaffer[66,44] D. Schaile[110] R. D. Schamberger[146] C. Scharf[18] M. M. Schefer[19] V. A. Schegelsky[37] D. Scheirich[134] F. Schenck[18] M. Schernau[160] C. Scheulen[55] C. Schiavi[57b,57a] M. Schioppa[43b,43a] B. Schlag[144,s] K. E. Schleicher[54] S. Schlenker[36] J. Schmeing[172] M. A. Schmidt[172] K. Schmieden[101] C. Schmitt[101] N. Schmitt[101] S. Schmitt[48] L. Schoeffel[136] A. Schoening[63b] P. G. Scholer[34] E. Schopf[127] M. Schott[101] J. Schovancova[36] S. Schramm[56] T. Schroer[56] H-C. Schultz-Coulon[63a] M. Schumacher[54] B. A. Schumm[137] Ph. Schune[136] A. J. Schuy[139] H. R. Schwartz[137] A. Schwartzman[144] T. A. Schwarz[107] Ph. Schwemling[136] R. Schwienhorst[108] A. Sciandra[29] G. Sciolla[26] F. Scuri[74a] C. D. Sebastiani[93] K. Sedlaczek[116] P. Seema[18] S. C. Seidel[113] A. Seiden[137] B. D. Seidlitz[41] C. Seitz[48] J. M. Seixas[83b] G. Sekhniaidze[72a] L. Selem[60] N. Semprini-Cesari[23b,23a] D. Sengupta[56] V. Senthilkumar[164] L. Serin[66] L. Serkin[69a,69b] M. Sessa[76a,76b] H. Severini[121] F. Sforza[57b,57a] A. Sfyrla[56] Q. Sha[14a] E. Shabalina[55] A. H. Shah[32] R. Shaheen[145] J. D. Shahinian[129] D. Shaked Renous[170] L. Y. Shan[14a] M. Shapiro[17a] A. Sharma[36] A. S. Sharma[165] P. Sharma[80] P. B. Shatalov[37] K. Shaw[147] S. M. Shaw[102] A. Shcherbakova[37] Q. Shen[62c,5] D. J. Sheppard[143] P. Sherwood[97] L. Shi[97] X. Shi[14a] C. O. Shimmin[173] J. D. Shinner[96] I. P. J. Shipsey[127] S. Shirabe[89] M. Shiyakova,[38,gg] J. Shlomi[170] M. J. Shochet[39] J. Shojaii[106] D. R. Shope[126] B. Shrestha[121] S. Shrestha,[120,hh] E. M. Shrif[33g] M. J. Shroff[166] P. Sicho[132] A. M. Sickles[163] E. Sideras Haddad[33g] A. C. Sidley[115] A. Sidoti[23b] F. Siegert[50] Dj. Sijacki[15] F. Sili[91] J. M. Silva[52] M. V. Silva Oliveira[29] S. B. Silverstein[47a] S. Simion,[66] R. Simoniello[36] E. L. Simpson[102] H. Simpson[147] L. R. Simpson[107] N. D. Simpson,[99] S. Simsek[82] S. Sindhu[55] P. Sinervo[156] S. Singh[156] S. Sinha[48] S. Sinha[102] M. Sioli[23b,23a] I. Siral[36] E. Sitnikova[48] J. Sjölin[47a,47b] A. Skaf[55] E. Skorda[20] P. Skubic[121] M. Slawinska[87] V. Smakhtin,[170] B. H. Smart[135] S. Yu. Smirnov[37] Y. Smirnov[37] L. N. Smirnova,[37,k] O. Smirnova[99] A. C. Smith[41] D. R. Smith,[160] E. A. Smith[39] H. A. Smith[127] J. L. Smith[102] R. Smith,[144] M. Smizanska[92] K. Smolek[133] A. A. Snesarev[37] S. R. Snider[156] H. L. Snoek[115] S. Snyder[29] R. Sobie,[166,n] A. Soffer[152] C. A. Solans Sanchez[36] E. Yu. Soldatov[37] U. Soldevila[164] A. A. Solodkov[37] S. Solomon[26] A. Soloshenko[38] K. Solovieva[54] O. V. Solovyanov[40] P. Sommer[36] A. Sonay[13] W. Y. Song[157b] A. Sopczak[133] A. L. Sopio[97] F. Sopkova[28b] J. D. Sorenson[113] I. R. Sotarriva Alvarez[155] V. Sothilingam,[63a] O. J. Soto Sandoval[138c,138b] S. Sottocornola[68] R. Soualah[161] Z. Soumaimi[35e] D. South[48] N. Soybelman[170] S. Spagnolo[70a,70b] M. Spalla[111] D. Sperlich[54] G. Spigo[36] S. Spinali[92] D. P. Spiteri[59] M. Spousta[134] E. J. Staats[34] R. Stamen[63a] A. Stampekis[20] M. Standke[24] E. Stanecka[87] W. Stanek-Maslouska[48] M. V. Stange[50] B. Stanislaus[17a] M. M. Stanitzki[48] B. Stapf[48] E. A. Starchenko[37] G. H. Stark[137] J. Stark[90] P. Staroba[132] P. Starovoitov[63a] S. Stärz[105] R. Staszewski[87] G. Stavropoulos[46] J. Steentoft[162] P. Steinberg[29] B. Stelzer[143,157a] H. J. Stelzer[130] O. Stelzer-Chilton[157a] H. Stenzel[58] T. J. Stevenson[147] G. A. Stewart[36] J. R. Stewart[122] M. C. Stockton[36] G. Stoicea[27b] M. Stolarski[131a] S. Stonjek[111] A. Straessner[50] J. Strandberg[145] S. Strandberg[47a,47b] M. Stratmann[172] M. Strauss[121] T. Strebler[103] P. Strizenec[28b] R. Ströhmer[167] D. M. Strom[124] R. Stroynowski[44] A. Strubig[47a,47b] S. A. Stucci[29] B. Stugu[16] J. Stupak[121] N. A. Styles[48] D. Su[144] S. Su[62a] W. Su[62d] X. Su[62a] D. Suchy[28a] K. Sugizaki[154] V. V. Sulin[37] M. J. Sullivan[93] D. M. S. Sultan[127] L. Sultanaliyeva[37] S. Sultansoy[3b] T. Sumida[88] S. Sun[107] S. Sun[171] O. Sunneborn Gudnadottir[162] N. Sur[103] M. R. Sutton[147] H. Suzuki[158] M. Svatos[132] M. Swiatlowski[157a] T. Swirski[167] I. Sykora[28a] M. Sykora[134] T. Sykora[134] D. Ta[101] K. Tackmann,[48,ff] A. Taffard[160] R. Tafirout[157a] J. S. Tafoya Vargas[66] Y. Takubo[84] M. Talby[103] A. A. Talyshev[37] K. C. Tam[64b] N. M. Tamir[152] A. Tanaka[154] J. Tanaka[154] R. Tanaka[66] M. Tanasini[146] Z. Tao[165] S. Tapia Araya[138f] S. Tapprogge[101] A. Tarek Abouelfadl Mohamed[108] S. Tarem[151] K. Tariq[14a] G. Tarna[27b] G. F. Tartarelli[71a] M. J. Tartarin[90] P. Tas[134] M. Tasevsky[132] E. Tassi[43b,43a] A. C. Tate[163] G. Tateno[154] Y. Tayalati,[35e,ii] G. N. Taylor[106] W. Taylor[157b] A. S. Tee[171] R. Teixeira De Lima[144] P. Teixeira-Dias[96] J. J. Teoh[156] K. Terashi[154] J. Terron[100] S. Terzo[13] M. Testa[53] R. J. Teuscher,[156,n] A. Thaler[79] O. Theiner[56] N. Themistokleous[52] T. Theveneaux-Pelzer[103] O. Thielmann[172] D. W. Thomas,[96] J. P. Thomas[20] E. A. Thompson[17a] P. D. Thompson[20] E. Thomson[129] R. E. Thornberry[44] Y. Tian[55] V. Tikhomirov,[37,k] Yu. A. Tikhonov[37] S. Timoshenko,[37] D. Timoshyn[134] E. X. L. Ting[1] P. Tipton[173] S. H. Tlou[33g] K. Todome[155]

S. Todorova-Nova,[134] S. Todt,[50] L. Toffolin,[69a,69c] M. Togawa,[84] J. Tojo,[89] S. Tokár,[28a] K. Tokushuku,[84] O. Toldaiev,[68] R. Tombs,[32] M. Tomoto,[84,112] L. Tompkins,[144,s] K. W. Topolnicki,[86b] E. Torrence,[124] H. Torres,[90] E. Torró Pastor,[164] M. Toscani,[30] C. Tosciri,[39] M. Tost,[11] D. R. Tovey,[140] A. Traeet,[16] I. S. Trandafir,[27b] T. Trefzger,[167] A. Tricoli,[29] I. M. Trigger,[157a] S. Trincaz-Duvoid,[128] D. A. Trischuk,[26] B. Trocmé,[60] L. Truong,[33c] M. Trzebinski,[87] A. Trzupek,[87] F. Tsai,[146] M. Tsai,[107] A. Tsiamis,[153,z] P. V. Tsiareshka,[37] S. Tsigaridas,[157a] A. Tsirigotis,[153,aa] V. Tsiskaridze,[156] E. G. Tskhadadze,[150a] M. Tsopoulou,[153] Y. Tsujikawa,[88] I. I. Tsukerman,[37] V. Tsulaia,[17a] S. Tsuno,[84] K. Tsuri,[119] D. Tsybychev,[146] Y. Tu,[64b] A. Tudorache,[27b] V. Tudorache,[27b] A. N. Tuna,[61] S. Turchikhin,[57b,57a] I. Turk Cakir,[3a] R. Turra,[71a] T. Turtuvshin,[38,jj] P. M. Tuts,[41] S. Tzamarias,[153,z] E. Tzovara,[101] F. Ukegawa,[158] P. A. Ulloa Poblete,[138c,138b] E. N. Umaka,[29] G. Unal,[36] A. Undrus,[29] G. Unel,[160] J. Urban,[28b] P. Urquijo,[106] P. Urrejola,[138a] G. Usai,[8] R. Ushioda,[155] M. Usman,[109] Z. Uysal,[82] V. Vacek,[133] B. Vachon,[105] T. Vafeiadis,[36] A. Vaitkus,[97] C. Valderanis,[110] E. Valdes Santurio,[47a,47b] M. Valente,[157a] S. Valentinetti,[23b,23a] A. Valero,[164] E. Valiente Moreno,[164] A. Vallier,[90] J. A. Valls Ferrer,[164] D. R. Van Arneman,[115] T. R. Van Daalen,[139] A. Van Der Graaf,[49] P. Van Gemmeren,[6] M. Van Rijnbach,[126] S. Van Stroud,[97] I. Van Vulpen,[115] P. Vana,[134] M. Vanadia,[76a,76b] W. Vandelli,[36] E. R. Vandewall,[122] D. Vannicola,[152] L. Vannoli,[53] R. Vari,[75a] E. W. Varnes,[7] C. Varni,[17b] T. Varol,[149] D. Varouchas,[66] L. Varriale,[164] K. E. Varvell,[148] M. E. Vasile,[27b] L. Vaslin,[84] G. A. Vasquez,[166] A. Vasyukov,[38] R. Vavricka,[101] F. Vazeille,[40] T. Vazquez Schroeder,[36] J. Veatch,[31] V. Vecchio,[102] M. J. Veen,[104] I. Veliscek,[29] L. M. Veloce,[156] F. Veloso,[131a,131c] S. Veneziano,[75a] A. Ventura,[70a,70b] S. Ventura Gonzalez,[136] A. Verbytskyi,[111] M. Verducci,[74a,74b] C. Vergis,[95] M. Verissimo De Araujo,[83b] W. Verkerke,[115] J. C. Vermeulen,[115] C. Vernieri,[144] M. Vessella,[104] M. C. Vetterli,[143,e] A. Vgenopoulos,[153,z] N. Viaux Maira,[138f] T. Vickey,[140] O. E. Vickey Boeriu,[140] G. H. A. Viehhauser,[127] L. Vigani,[63b] M. Villa,[23b,23a] M. Villaplana Perez,[164] E. M. Villhauer,[52] E. Vilucchi,[53] M. G. Vincter,[34] A. Visibile,[115] C. Vittori,[36] I. Vivarelli,[23b,23a] E. Voevodina,[111] F. Vogel,[110] J. C. Voigt,[50] P. Vokac,[133] Yu. Volkotrub,[86b] J. Von Ahnen,[48] E. Von Toerne,[24] B. Vormwald,[36] V. Vorobel,[134] K. Vorobev,[37] M. Vos,[164] K. Voss,[142] M. Vozak,[115] L. Vozdecky,[121] N. Vranjes,[15] M. Vranjes Milosavljevic,[15] M. Vreeswijk,[115] N. K. Vu,[62d,62c] R. Vuillermet,[36] O. Vujinovic,[101] I. Vukotic,[39] S. Wada,[158] C. Wagner,[104] J. M. Wagner,[17a] W. Wagner,[172] S. Wahdan,[172] H. Wahlberg,[91] M. Wakida,[112] J. Walder,[135] R. Walker,[110] W. Walkowiak,[142] A. Wall,[129] E. J. Wallin,[99] T. Wamorkar,[6] A. Z. Wang,[137] C. Wang,[101] C. Wang,[11] H. Wang,[17a] J. Wang,[64c] R.-J. Wang,[101] R. Wang,[61] R. Wang,[6] S. M. Wang,[149] S. Wang,[62b] S. Wang,[14a] T. Wang,[62a] W. T. Wang,[80] W. Wang,[14a] X. Wang,[14c] X. Wang,[163] X. Wang,[62c] Y. Wang,[62d] Y. Wang,[14c] Z. Wang,[107] Z. Wang,[62d,51,62c] Z. Wang,[107] A. Warburton,[105] R. J. Ward,[20] N. Warrack,[59] S. Waterhouse,[96] A. T. Watson,[20] H. Watson,[59] M. F. Watson,[20] E. Watton,[59,135] G. Watts,[139] B. M. Waugh,[97] J. M. Webb,[54] C. Weber,[29] H. A. Weber,[18] M. S. Weber,[19] S. M. Weber,[63a] C. Wei,[62a] Y. Wei,[54] A. R. Weidberg,[127] E. J. Weik,[118] J. Weingarten,[49] M. Weirich,[101] C. Weiser,[54] C. J. Wells,[48] T. Wenaus,[29] B. Wendland,[49] T. Wengler,[36] N. S. Wenke,[111] N. Wermes,[24] M. Wessels,[63a] A. M. Wharton,[92] A. S. White,[61] A. White,[8] M. J. White,[1] D. Whiteson,[160] L. Wickremasinghe,[125] W. Wiedenmann,[171] M. Wielers,[135] C. Wiglesworth,[42] D. J. Wilbern,[121] H. G. Wilkens,[36] J. J. H. Wilkinson,[32] D. M. Williams,[41] H. H. Williams,[129] S. Williams,[32] S. Willocq,[104] B. J. Wilson,[102] P. J. Windischhofer,[39] F. I. Winkel,[30] F. Winklmeier,[124] B. T. Winter,[54] J. K. Winter,[102] M. Wittgen,[144] M. Wobisch,[98] T. Wojtkowski,[60] Z. Wolffs,[115] J. Wollrath,[160] M. W. Wolter,[87] H. Wolters,[131a,131c] M. C. Wong,[137] E. L. Woodward,[41] S. D. Worm,[48] B. K. Wosiek,[87] K. W. Woźniak,[87] S. Wozniewski,[55] K. Wraight,[59] C. Wu,[20] M. Wu,[14d] M. Wu,[114] S. L. Wu,[171] X. Wu,[56] Y. Wu,[62a] Z. Wu,[4] J. Wuerzinger,[111,v] T. R. Wyatt,[102] B. M. Wynne,[52] S. Xella,[42] L. Xia,[14c] M. Xia,[14b] J. Xiang,[64c] M. Xie,[62a] X. Xie,[62a] S. Xin,[14a,14e] A. Xiong,[124] J. Xiong,[17a] D. Xu,[14a] H. Xu,[62a] L. Xu,[62a] R. Xu,[129] T. Xu,[107] Y. Xu,[14b] Z. Xu,[52] Z. Xu,[14c] B. Yabsley,[148] S. Yacoob,[33a] Y. Yamaguchi,[155] E. Yamashita,[154] H. Yamauchi,[158] T. Yamazaki,[17a] Y. Yamazaki,[85] J. Yan,[62c] S. Yan,[59] Z. Yan,[104] H. J. Yang,[62c,62d] H. T. Yang,[62a] S. Yang,[62a] T. Yang,[64c] X. Yang,[36] X. Yang,[14a] Y. Yang,[44] Y. Yang,[62a] Z. Yang,[62a] W-M. Yao,[17a] H. Ye,[14c] H. Ye,[55] J. Ye,[14a] S. Ye,[29] X. Ye,[62a] Y. Yeh,[97] I. Yeletskikh,[38] B. K. Yeo,[17b] M. R. Yexley,[97] T. P. Yildirim,[127] P. Yin,[41] K. Yorita,[169] S. Younas,[27b] C. J. S. Young,[36] C. Young,[144] C. Yu,[14a,14e] Y. Yu,[62a] M. Yuan,[107] R. Yuan,[62d,62c] L. Yue,[97] M. Zaazoua,[62a] B. Zabinski,[87] E. Zaid,[52] Z. K. Zak,[87] T. Zakareishvili,[164] N. Zakharchuk,[34] S. Zambito,[56] J. A. Zamora Saa,[138d,138b] J. Zang,[154] D. Zanzi,[54] O. Zaplatilek,[133] C. Zeitnitz,[172] H. Zeng,[14a]

J. C. Zeng,[163] D. T. Zenger Jr.,[26] O. Zenin,[37] T. Ženiš,[28a] S. Zenz,[95] S. Zerradi,[35a] D. Zerwas,[66] M. Zhai,[14a,14e] D. F. Zhang,[140] J. Zhang,[62b] J. Zhang,[6] K. Zhang,[14a,14e] L. Zhang,[62a] L. Zhang,[14c] P. Zhang,[14a,14e] R. Zhang,[171] S. Zhang,[107] S. Zhang,[44] T. Zhang,[154] X. Zhang,[62c] X. Zhang,[62b] Y. Zhang,[62c,5] Y. Zhang,[97] Y. Zhang,[14c] Z. Zhang,[17a] Z. Zhang,[66] H. Zhao,[139] T. Zhao,[62b] Y. Zhao,[137] Z. Zhao,[62a] Z. Zhao,[62a] A. Zhemchugov,[38] J. Zheng,[14c] K. Zheng,[163] X. Zheng,[62a] Z. Zheng,[144] D. Zhong,[163] B. Zhou,[107] H. Zhou,[7] N. Zhou,[62c] Y. Zhou,[14c] Y. Zhou,[7] C. G. Zhu,[62b] J. Zhu,[107] X. Zhu,[62d] Y. Zhu,[62c] Y. Zhu,[62a] X. Zhuang,[14a] K. Zhukov,[37] N. I. Zimine,[38] J. Zinsser,[63b] M. Ziolkowski,[142] L. Živković,[15] A. Zoccoli,[23b,23a] K. Zoch,[61] T. G. Zorbas,[140] O. Zormpa,[46] W. Zou,[41] and L. Zwalinski[36]

(ATLAS Collaboration)

[1]*Department of Physics, University of Adelaide, Adelaide, Australia*
[2]*Department of Physics, University of Alberta, Edmonton, Alberta, Canada*
[3a]*Department of Physics, Ankara University, Ankara, Türkiye*
[3b]*Division of Physics, TOBB University of Economics and Technology, Ankara, Türkiye*
[4]*LAPP, Université Savoie Mont Blanc, CNRS/IN2P3, Annecy, France*
[5]*APC, Université Paris Cité, CNRS/IN2P3, Paris, France*
[6]*High Energy Physics Division, Argonne National Laboratory, Argonne, Illinois, USA*
[7]*Department of Physics, University of Arizona, Tucson, Arizona, USA*
[8]*Department of Physics, University of Texas at Arlington, Arlington, Texas, USA*
[9]*Physics Department, National and Kapodistrian University of Athens, Athens, Greece*
[10]*Physics Department, National Technical University of Athens, Zografou, Greece*
[11]*Department of Physics, University of Texas at Austin, Austin, Texas, USA*
[12]*Institute of Physics, Azerbaijan Academy of Sciences, Baku, Azerbaijan*
[13]*Institut de Física d'Altes Energies (IFAE), Barcelona Institute of Science and Technology, Barcelona, Spain*
[14a]*Institute of High Energy Physics, Chinese Academy of Sciences, Beijing, China*
[14b]*Physics Department, Tsinghua University, Beijing, China*
[14c]*Department of Physics, Nanjing University, Nanjing, China*
[14d]*School of Science, Shenzhen Campus of Sun Yat-sen University, China*
[14e]*University of Chinese Academy of Science (UCAS), Beijing, China*
[15]*Institute of Physics, University of Belgrade, Belgrade, Serbia*
[16]*Department for Physics and Technology, University of Bergen, Bergen, Norway*
[17a]*Physics Division, Lawrence Berkeley National Laboratory, Berkeley, California, USA*
[17b]*University of California, Berkeley, California, USA*
[18]*Institut für Physik, Humboldt Universität zu Berlin, Berlin, Germany*
[19]*Albert Einstein Center for Fundamental Physics and Laboratory for High Energy Physics, University of Bern, Bern, Switzerland*
[20]*School of Physics and Astronomy, University of Birmingham, Birmingham, United Kingdom*
[21a]*Department of Physics, Bogazici University, Istanbul, Türkiye*
[21b]*Department of Physics Engineering, Gaziantep University, Gaziantep, Türkiye*
[21c]*Department of Physics, Istanbul University, Istanbul, Türkiye*
[22a]*Facultad de Ciencias y Centro de Investigaciónes, Universidad Antonio Nariño, Bogotá, Colombia*
[22b]*Departamento de Física, Universidad Nacional de Colombia, Bogotá, Colombia*
[23a]*Dipartimento di Fisica e Astronomia A. Righi, Università di Bologna, Bologna, Italy*
[23b]*INFN Sezione di Bologna, Italy*
[24]*Physikalisches Institut, Universität Bonn, Bonn, Germany*
[25]*Department of Physics, Boston University, Boston, Massachusetts, USA*
[26]*Department of Physics, Brandeis University, Waltham, Massachusetts, USA*
[27a]*Transilvania University of Brasov, Brasov, Romania*
[27b]*Horia Hulubei National Institute of Physics and Nuclear Engineering, Bucharest, Romania*
[27c]*Department of Physics, Alexandru Ioan Cuza University of Iasi, Iasi, Romania*
[27d]*National Institute for Research and Development of Isotopic and Molecular Technologies, Physics Department, Cluj-Napoca, Romania*
[27e]*National University of Science and Technology Politechnica, Bucharest, Romania*
[27f]*West University in Timisoara, Timisoara, Romania*
[27g]*Faculty of Physics, University of Bucharest, Bucharest, Romania*
[28a]*Faculty of Mathematics, Physics and Informatics, Comenius University, Bratislava, Slovak Republic*

[28b]*Department of Subnuclear Physics, Institute of Experimental Physics of the Slovak Academy of Sciences, Kosice, Slovak Republic*

[29]*Physics Department, Brookhaven National Laboratory, Upton, New York, USA*

[30]*Universidad de Buenos Aires, Facultad de Ciencias Exactas y Naturales, Departamento de Física, y CONICET, Instituto de Física de Buenos Aires (IFIBA), Buenos Aires, Argentina*

[31]*California State University, California, USA*

[32]*Cavendish Laboratory, University of Cambridge, Cambridge, United Kingdom*

[33a]*Department of Physics, University of Cape Town, Cape Town, South Africa*

[33b]*iThemba Labs, Western Cape, South Africa*

[33c]*Department of Mechanical Engineering Science, University of Johannesburg, Johannesburg, South Africa*

[33d]*National Institute of Physics, University of the Philippines Diliman (Philippines), Philippines*

[33e]*University of South Africa, Department of Physics, Pretoria, South Africa*

[33f]*University of Zululand, KwaDlangezwa, South Africa*

[33g]*School of Physics, University of the Witwatersrand, Johannesburg, South Africa*

[34]*Department of Physics, Carleton University, Ottawa, Ontario, Canada*

[35a]*Faculté des Sciences Ain Chock, Réseau Universitaire de Physique des Hautes Energies—Université Hassan II, Casablanca, Morocco*

[35b]*Faculté des Sciences, Université Ibn-Tofail, Kénitra, Morocco*

[35c]*Faculté des Sciences Semlalia, Université Cadi Ayyad, LPHEA-Marrakech, Morocco*

[35d]*LPMR, Faculté des Sciences, Université Mohamed Premier, Oujda, Morocco*

[35e]*Faculté des sciences, Université Mohammed V, Rabat, Morocco*

[35f]*Institute of Applied Physics, Mohammed VI Polytechnic University, Ben Guerir, Morocco*

[36]*CERN, Geneva, Switzerland*

[37]*Affiliated with an institute covered by a cooperation agreement with CERN*

[38]*Affiliated with an international laboratory covered by a cooperation agreement with CERN*

[39]*Enrico Fermi Institute, University of Chicago, Chicago, Illinois, USA*

[40]*LPC, Université Clermont Auvergne, CNRS/IN2P3, Clermont-Ferrand, France*

[41]*Nevis Laboratory, Columbia University, Irvington, New York, USA*

[42]*Niels Bohr Institute, University of Copenhagen, Copenhagen, Denmark*

[43a]*Dipartimento di Fisica, Università della Calabria, Rende, Italy*

[43b]*INFN Gruppo Collegato di Cosenza, Laboratori Nazionali di Frascati, Italy*

[44]*Physics Department, Southern Methodist University, Dallas, Texas, USA*

[45]*Physics Department, University of Texas at Dallas, Richardson, Texas, USA*

[46]*National Centre for Scientific Research "Demokritos", Agia Paraskevi, Greece*

[47a]*Department of Physics, Stockholm University, Sweden*

[47b]*Oskar Klein Centre, Stockholm, Sweden*

[48]*Deutsches Elektronen-Synchrotron DESY, Hamburg and Zeuthen, Germany*

[49]*Fakultät Physik, Technische Universität Dortmund, Dortmund, Germany*

[50]*Institut für Kern- und Teilchenphysik, Technische Universität Dresden, Dresden, Germany*

[51]*Department of Physics, Duke University, Durham, North Carolina, USA*

[52]*SUPA—School of Physics and Astronomy, University of Edinburgh, Edinburgh, United Kingdom*

[53]*INFN e Laboratori Nazionali di Frascati, Frascati, Italy*

[54]*Physikalisches Institut, Albert-Ludwigs-Universität Freiburg, Freiburg, Germany*

[55]*II. Physikalisches Institut, Georg-August-Universität Göttingen, Göttingen, Germany*

[56]*Département de Physique Nucléaire et Corpusculaire, Université de Genève, Genève, Switzerland*

[57a]*Dipartimento di Fisica, Università di Genova, Genova, Italy*

[57b]*INFN Sezione di Genova, Italy*

[58]*II. Physikalisches Institut, Justus-Liebig-Universität Giessen, Giessen, Germany*

[59]*SUPA—School of Physics and Astronomy, University of Glasgow, Glasgow, United Kingdom*

[60]*LPSC, Université Grenoble Alpes, CNRS/IN2P3, Grenoble INP, Grenoble, France*

[61]*Laboratory for Particle Physics and Cosmology, Harvard University, Cambridge, Massachusetts, USA*

[62a]*Department of Modern Physics and State Key Laboratory of Particle Detection and Electronics, University of Science and Technology of China, Hefei, China*

[62b]*Institute of Frontier and Interdisciplinary Science and Key Laboratory of Particle Physics and Particle Irradiation (MOE), Shandong University, Qingdao, China*

[62c]*School of Physics and Astronomy, Shanghai Jiao Tong University, Key Laboratory for Particle Astrophysics and Cosmology (MOE), SKLPPC, Shanghai, China*

[62d]*Tsung-Dao Lee Institute, Shanghai, China*

[62e]*School of Physics and Microelectronics, Zhengzhou University, China*

[63a]*Kirchhoff-Institut für Physik, Ruprecht-Karls-Universität Heidelberg, Heidelberg, Germany*
[63b]*Physikalisches Institut, Ruprecht-Karls-Universität Heidelberg, Heidelberg, Germany*
[64a]*Department of Physics, Chinese University of Hong Kong, Shatin, N.T., Hong Kong, China*
[64b]*Department of Physics, University of Hong Kong, Hong Kong, China*
[64c]*Department of Physics and Institute for Advanced Study, Hong Kong University of Science and Technology, Clear Water Bay, Kowloon, Hong Kong, China*
[65]*Department of Physics, National Tsing Hua University, Hsinchu, Taiwan*
[66]*IJCLab, Université Paris-Saclay, CNRS/IN2P3, 91405, Orsay, France*
[67]*Centro Nacional de Microelectrónica (IMB-CNM-CSIC), Barcelona, Spain*
[68]*Department of Physics, Indiana University, Bloomington, Indiana, USA*
[69a]*INFN Gruppo Collegato di Udine, Sezione di Trieste, Udine, Italy*
[69b]*ICTP, Trieste, Italy*
[69c]*Dipartimento Politecnico di Ingegneria e Architettura, Università di Udine, Udine, Italy*
[70a]*INFN Sezione di Lecce, Italy*
[70b]*Dipartimento di Matematica e Fisica, Università del Salento, Lecce, Italy*
[71a]*INFN Sezione di Milano, Italy*
[71b]*Dipartimento di Fisica, Università di Milano, Milano, Italy*
[72a]*INFN Sezione di Napoli, Italy*
[72b]*Dipartimento di Fisica, Università di Napoli, Napoli, Italy*
[73a]*INFN Sezione di Pavia, Italy*
[73b]*Dipartimento di Fisica, Università di Pavia, Pavia, Italy*
[74a]*INFN Sezione di Pisa, Italy*
[74b]*Dipartimento di Fisica E. Fermi, Università di Pisa, Pisa, Italy*
[75a]*INFN Sezione di Roma, Italy*
[75b]*Dipartimento di Fisica, Sapienza Università di Roma, Roma, Italy*
[76a]*INFN Sezione di Roma Tor Vergata, Italy*
[76b]*Dipartimento di Fisica, Università di Roma Tor Vergata, Roma, Italy*
[77a]*INFN Sezione di Roma Tre, Italy*
[77b]*Dipartimento di Matematica e Fisica, Università Roma Tre, Roma, Italy*
[78a]*INFN-TIFPA, Italy*
[78b]*Università degli Studi di Trento, Trento, Italy*
[79]*Universität Innsbruck, Department of Astro and Particle Physics, Innsbruck, Austria*
[80]*University of Iowa, Iowa City, Iowa, USA*
[81]*Department of Physics and Astronomy, Iowa State University, Ames, Iowa, USA*
[82]*Istinye University, Sariyer, Istanbul, Türkiye*
[83a]*Departamento de Engenharia Elétrica, Universidade Federal de Juiz de Fora (UFJF), Juiz de Fora, Brazil*
[83b]*Universidade Federal do Rio De Janeiro COPPE/EE/IF, Rio de Janeiro, Brazil*
[83c]*Instituto de Física, Universidade de São Paulo, São Paulo, Brazil*
[83d]*Rio de Janeiro State University, Rio de Janeiro, Brazil*
[83e]*Federal University of Bahia, Bahia, Brazil*
[84]*KEK, High Energy Accelerator Research Organization, Tsukuba, Japan*
[85]*Graduate School of Science, Kobe University, Kobe, Japan*
[86a]*AGH University of Krakow, Faculty of Physics and Applied Computer Science, Krakow, Poland*
[86b]*Marian Smoluchowski Institute of Physics, Jagiellonian University, Krakow, Poland*
[87]*Institute of Nuclear Physics Polish Academy of Sciences, Krakow, Poland*
[88]*Faculty of Science, Kyoto University, Kyoto, Japan*
[89]*Research Center for Advanced Particle Physics and Department of Physics, Kyushu University, Fukuoka, Japan*
[90]*L2IT, Université de Toulouse, CNRS/IN2P3, UPS, Toulouse, France*
[91]*Instituto de Física La Plata, Universidad Nacional de La Plata and CONICET, La Plata, Argentina*
[92]*Physics Department, Lancaster University, Lancaster, United Kingdom*
[93]*Oliver Lodge Laboratory, University of Liverpool, Liverpool, United Kingdom*
[94]*Department of Experimental Particle Physics, Jožef Stefan Institute and Department of Physics, University of Ljubljana, Ljubljana, Slovenia*
[95]*School of Physics and Astronomy, Queen Mary University of London, London, United Kingdom*
[96]*Department of Physics, Royal Holloway University of London, Egham, United Kingdom*
[97]*Department of Physics and Astronomy, University College London, London, United Kingdom*
[98]*Louisiana Tech University, Ruston, Los Angeles, USA*
[99]*Fysiska institutionen, Lunds universitet, Lund, Sweden*

[100]Departamento de Física Teorica C-15 and CIAFF, Universidad Autónoma de Madrid, Madrid, Spain

[101]Institut für Physik, Universität Mainz, Mainz, Germany

[102]School of Physics and Astronomy, University of Manchester, Manchester, United Kingdom

[103]CPPM, Aix-Marseille Université, CNRS/IN2P3, Marseille, France

[104]Department of Physics, University of Massachusetts, Amherst, Massachusetts, USA

[105]Department of Physics, McGill University, Montreal, Quebec, Canada

[106]School of Physics, University of Melbourne, Victoria, Australia

[107]Department of Physics, University of Michigan, Ann Arbor, Michigan, USA

[108]Department of Physics and Astronomy, Michigan State University, East Lansing, Michigan, USA

[109]Group of Particle Physics, University of Montreal, Montreal, Quebec, Canada

[110]Fakultät für Physik, Ludwig-Maximilians-Universität München, München, Germany

[111]Max-Planck-Institut für Physik (Werner-Heisenberg-Institut), München, Germany

[112]Graduate School of Science and Kobayashi-Maskawa Institute, Nagoya University, Nagoya, Japan

[113]Department of Physics and Astronomy, University of New Mexico, Albuquerque, New Mexico, USA

[114]Institute for Mathematics, Astrophysics and Particle Physics, Radboud University/Nikhef,
Nijmegen, Netherlands

[115]Nikhef National Institute for Subatomic Physics and University of Amsterdam, Amsterdam, Netherlands

[116]Department of Physics, Northern Illinois University, DeKalb, Illinois, USA

[117a]New York University Abu Dhabi, Abu Dhabi, United Arab Emirates

[117b]United Arab Emirates University, Al Ain, United Arab Emirates

[118]Department of Physics, New York University, New York, New York, USA

[119]Ochanomizu University, Otsuka, Bunkyo-ku, Tokyo, Japan

[120]Ohio State University, Columbus, Ohio, USA

[121]Homer L. Dodge Department of Physics and Astronomy, University of Oklahoma,
Norman, Oklahoma, USA

[122]Department of Physics, Oklahoma State University, Stillwater, Oklahoma, USA

[123]Palacký University, Joint Laboratory of Optics, Olomouc, Czech Republic

[124]Institute for Fundamental Science, University of Oregon, Eugene, Oregon, USA

[125]Graduate School of Science, Osaka University, Osaka, Japan

[126]Department of Physics, University of Oslo, Oslo, Norway

[127]Department of Physics, Oxford University, Oxford, United Kingdom

[128]LPNHE, Sorbonne Université, Université Paris Cité, CNRS/IN2P3, Paris, France

[129]Department of Physics, University of Pennsylvania, Philadelphia, Pennsylvania, USA

[130]Department of Physics and Astronomy, University of Pittsburgh, Pittsburgh, Pennsylvania, USA

[131a]Laboratório de Instrumentação e Física Experimental de Partículas—LIP, Lisboa, Portugal

[131b]Departamento de Física, Faculdade de Ciências, Universidade de Lisboa, Lisboa, Portugal

[131c]Departamento de Física, Universidade de Coimbra, Coimbra, Portugal

[131d]Centro de Física Nuclear da Universidade de Lisboa, Lisboa, Portugal

[131e]Departamento de Física, Universidade do Minho, Braga, Portugal

[131f]Departamento de Física Teórica y del Cosmos, Universidad de Granada, Granada (Spain), Spain

[131g]Departamento de Física, Instituto Superior Técnico, Universidade de Lisboa, Lisboa, Portugal

[132]Institute of Physics of the Czech Academy of Sciences, Prague, Czech Republic

[133]Czech Technical University in Prague, Prague, Czech Republic

[134]Charles University, Faculty of Mathematics and Physics, Prague, Czech Republic

[135]Particle Physics Department, Rutherford Appleton Laboratory, Didcot, United Kingdom

[136]IRFU, CEA, Université Paris-Saclay, Gif-sur-Yvette, France

[137]Santa Cruz Institute for Particle Physics, University of California Santa Cruz,
Santa Cruz, California, USA

[138a]Departamento de Física, Pontificia Universidad Católica de Chile, Santiago, Chile

[138b]Millennium Institute for Subatomic physics at high energy frontier (SAPHIR), Santiago, Chile

[138c]Instituto de Investigación Multidisciplinario en Ciencia y Tecnología, y Departamento de Física,
Universidad de La Serena, Chile

[138d]Universidad Andres Bello, Department of Physics, Santiago, Chile

[138e]Instituto de Alta Investigación, Universidad de Tarapacá, Arica, Chile

[138f]Departamento de Física, Universidad Técnica Federico Santa María, Valparaíso, Chile

[139]Department of Physics, University of Washington, Seattle, Washington, USA

[140]Department of Physics and Astronomy, University of Sheffield, Sheffield, United Kingdom

[141]Department of Physics, Shinshu University, Nagano, Japan

[142]Department Physik, Universität Siegen, Siegen, Germany

[143]Department of Physics, Simon Fraser University, Burnaby, British Columbia, Canada

[144]*SLAC National Accelerator Laboratory, Stanford, California, USA*

[145]*Department of Physics, Royal Institute of Technology, Stockholm, Sweden*

[146]*Departments of Physics and Astronomy, Stony Brook University, Stony Brook, New York, USA*

[147]*Department of Physics and Astronomy, University of Sussex, Brighton, United Kingdom*

[148]*School of Physics, University of Sydney, Sydney, Australia*

[149]*Institute of Physics, Academia Sinica, Taipei, Taiwan*

[150a]*E. Andronikashvili Institute of Physics, Iv. Javakhishvili Tbilisi State University, Tbilisi, Georgia*

[150b]*High Energy Physics Institute, Tbilisi State University, Tbilisi, Georgia*

[150c]*University of Georgia, Tbilisi, Georgia*

[151]*Department of Physics, Technion, Israel Institute of Technology, Haifa, Israel*

[152]*Raymond and Beverly Sackler School of Physics and Astronomy, Tel Aviv University, Tel Aviv, Israel*

[153]*Department of Physics, Aristotle University of Thessaloniki, Thessaloniki, Greece*

[154]*International Center for Elementary Particle Physics and Department of Physics, University of Tokyo, Tokyo, Japan*

[155]*Department of Physics, Tokyo Institute of Technology, Tokyo, Japan*

[156]*Department of Physics, University of Toronto, Toronto, Ontario, Canada*

[157a]*TRIUMF, Vancouver, British Columbia, Canada*

[157b]*Department of Physics and Astronomy, York University, Toronto, Ontario, Canada*

[158]*Division of Physics and Tomonaga Center for the History of the Universe, Faculty of Pure and Applied Sciences, University of Tsukuba, Tsukuba, Japan*

[159]*Department of Physics and Astronomy, Tufts University, Medford, Massachusetts, USA*

[160]*Department of Physics and Astronomy, University of California Irvine, Irvine, California, USA*

[161]*University of Sharjah, Sharjah, United Arab Emirates*

[162]*Department of Physics and Astronomy, University of Uppsala, Uppsala, Sweden*

[163]*Department of Physics, University of Illinois, Urbana, Illinois, USA*

[164]*Instituto de Física Corpuscular (IFIC), Centro Mixto Universidad de Valencia—CSIC, Valencia, Spain*

[165]*Department of Physics, University of British Columbia, Vancouver, British Columbia, Canada*

[166]*Department of Physics and Astronomy, University of Victoria, Victoria, British Columbia, Canada*

[167]*Fakultät für Physik und Astronomie, Julius-Maximilians-Universität Würzburg, Würzburg, Germany*

[168]*Department of Physics, University of Warwick, Coventry, United Kingdom*

[169]*Waseda University, Tokyo, Japan*

[170]*Department of Particle Physics and Astrophysics, Weizmann Institute of Science, Rehovot, Israel*

[171]*Department of Physics, University of Wisconsin, Madison, Wisconsin, USA*

[172]*Fakultät für Mathematik und Naturwissenschaften, Fachgruppe Physik, Bergische Universität Wuppertal, Wuppertal, Germany*

[173]*Department of Physics, Yale University, New Haven, Connecticut, USA*

[a]Deceased.

[b]Also at Department of Physics, King's College London, London, United Kingdom.

[c]Also at Institute of Physics, Azerbaijan Academy of Sciences, Baku, Azerbaijan.

[d]Also at Lawrence Livermore National Laboratory, Livermore, USA.

[e]Also at TRIUMF, Vancouver, British Columbia, Canada.

[f]Also at Department of Physics, University of Thessaly, Greece.

[g]Also at An-Najah National University, Nablus, Palestine.

[h]Also at Department of Physics, University of Fribourg, Fribourg, Switzerland.

[i]Also at Department of Physics, Westmont College, Santa Barbara, USA.

[j]Also at Departament de Fisica de la Universitat Autonoma de Barcelona, Barcelona, Spain.

[k]Also at Affiliated with an institute covered by a cooperation agreement with CERN.

[l]Also at The Collaborative Innovation Center of Quantum Matter (CICQM), Beijing, China.

[m]Also at Università di Napoli Parthenope, Napoli, Italy.

[n]Also at Institute of Particle Physics (IPP), Canada.

[o]Also at University of Colorado Boulder, Department of Physics, Colorado, USA.

[p]Also at Borough of Manhattan Community College, City University of New York, New York, New York, USA.

[q]Also at National Institute of Physics, University of the Philippines Diliman (Philippines), Philippines.

[r]Also at Department of Financial and Management Engineering, University of the Aegean, Chios, Greece.

[s]Also at Department of Physics, Stanford University, Stanford, California, USA.

[t]Also at Centro Studi e Ricerche Enrico Fermi, Italy.

[u]Also at Institucio Catalana de Recerca i Estudis Avancats, ICREA, Barcelona, Spain.

[v]Also at Technical University of Munich, Munich, Germany.

[w]Also at Yeditepe University, Physics Department, Istanbul, Türkiye.

[x]Also at Institute of Theoretical Physics, Ilia State University, Tbilisi, Georgia.

[y]Also at CERN, Geneva, Switzerland.

[z]Also at Center for Interdisciplinary Research and Innovation (CIRI-AUTH), Thessaloniki, Greece.

[aa]Also at Hellenic Open University, Patras, Greece.

[bb]Also at Center for High Energy Physics, Peking University, China.

[cc]Also at Department of Physics, Stellenbosch University, South Africa.

[dd]Also at Department of Physics, California State University, Sacramento, USA.

[ee]Also at Département de Physique Nucléaire et Corpusculaire, Université de Genève, Genève, Switzerland.

[ff]Also at Institut für Experimentalphysik, Universität Hamburg, Hamburg, Germany.

[gg]Also at Institute for Nuclear Research and Nuclear Energy (INRNE) of the Bulgarian Academy of Sciences, Sofia, Bulgaria.

[hh]Also at Washington College, Chestertown, Maryland, USA.

[ii]Also at Institute of Applied Physics, Mohammed VI Polytechnic University, Ben Guerir, Morocco.

[jj]Also at Institute of Physics and Technology, Mongolian Academy of Sciences, Ulaanbaatar, Mongolia.